The University Of Sheffield.

Understanding the Mechanisms Driving Hair Cell Maturation in the Mammalian Cochlea *ex vivo*

By:

Hubashia Gazanfar Rizvi

A thesis submitted in partial fulfilment of the requirements for the degree of Doctor of Philosophy

The University of Sheffield

Faculty of Science

School of Biosciences

September 2022

Acknowledgements

I would like to thank both my supervisors, Professor Walter Marcotti and Dr. Stuart Johnson. They provided me with support, sage guidance, and advice when it was most important. I would not be here without their foresight and vision. I am truly grateful in more ways than one.

I would also like to thank my advisors Professor Marcelo Rivolta and Dr. Anton Nikolaev for their inputs on my ideas and overall project. It was extremely interesting to look at my work from a different perspective and think of new ideas. Additionally, I would like to thank Dr. Federico Ceriani, for helping me understand how to build my setup, and explaining concepts that were difficult for me to grasp initially. I would like to extend thanks to all the post-docs and technicians in the lab. Specifically, thank you very much Dr. Jing-Yi Jeng, for your guidance on immunostaining and for entertaining every silly question I had about everything under the sun. I thank all my colleagues in the lab who taught me python, various analysis, and innumerable techniques. Piece, I relished every single food and idea we exchanged. Anna, thanks so much for always lending an ear and teaching me SEM. Shout out to Catherine, Sam, Andy, Heather, Jianbo and Laila. The true strength of a lab is the willingness of its members to communicate and impart knowledge unto others. I have nothing but respect for everyone in the hearing group, who work tirelessly to broaden our collective horizons in this field.

I would like to thank my family, who have supported me through my PhD. In many ways this is their achievement. I could not have done this without them. My mum and dad, who always reminded me to be focussed, and my sister and brother, who made sure I don't take myself too seriously. I would also like to thank all my friends, inside the lab and outside; Alice, Erik and Tania, for being incredible. Paolo, thank you for spending hours listening to me, giving me ideas, and supporting me in more ways than I can count.

Lastly, thank you, Dr Jarema Malicki, and may you rest in peace.

Abstract

The remarkable ability of the auditory system to accurately transduce acoustic signals from the environment into electrical signals in the brain is the product of finely tuned developmental and functional pathways. Before the onset of hearing, cochlear inner hair cells undergo a series of developmental steps, which involve changes to their biophysical and molecular properties.

One of these developmental steps, called spontaneous activity is driven by stimulus-independent action potentials, generated by immature hair cells in the prehearing stage of the mammalian cochlea. Spontaneous activity is calcium-dependent and generates rhythmic waves in levels of intracellular calcium within the organ of Corti (Kros *et al.*, 1998; Johnson *et al.*, 2017a). Similar to its role in other sensory systems (such as the visual system; Fisher, 1979; Soto *et al.*, 2012), spontaneous activity in the cochlear inner hair cells serves to develop the ribbon synapse, refine afferent circuits (Johnson *et al.*, 2013; Clause *et al.*, 2014) and influence neuronal survival (Zhang-Hooks *et al.*, 2016). Within the auditory system specifically, spontaneous activity aids to also regulate hair cell maturation. However, how precisely spontaneous activity regulates hair cell maturation is not well understood. The true extent of the role of spontaneous activity in development, and even the generation of the activity itself, is still an area of dynamic research.

Understanding the full influence of spontaneous activity on inner hair cell maturation, especially during ribbon synapse development can provide insight into the development of the complex hair cell machinery. Additionally, it would be noteworthy to study inner hair cell development *ex vivo* in a context isolated from the central nervous system, as this could aid future investigations in drug development and the generation of novel targeted therapeutic strategies to combat hearing loss. Therefore, the aim of this project is to study how spontaneous activity (or lack thereof) in immature inner hair cells contributes to development and biophysical maturation of inner hair cells *ex vivo* by utilising optogenetic techniques and super resolution imaging. The following introduction will provide a summary to what is known so far in terms of hair cell development and postulate the hypothesis underpinning this project.

Table of Contents

List of Figures

List of Tables

List of Graphs

List of Abbreviations

Na^+	Sodium
ACh	Acetylcholine
ATOH1	Atonal BHLH Transcription Factor 1
ATP	Adenosine triphosphate
AZ	Active zone
BDNF	Brain Derived Neurotrophic Factor
BK	Large conductance Ca^{2+} activated K^+ channel
Ca^{2+}	Calcium
$CaCl_2$	Calcium chloride
$Cav_{1.3}$	Calcium channel, voltage-dependent, L type, alpha 1D subunit
CDH23	Cadherin 23
ChR2	Channelrhodopsin-2
Cl^-	Chlorine
CNS	Central Nervous System
CNTF	Ciliary Neurotrophic Factor
CSF	Cerebrospinal fluid
CtBP1	C-Terminal Binding Protein 1
CtBP2	C-Terminal Binding Protein 2
CVG	Cochleovestibular ganglion
DCs	Deiters' cells
DCV	Dense core vesicle
DIV	Days *in vitro*
DMEM/F-12	Dulbecco's Modified Eagle Medium/Nutrient Mixture F-12
E12/14	Embryonic day 12/14
EP	Endocochlear potential
Eps8	Epidermal growth factor receptor kinase substrate 8
EPSCs	Excitatory postsynaptic currents
ERC2	ELKS/RAB6-Interacting/CAST Family Member 2
EYFP	Enhanced yellow fluorescent protein
FBS	Fetal bovine serum
FGF	Fibroblast growth factor
GER	Greater epithelial ridge

GluA2/3	AMPA subunit GluA2 and GluA3
GluR4	AMPA receptor subunit GluR4
HBSS	Hanks' Balanced Salt Solution
HCO_3^-	Bicarbonate
HEDTA	Hydroxyethylethylenediaminetriacetic acid
HEPES	Hydroxyethyl piperazineethanesulfonic acid
I_{Ca}	Calcium current
IGF-1	Insulin-like growth factor-1
IgG	Immunoglobulin G
IHCs	Inner hair cells
$I_{K,f}$	Fast outward potassium current
$I_{K,n}$	Potassium current from Kcnq4
I_{Na}	Sodium current
IPhCs	Inner phalangeal cells
IR	insulin receptor
I_{SK2}	Current from small conductance Ca^{2+}-activated K^+ channels
K^+	Potassium
KCl	Potassium chloride
Kcnq4	Voltage-gated K^+ channel
KIF3A	Kinesin family 3A
$K_{v7.4}$	Voltage-gated K+ channel encoded by Kcnq4
LED	Light-emitting diode
LOC	Lateral olivocochlear
MET	Mechano-electrical transduction
Mg^{2+}	Magnesium
MOC	Medial olivocochlear
mRNA	Messenger RNA
nAChR	Nicotinic acetylcholine receptor
NAD+	Nicotinamide adenine dinucleotide
NGF	Nerve growth factor
NT3	Neurotrophin-3
OHC	Outer hair cell
OS	Optogenetically stimulated
OTOF	Otoferlin
PBS	Phosphate buffered saline

PBST	Phosphate-buffered saline with Tween® detergent
PCDH15	Protocadherin 15
PFA	Paraformaldehyde
P(X)	Postnatal day
RIM2	Rab3-interacting molecule
RRP	Readily releasable pool
SCs	Supporting cells
SGNs	Spiral ganglion neurons
SK2	Small-conductance potassium channel
STORM	Stochastic optical reconstruction microscopy
SVs	Synaptic vesicles
Syt1	Synaptotagmin 1
Syt2	Synaptotagmin 2
Syt4	Synaptotagmin 4
T3	Triiodothyronine
T4	Thyroxine
TH	Thyroid hormone
TSH	Thyroid stimulating hormone
VAMP	Vesicle associated membrane protein
VGSCs	Voltage gated sodium channels
Vm	Membrane potential
YFP	Yellow fluorescent protein

1. Main Introduction

1.1 General anatomy of the cochlea

The mammalian auditory system is comprised of three parts (figure 1.1): the outer ear, the middle ear, and the inner ear. The outer ear consists of the external facing ear pinna (auricle) and is attached to the ear canal. The external ear pinna acts as a wide receiver of external sound waves. The ear canal functions to effectively direct acoustic vibration towards the tympanic membrane (eardrum) at the end of the ear canal. The middle ear begins at the tympanic membrane. Sound waves hit the tympanic membrane and trigger vibrations of the three ear ossicles: the malleus, incus, and stapes in succession. The movement of the stapes directs sound vibrations into the inner ear via the oval window. The oval window allows vibrations to reach into the fluid-filled cochlea, while the concurrent movement of the flexible round window enables fluid displacement in the cochlea. The inner ear consists of two main parts: the vestibular system, which comprises of the semicircular canals, the utricle, and the saccule (i.e., the otoliths, which are positioned in the vestibule), and the cochlea. The vestibular system senses head movement and gravity acting on the body. This helps to maintain spatial orientation and balance within 3-dimensional space. The cochlea is primarily responsible for the transduction of auditory stimulus. Auditory and vestibular sensory data is transmitted to the brain via the cranial nerve VIII- vestibulocochlear nerve.

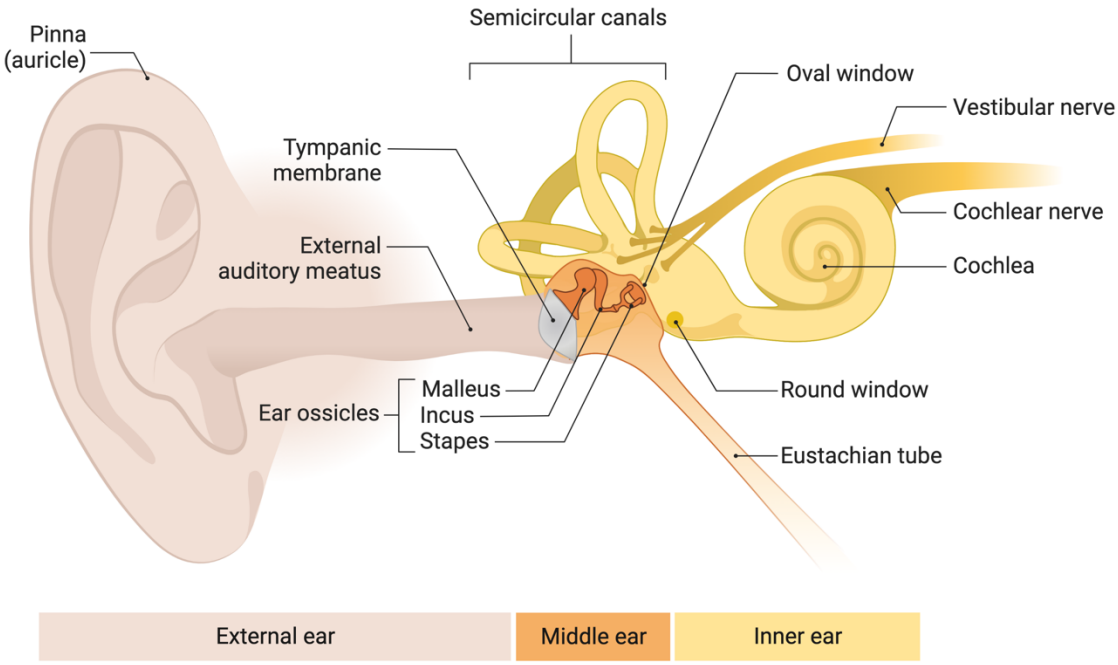

Figure 1.1 General anatomy of the external middle and inner ear.

The outer ear consists of the ear pinna (auricle) and external auditory meatus (ear canal), which directs sound towards the tympanic membrane (eardrum) at the middle ear. The middle ear is composed of the three ear ossicles (malleus, incus and stapes) that work alongside the tympanic membrane as an impedance transformer to compensate for the characteristic impedance between air and cochlear fluid. This is attained by the combination of pressure amplification and the lever motion of the ossicles. The stimulus is concentrated towards the inner ear which is composed of the vestibule (vestibular system) with semicircular canals and the cochlea (auditory system). The stimulus travels into the cochlea via the oval window, where the transduction of sound stimulus takes place. Figure created with BioRender.com under academic license.

The cochlea is a hollow, spiral cavity located in the bony labyrinth (the bony wall of the inner ear in the temporal bone) in the inner ear (figure 1.2 A-C). The coiled structure of the cochlea has influenced its name from Ancient Greek, meaning 'snail shell'. In humans, this spiral is almost 42 mm long (Erixon *et al.*, 2009), and consists of 2¾ turns around an axis, the modiolus (Slepecky *et al.*, 1980; Bogart, 2008), and is innervated by the cranial nerve VIII. The cochlear spiral cavity is divided into three chambers (i.e., scalae): the superior scala vestibuli, the inferior scala tympani, and in the medial scala media (also known as the cochlear duct). The scala vestibuli is connected to the oval window. The scala vestibuli and scala media are divided by a membrane called the Reissner's membrane. Similarly, the scala media and scala tympani are separated by the basilar membrane. The scala media separates the scala vestibuli and scala tympani for almost the entire length of the cochlea. However, the scala vestibuli and scala tympani meet at the apex through a small opening, called the helicotrema.

The scala vestibuli and scala tympani are filled with an ionic solution rich in Na^+ called perilymph. The scala media, in contrast, is filled with a solution rich in K^+ but low in Na^+ and Ca^{2+} (Wangemann, 2006), called endolymph. The reticular lamina separates the ionic fluids between the scala media and scala tympani and prevents diffusion across the chambers. Resting on the basilar membrane within the scala media is the organ of Corti. Situated above the organ of Corti is an acellular membrane called tectorial membrane. The tectorial membrane runs parallel to the basilar membrane throughout the longitudinal axis of the cochlea. The organ of Corti, tectorial membrane and basilar membrane together are known as the cochlear partition.

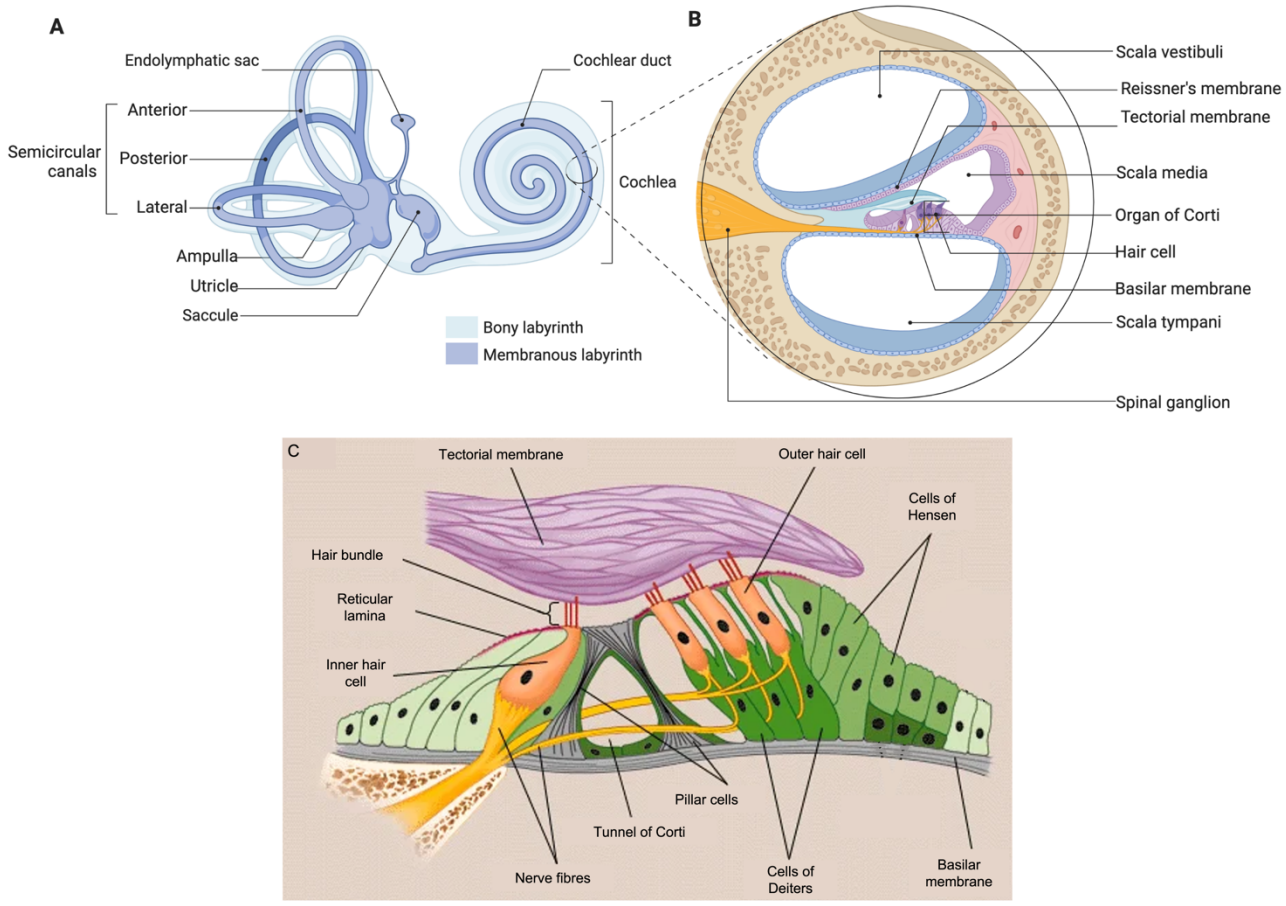

<u>Figure 1.2</u> General anatomy of the inner ear, cochlea, and organ of Corti: sectional view

A) External morphology of the inner ear containing the vestibule, semicircular canals, and cochlea. The vestibular system provides spatial orientation and balance. It contains

three semicircular canals, and the vestibule. The semicircular canals provide rotary information in the transverse, sagittal and coronal plane. The vestibule consists of the utricle and saccule (the otoliths), which detect linear acceleration and gravitational force. The spiral cochlea is responsible for the transduction of auditory stimulus to the brain and contains the organ of Corti. B) Sectional view of the cochlea, displaying its three chambers, namely the scala vestibuli, scala tympani and scala media. The Reissner's membrane divides the scala vestibuli from the scala media, while the basilar membrane divides the scala media from the scala tympani. The scala media contains the organ of Corti. C) Enlarged view of the organ of Corti. The organ of Corti is situated atop the basilar membrane with the overhanging tectorial membrane. The organ of Corti houses the inner and outer hair cells (IHCs and OHCs respectively). IHCs are the primary transducers of auditory stimulus, while OHCs are acoustic amplifiers. IHCs are mostly innervated by afferent type I SGNs (90-95%) while OHCs are mostly innervated by efferent MOC fibres and type II SGNs (5%). Figure A and B: Created with BioRender.com under academic license. Figure C: Adapted and inspired from Encyclopaedia Britannica Inc., (1997).

During an incoming sound wave, the basilar membrane flexes in response to the stimulus. The membrane is tonotopically arranged, such that higher frequency sound waves induce vibration at the base, and lower frequency sound waves vibrate the membrane at the apex (figure 1.3 A-B). This is because the basilar membrane is stiff and relatively narrower in width at the base compared to the apex, where it is relatively thinner, wider and more flexible (Emadi *et al.*, 2004; Teudt and Richter, 2014). In response to the movement of the basilar membrane, the organ of Corti above it moves correspondingly.

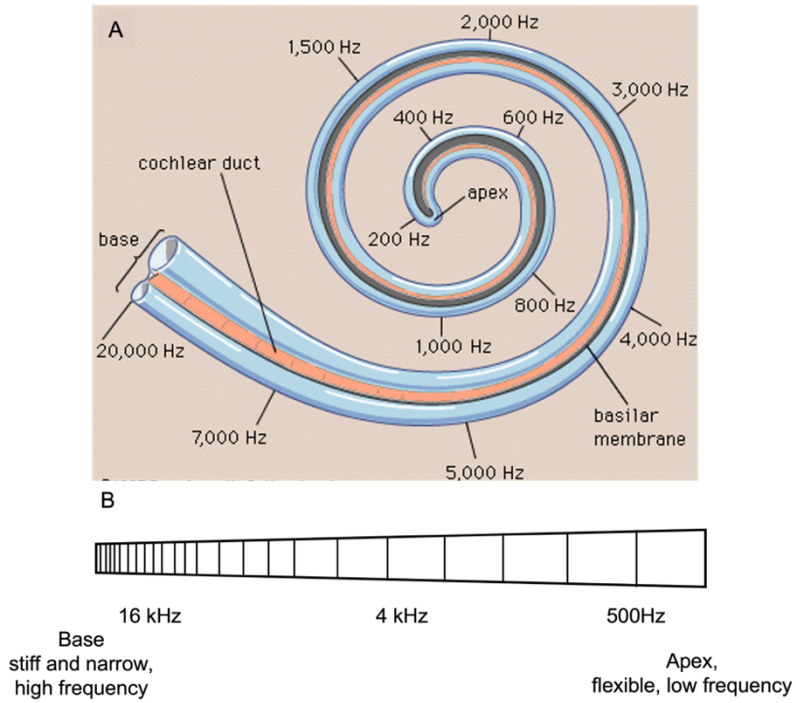

Figure 1.3 Tonotopic organisation of the basilar membrane

A) Frequency distribution of the basilar membrane ranging from the apex to the base. B) The uncoiled basilar membrane. The base of the membrane is narrow and rigid. The membrane gradually becomes broader and more flexible towards the apex. Consequently, each section of the membrane vibrates selectively to a specific frequency along the length of the cochlea. The basilar membrane at the base induces preferential vibration at high frequency. Medium frequencies vibrate the central region of the membrane, and the apex is better adapted to vibrate in response to lower frequencies. Figure A: Adapted and inspired from Encyclopaedia Britannica Inc., (1997). Figure B: Redrawn from Kim and Koo, (2015a).

The organ of Corti houses the cells responsible for the mechanotransduction of sensory information in the ear: the hair cells (figure 1.2. C). The two types of hair cells in the organ of Corti are the inner hair cells (IHCs) and outer hair cells (OHCs). The mammalian cochlea contains one row of IHCs, and three rows of OHCs. These highly specialised cells receive their title from hair-like structures

essentially similar to microvilli, that project out their apical end, called stereocilia. Each hair cell may contain 50-100 stereocilia extending from its apical end (Schwander *et al.*, 2010; McPherson, 2018). The stereocilia together in unison are also called hair bundles, and are arranged on each hair cell in two to four rows following a staircase-like structure (Tilney *et al.*, 1992; Goutman *et al.*, 2015).

During an incoming stimulus, the movement of the basilar membrane causes shearing motion (Fridberger *et al.*, 2002) between the OHCs stereocilia and the overhanging tectorial membrane. This movement causes the hair bundles to deflect and either open or close ion channels present at the tips of the stereocilia, depending on the direction of movement. This enables K^+ ions to flow down the electrochemical gradient into the cells and cause their depolarization.

In mice, there are 700-800 IHCs arranged in one row and ~2600 OHCs arranged in three rows (Ehret and Frankenreiter, 1977). The hair cells are arranged in a spiral fashion within the organ of Corti, following the spiral shape of the cochlea (Slepecky *et al.*, 1980; Robles and Ruggero, 2001). The hair cells are also surrounded by complementary supporting cells (SCs), which play critical roles in the structural development and maintenance of hair cells, and functional K^+ homeostasis in the cochlea. Unique populations of SCs rest on the basilar membrane and are morphologically distinct. SCs are organised along the length of the organ of Corti as follows (from the outer periphery to the interior edge): Hensen's cells, Deiters' cells (DCs), pillar cells, inner phalangeal cells (IPhCs) and border cells.

Hair cells transduce mechanosensory information (sound stimuli) into electrochemical signals which are conveyed to the brain. The cells primarily responsible for this task are the IHCs, which are able to transduce acoustic information with remarkable accuracy. OHCs, in contrast, are responsible for mechanical amplification and frequency selection of stimuli. Hair cells synapse with afferent spiral ganglion neurons (SGNs), which relay the transduced information to the central nervous system (CNS). 90-95% of these afferent neurons innervate the IHCs and are called type I SGNs. Incoming acoustic stimulus causes IHCs to release the neurotransmitter glutamate in a Ca^{2+}-dependent

manner, thus causing excitation in type I SGNs. Type I SGNs of the IHC are also contacted by lateral olivocochlear (LOC) efferent fibres though axodendritic synapses.

A small amount of afferent SGNs (around 5%), shoot collateral projections with multiple OHCs. These fibres are called type II SGNs. However, the major fibres innervating OHCs are cholinergic, efferent fibres, called medial olivocochlear (MOC) neurons. The MOC fibres form axosomatic synapses with OHCs in close proximity to the type II afferents. During mechanosensory stimulation, the stereocilia atop OHCs deflect and cause the OHCs to produce a mechanical reaction to the stimulus, called electromotility. This is made possible due to the membrane protein prestin (Fettiplace, 2017). OHC depolarization generates voltage-dependent length change in the cell body, leading to physical extension and contraction (Beurg *et al.*, 2009). This imparts pressure to the tectorial membrane, consequently amplifying the movement of the organ of Corti by a thousandfold.

The stereocilia of OHCs are embedded in the tectorial membrane. The protein stereocilin assists OHCs to attach the tips of the tallest row of stereocilia to the tectorial membrane and to one another (Verpy *et al.*, 2011). Until recently, it was assumed that the stereocilia of IHCs are free-standing, and not embedded in the tectorial membrane. However, recent studies revealed that filamentous Ca^{2+}-rich structures called Ca^{2+} ducts link the tectorial membrane to the stereocilia of IHCs, similar to OHCs (Hakizimana and Fridberger, 2021).

Stereocilia are composed of compact actin filaments and are connected to each other by extracellular links (figure 1.4). They also possess specialised tip links, that connect the tips of shorter stereocilia to the longer one in the bundle in the next row. The heights of stereocilia increase as one moves towards the apex, in the characteristic staircase configuration. However, the individual lengths of the stereocilia within each row and equivalent rows on adjacent cells remain alike (Tilney *et al.*, 1992; Robles and Ruggero, 2001).

At the core of the stereocilia lie parallel, crosslinked actin filaments. The two main isoforms of actin expressed by hair cells are β-actin and γ-actin (McGrath *et al.*, 2017). The tip links of the stereocilia

are mainly formed of two Ca^{2+}-dependent transmembrane proteins, cadherin 23 (CHD23) and protocadherin 15 (PCDH15; Ahmed *et al.*, 2006; Schwander *et al.*, 2010; Alagramam *et al.*, 2011). These proteins lie at opposite ends of the tip link (figure 1.4.); PCDH15 at the apical tip of the shorter stereocilia and CHD23 at the lateral tip of the taller stereocilia. CDH23 homodimers interact in trans with PCDH15 homodimers to form single filaments, which link the two stereociliary apexes (Müller, 2008; Sotomayor *et al.*, 2012; Geng *et al.*, 2013).

The top of the stereocilia contains an important non-selective cation channel called the mechano-electrical transducer channel (MET channel), which is responsible for the generation of the MET current. It is present in the form of a protein complex, called the MET complex. Each PCDH15 at the lower end of the tip link is believed to be attached to two MET channels (Beurg *et al.*, 2009). Due to the resting tension of the tip links, the MET channels are constantly slightly open. The slight inward current causes a small shift in the overall potential of the cell towards depolarised values. The incoming stimulus therefore requires a smaller amount of effort to trigger synaptic release of glutamate. MET channels are suggested to be absent from the tallest stereociliary row and exclusively located on the second and third row of stereocilia in IHCs and OHCs (Beurg *et al.*, 2009).

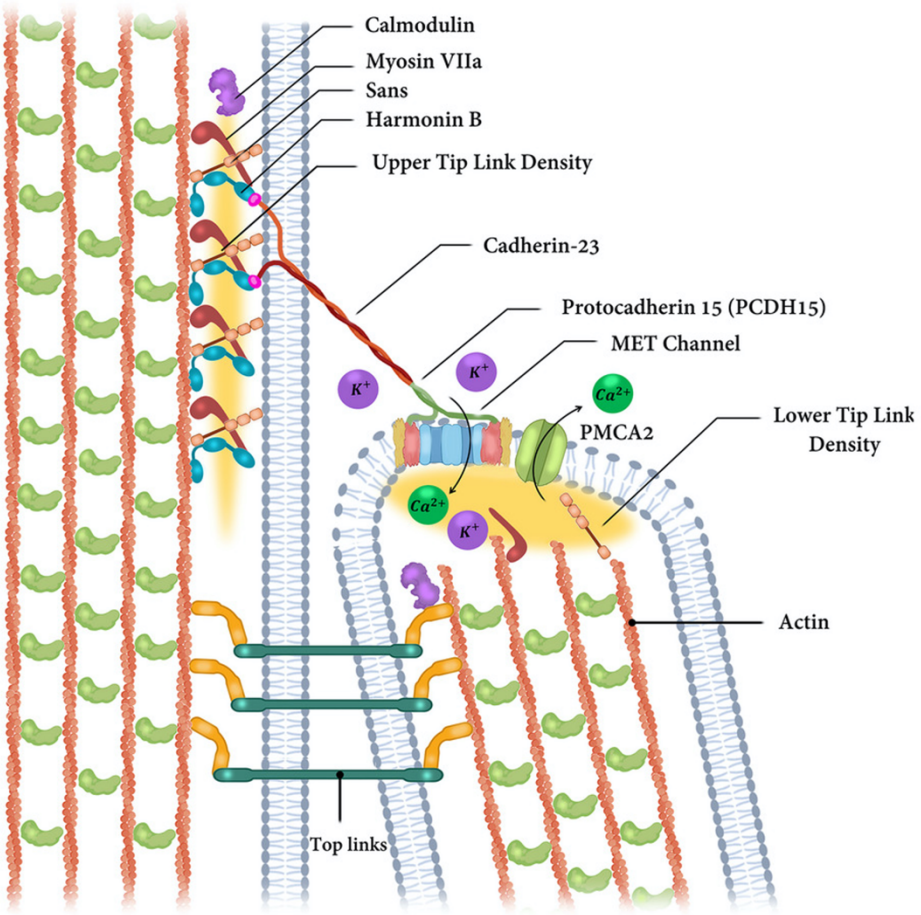

Figure 1.4 Diagrammatic representation of the hair cell stereocilia

The tip link is composed of Cadherin-23 and Protocadherin-15 (PCDH15), both of which enter into the membrane of the stereocilium at the positions of the upper and lower tip densities, respectively. The tip link is anchored by scaffolding proteins, such as Myosin VIIa, Harmonin, and Sans, which bind to cadherin-23. Each PCDH15 at the lower end of the tip link is attached to two MET channels. Yellow regions represent the upper and lower tip link densities. Calmodulin attaches to stereocilin as well as Ca2+, and the stereocilin consequently links two stereocilia. The core of the stereocilia consists of parallel, crosslinked actin filaments. The two main isoforms of actin expressed by hair cells are β-actin and γ-actin. Stimulus entering the cochlea causes deflections of the stereocilia, consequently opening of the MET channel, and allowing the influx of Ca2+ and K+ ions. Figure adapted from Farhadi et al., (2021).

Cochlear fluids have a variety of sources. The perilymph in the scala vestibuli originates from blood plasma, by utilising a hemto-perilymphatic barrier. The perilymph filling the scala tympani arises via the cerebrospinal fluid CSF. The endolymph originates from the CSF and its unique ionic composition is created and maintained by the stria vascularis (Zdebik *et al.*, 2009; Uetsuka *et al.*, 2015).

The stria vascularis is an epithelial tissue bordering the lateral wall of the cochlea. It is composed of cell layers (marginal, intermediate, and basal cells) and is extensively vascularized. Due to the presence of claudin-based tight junctions (Ben-Yosef *et al.*, 2003; Elkouby-Naor and Ben-Yosef, 2010) they provide a barrier between the cells that surround the scala media, any solute exchange between the endolymph and perilymph is prevented.

The composition of the perilymph is 148 mM Na^+, 4.2 mM K^+, 1.3 mM Ca^{2+}, 0.7 mM Mg^{2+}, 119 mM Cl^- and 21 mM $HCO3^-$ (pH 7.3). The composition of endolymph is 1.3 mM Na^+, 157 mM K^+, 0.02 mM Ca^{2+}, 0.01mM Mg^{2+}, 132 mM Cl^- and 31 mM $HCO3^-$ (pH 7.4) (Scheibe *et al.*, 1999; Wangemann, 2006). Due to its ionic characteristics, the endolymph possesses an electric potential of around +90mV known as the endocochlear potential (EP).

In contrast, the resting membrane potential of hair cells is -60mV (in mature hair cells). This brings the total ionic difference between the endolymph and the hair cell to around 150 mV, which is the largest difference in electrical potential observed in the body. This provides the driving force for the influx of K^+ and Ca^{2+} ions into the cell via the apical MET channel. K^+ then gets driven out into the perilymph by means of K^+ channels such as Kcnma1/BK ($I_{K,f}$), Kcnq4 ($I_{K,n}$), Kcnn2/SK2 (I_{SK2}) at the basolateral membrane (Johnstone *et al.*, 1989; Kros, 1996; Oliver *et al.*, 2003). The stria vascularis fulfils the role of keeping the concentration of K^+ high along with recycling K^+, and thus maintaining the EP (Wangemann, 2006).

Hair bundles are constantly bathed in the endolymph (figure 1.5). In contrast, the body of hair cells, located closer to the basolateral membrane, is bathed in perilymph (Sterkers *et al.*, 1988; Echteler

et al., 1994). This exquisite separation, provided by reticular lamina, maintains the ionic gradient that allows hair cell firing.

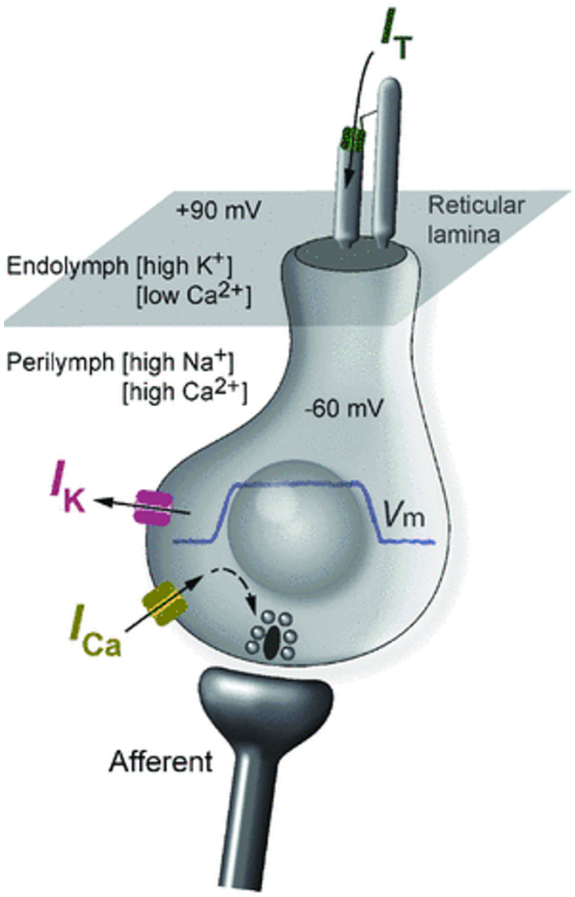

Figure 1.5 Diagram illustrating the fundamental physiology of mature IHCs

The reticular lamina acts as a barrier between the hair bundles that are bathed in the endolymph and the basilar membrane, which is bathed in perilymph. The endolymph and perilymph are dissimilar in their ionic composition. The endocochlear potential (around +90mV) and resting membrane potential of the IHC (around -60mV) together provide the driving force for the transducer current (IT). This triggers IHC depolarisation, and consequently generates the receptor potential and Ca2+ driven exocytosis of glutamate. The release of glutamate causes the activation of type I afferent fibres. Image adapted from Marcotti et al., (2012).

1.1.1 Initiation of mechanotransduction

Mechanotransduction in the IHC takes place in a series of steps (both IHCs and OHCs have similarities in transduction mechanisms, however, here it will be discussed in the context of IHCs specifically).

Mature IHCs produce graded receptor potentials (similar to photoreceptors), as opposed to the all-or-none action potentials, that are seen in various other sensory neurons (such as olfactory receptors). As explained earlier, the resting potential of IHCs is around −60 mV and the surrounding endocochlear potential is around + 90 mV. This vast difference is the driving force for the generation of the transducer current. L-type voltage-gated calcium channels ($Ca_V1.3$) are present at the presynaptic membrane, and have low activation threshold and very little inactivation. These factors, along with the resting membrane potential of the IHCs, cause some of the Ca^{2+} channels to remain open in the absence of sound stimuli. Therefore, the IHCs are constantly slightly active at resting membrane potential. Further investigations demonstrate that monophasic excitatory postsynaptic potentials (EPSCs) are present at synaptic terminals (Grant *et al.*, 2010), aiding continuous graded vesicle release and promoting background activity at the synapse.

As mentioned previously, stimulus reaching the cochlea creates vibrations that oscillate the basolateral membrane and the endolymph, which causes a shearing force between the tectorial membrane and the basilar membrane. This results in pressure changes in the endolymphatic fluid bathing the hair cell stereocilia in the direction of the sound stimulus. Consequently, this produces tension on the tip links of the stereocilia, which subsequently get deflected. If the deflection of the stereocilia is towards the direction of tallest stereocilium, it fully opens the MET channels, which allow K^+ ions (and some Ca^{2+} ions) to flow into the cell. This is known as the MET current. When acted upon by a large enough current, the IHC membrane gets depolarised and generates a receptor potential which causes the $Ca_V1.3$ channels to open. This allows the influx of Ca^{2+} from the

surrounding perilymph. This triggers the fusion of synaptic vesicles at the presynaptic site, leading to the subsequent release of glutamate. Thus, the release of glutamate from IHCs is Ca^{2+}-dependent.

During this period, the Ca^{2+} ions that are able to enter the MET channel also drive its closure, acting as a negative feedback, called adaptation (Peng *et al.*, 2011; Corns *et al.*, 2014). This consequently resets the sensitivity of the MET channels.

In contrast, deflection of the hair bundle towards the shortest stereocilia hyperpolarises the MET channels, causing them to close (Qiu and Müller, 2018), and no glutamate is released. This shows that the mature IHC receptor potential is in fact, biphasic, and allows the IHC to generate sinusoidal potentials in response to sinusoidal sound stimuli. This is beneficial as it conserves the temporal information in the stimulus reaching the cochlea.

1.1.2 General development of the hair cells

In mice, hair cell differentiation starts around terminal mitosis (embryonic days 12-14; i.e., E12-E14 in mice) and takes approximately three weeks. The onset of hearing in mice is almost two weeks after birth, at postnatal day 12 (P12; Pujol *et al.*, 1998). Hair cell growth and subsequent maturation relies on organised molecular cues and electrical activity during development. These signals arise at specific checkpoints throughout early development. Although IHCs and OHCs are already morphologically distinguishable as hair cells during early development, they are biophysically not identifiable (Marcotti *et al.*, 2003). In mice, this biophysical differentiation starts around birth (P0). OHCs mature earlier than IHCs, at around P8 and IHCs mature subsequently at P12 (Kros *et al.*, 1998; Marcotti and Kros, 1999).

In the mouse cochlea, hair cell progenitors are produced around E12.5-E14.5 following an apical to basal pattern down the entire length of the cochlea (Lee *et al.*, 2006; Yang *et al.*, 2010). Newly formed hair cells start to differentiate, beginning at the base at E14.5 (Chen *et al.*, 2002). In mice, stereocilia development is evident at E15. A layer of minute projections can be seen from the surface of the hair cells (figure 1.6.A), i.e., microvilli. Microvilli are initially observed developing at the basal end of the cochlea, and subsequently seen towards the apical end.

During initial development, the microvilli are accompanied by a distinct projection on the apical pole of the cell (figure 1.6 A-B), consisting of a microtubule core (classic 9+2 microtubule structural configuration), called the kinocilium. The kinocilium is theorised to facilitate the development of planar polarity within the cell (Kaltenbach *et al.*, 1994). The kinocilium subsequently moves towards the lateral edge of the immature hair cell. Successive development is characterised by the initiation of microvilli elongation and formation of the distinctive staircase structure. Each row of immature stereocilia follow elongation within their respective rows. Thus, the stereociliary bundles start to take form.

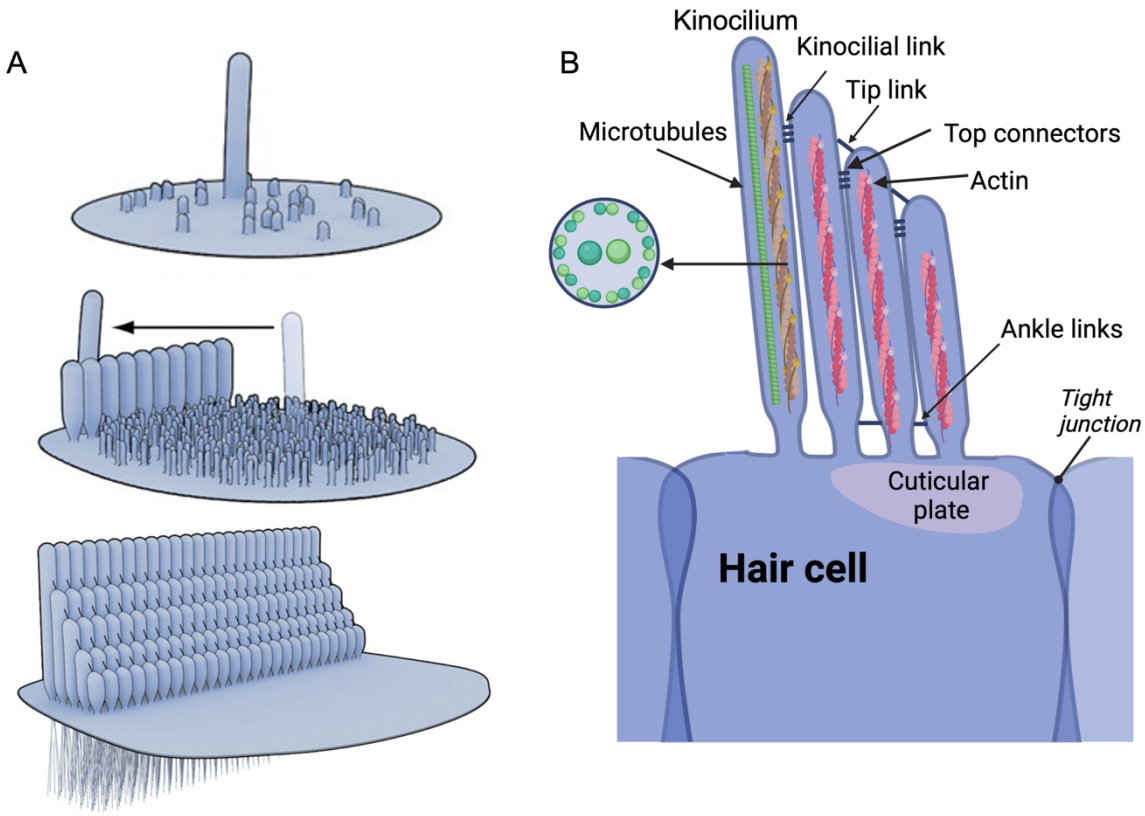

Figure 1.6 Development of hair cell stereocilia

A) Hair bundle development. Initially, the hair cell has a single kinocilium and multiple microvilli emerging from the apical pole. The kinocilium migrates to the edge of the apical pole, while adjacent microvilli grow in length. The kinocilium facilitates the establishment of planar polarity of the stereocilia. By the end, the stereocilia staircase has developed, and the kinocilium gets degenerated. B) Sectional view of a growing hair bundle. The kinocilium consists of microtubules, while stereocilia consist of actin. Green spheres show the expanded sectional view of the kinocilium microtubule core (showing the classic 9+2 microtubule structural configuration). Cadherin-23 and protocadherin-15 make up the tip links between stereocilia. Protocadherin-15 is associated on either side of the MET channel. Figure A: Adapted from (Schwander et al., 2010). Figure B: redrawn from Schwander et al., (2010) with BioRender.com under academic license.

Hair cell development carries on after birth, consisting of further elongation of the stereocilia postnatally (Kaltenbach *et al.*, 1994). In mice, elongation first terminates in the shortest stereociliary row at around P5, subsequently terminating in each row and finally in the tallest row at around P15. By this time, the initial kinocilium is eliminated and any excess microvilli are reabsorbed (Peng *et al.*, 2009). Mature stereocilia are highly organised structures, oriented along the axis of mechanosensitivity and localised asymmetrically with respect to the preceding kinocilium.

Several stereociliary proteins are suggested to be crucial for the development of stereocilia length. For example, epidermal growth factor receptor pathway substrate 8 (Eps8) is present at the tips of all stereocilia and is suggested to be important for their elongation (Zampini *et al.*, 2011). In contrast, the proteins twinfilin 2 and gelsolin are more exclusively expressed at the tips of short and mid-length stereocilia and function to inhibit the growth of actin filaments, thus regulating the overall length of the stereocilia (Peng *et al.*, 2009; Mburu *et al.*, 2010). Other proteins which have been implicated in stereociliary development and maintenance are espin, whirlin, myosin VIIa and myosin XV (Petit and Richardson, 2009; Schwander *et al.*, 2010). Mature stereociliary tip links are formed of the proteins CDH23 and PCDH15 (figure 1.4).

CDH23 is not only present in mature tip links, but also in immature hair bundles, in the form of transient lateral links between adjacent stereocilia. These links are cleared as the hair bundles mature. Recent studies suggest that the protein myosin VI is responsible for removing these transient links, so that the MET channels acquire their resting tension and Ca^{2+}-dependent adaptation properties (Marcotti *et al.*, 2016). Myosin VI (encoded by the deafness gene *Myo6*), maintains the structural integrity of hair bundles during postnatal maturation and the absence of myosin VI results in impediment of the maturation of hair cells (Hertzano *et al.*, 2008; Pylypenko *et al.*, 2015; Marcotti *et al.*, 2016).

Following terminal mitosis, both IHCs and OHCs start displaying inward rectifier (I_{K1}) and the outward delayed rectifier (I_K) currents at their basolateral membrane (figure 1.7). These cells can show small, slow voltage responses when injected with current (Marcotti *et al.*, 2003).

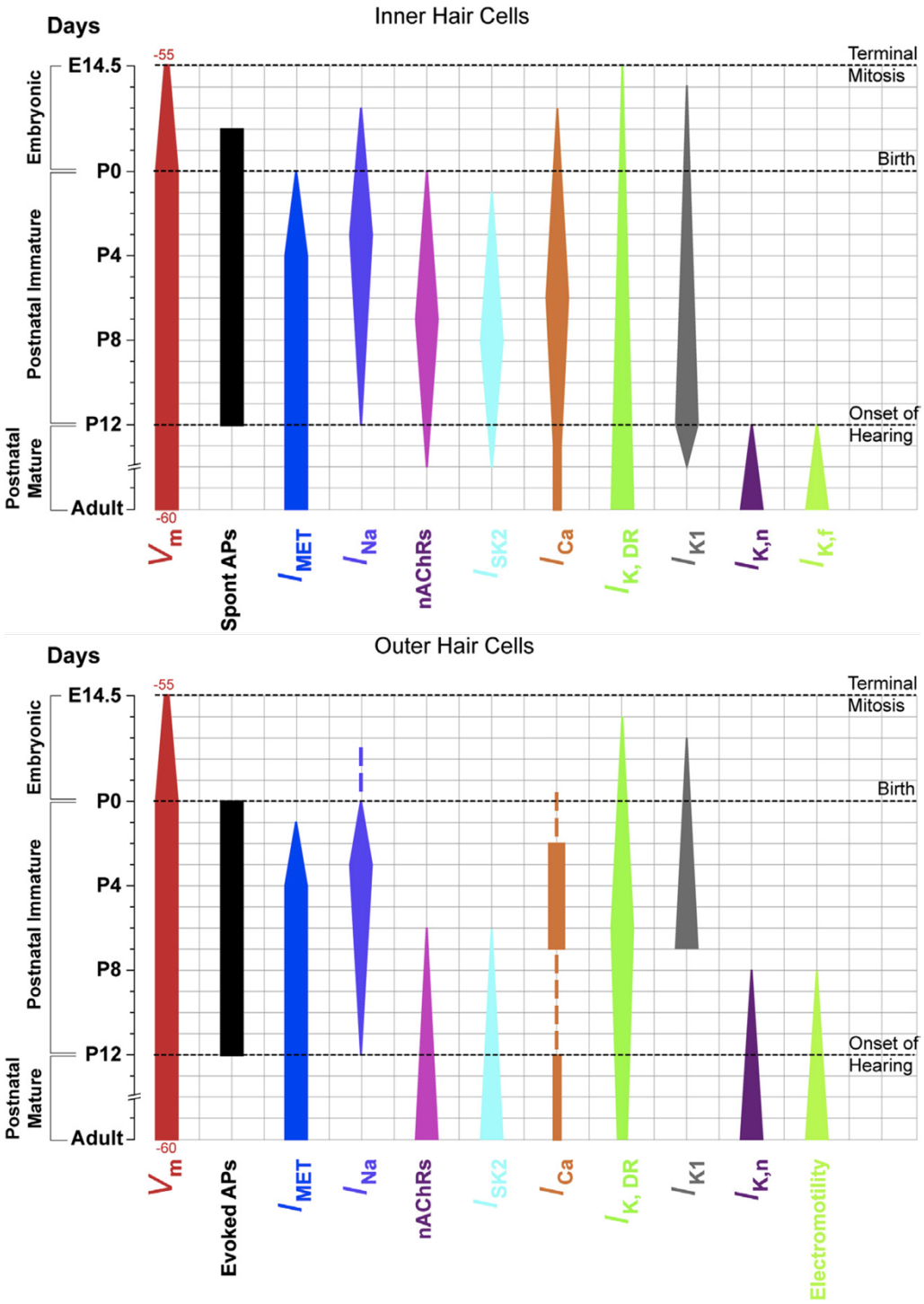

Figure 1.7 Developmental progression of biophysical properties in hair cells

Electrophysiological membrane properties of developing hair cells (mostly from mice): A) for IHCs and (B) for OHCs. Vertical columns indicate the prevalence of each current throughout development. The thickness of each column represents the scale of every individual current. Bands with dashes represent areas of uncertainty. Spont Aps:

spontaneous action potential, Vm: membrane potential. Figure adapted from Corns et al., (2014a).

Hair cells also express (I_{Ca}), carried by L-type $Ca_V1.3$ channels and (I_{Na}), carried by the voltage gated Na^+ channel (VGSCs) though to be carried by $Na_V1.1$ and $Na_V1.6$ (Eckrich *et al.*, 2012). Recent research has revealed that immature IHCs have nine VGSC subtypes ($Na_v1.1\alpha$-1.9α). For developing hair cells, $Na_v1.7\alpha$ was the most commonly expressed type and the primary contributor for generating Na^+ currents (Zhou *et al.*, 2020). During the late embryogenic stage, IHCs are also observed to show Ca^{2+}-driven exocytotic membrane capacitance changes following membrane depolarization, which are suggestive of exocytosis at the presynaptic plasma membrane.

Prior to the differentiation of nascent hair cells (~E12.5), both classes of afferents extend neurites along the embryonic cochlear epithelium, but they stop at the boundary of the spiral lamina until hair cells differentiate, after which they eventually initiate synapses (Kim *et al.*, 2001; Koundakjian *et al.*, 2007). Around birth, IHCs (by radial type I SGNs) and OHCs (by spiralling type II SGNs) are already observed to be differentially innervated for the most part. However, a lot of refinement still takes place postnatally. After birth, and until P3 (P0-P3) the OHCs undergo neurite refinement first, from both classes ('few temporary type I' and the predominant type II) of SGNs (Huang *et al.*, 2007).

Following P3 and up to P6, any excess terminals are pruned in order to generate mature synaptic innervation. Any temporary type I synapses are also heavily pruned and refined (Sobkowicz *et al.*, 1982; Pujol *et al.*, 1998; Huang *et al.*, 2007). In contrast, IHCs undergo synaptic development until P12. At birth, IHCs display initial functional innervation by type I SGN afferents in a greatly branched pattern. At this point, the type I SGNs may project to several IHCs, and even some OHCs. Over the course of the first postnatal week, the connections undergo significant refinement, leading to unbranched, axosomatic neurons that synapse with a single IHC (figure 1.8).

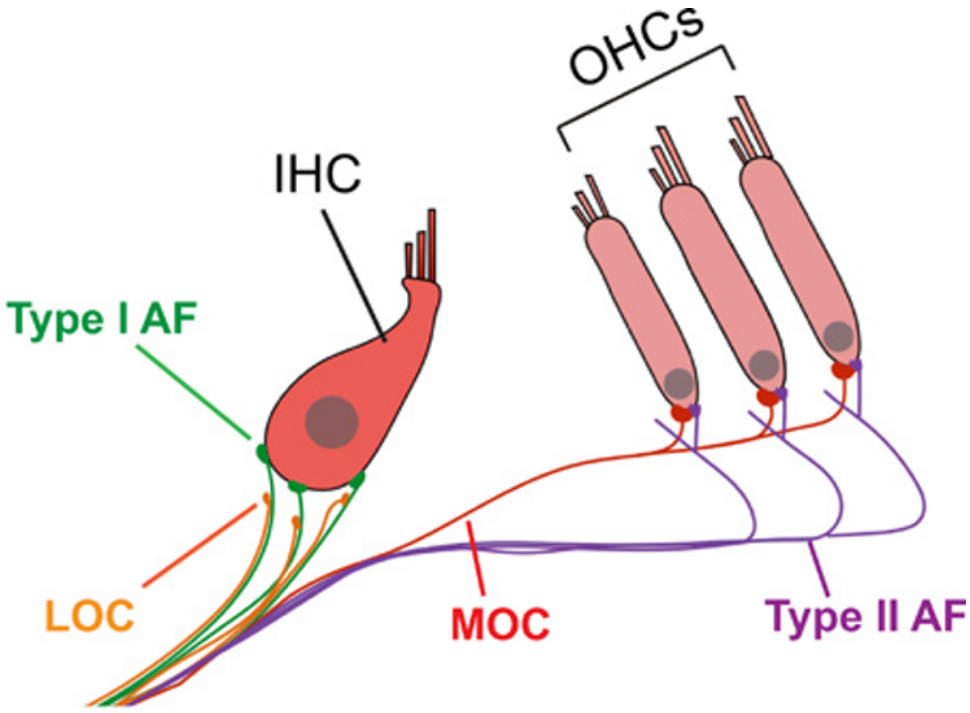

Figure 1.8 Innervation of mature IHCs and OHCs

Mature hair cells are innervated by different populations of afferent and efferent neurons. IHCs are innervated majorly (90-95%) by type I afferent SGNs (shown in green) while OHCs are innervated by type II afferent spiral SGNs (5%; shown in purple). OHCs are predominantly innervated with efferent neurons of the medial olivocochlear (MOC) neurons via axosomatic synapses (shown in red). Mature IHCs show efferent innervation with lateral olivocochlear (LOC) neurons via axodendritic synapses with type I SGNs (shown in orange). Figure adapted from Webber et al., (2021).

During this period, IHCs also drive EPSCs in the afferent fibres which is triggered by spontaneous activity in the immature IHCs (Kros et al., 1998; Glowatzki and Fuchs, 2002; Johnson *et al.*, 2012a). This signal travels to the CNS, to neurons in the auditory brainstem as rhythmic activity, presenting as burst of electrical activity (Kandler *et al.*, 2009; Tritsch *et al.*, 2010). Besides having afferent, glutamatergic synaptic boutons, developing IHCs also receive transient inputs from efferent-

cholinergic fibres of medial olivocochlear neurons (MOC; Warr and Guinan, 1979; Simmons *et al.*, 1996; Glowatzki and Fuchs, 2000; Guinan, 2006). Input from the MOC fibres activate the small-conductance potassium (SK2) channels in the IHCs.

Studies with current-clamp experiments in IHCs have demonstrated that the SK2 current is essential for the maintenance of the action potential train and additionally regulates their frequency when triggered by Ach (Marcotti *et al.*, 2004). These efferent inputs decline after the onset of hearing and are presumed to exert significant developmental influence. It is possible that the transitory cholinergic regulation of immature IHCs regulates the degree or temporal pattern of the prehearing activity (Johnson *et al.*, 2011a; Clause *et al.*, 2014). Mature IHCs are also innervated by efferents from LOC fibres, which form axodendritic synapses with the type I afferents below the IHCs (figure 1.8).

1.2 Ribbon synapses

1.2.1 Gross morphology and significance of the ribbon synapse

An important feature of the hair cells is a specialised presynaptic structure called ribbon synapse (figure 1.9 A-B). Similar to their function in primary transducers of stimuli in the visual system (photoreceptors), ribbon synapses in hair cells enable the transmission of graded information to afferent fibres, allowing for rapid, millisecond-scale discharges that may be sustained for an extensive duration (Nouvian *et al.*, 2006; Rutherford and Moser, 2016). Synaptic ribbons in the mammalian cochlea were first classified by Smith and Sjöstrand (1961).

Across the auditory system, a key feature of sound-evoked potentials is phase-locking. Hair cells are able to accurately process sinusoidal cycles for low-frequency sound waves with their membrane potentials (Crawford and Fettiplace, 1986). Similarly, auditory nerve fibres have a tendency to produce spikes at a certain period (phase) through each sinusoidal cycle. By comparing the waveforms arriving in each ear, it is possible to localise incoming sound stimuli for low frequency sounds (Palmer and Russell, 1986). However, phase-locking at higher frequencies is not viable. Consequently, hair cells induce sustained graded changes in the membrane potential in an effort to accurately represent sound intensity for localisation (Palmer and Russell, 1986; Khimich *et al.*, 2005). Sound is also localised through interaural time differences.

Ribbon synapses contain an electron-dense structure known as the synaptic ribbon (figure 1.9. B). The synaptic ribbon is ellipsoid, or raindrop in shape and is anchored to the presynaptic plasma membrane. A small percentage (<5%) of ribbons are not attached to the plasma membrane (“floating” ribbons) and are thought to reflect the normal turnover of ribbons in the cell (Khimich *et al.*, 2005). Synaptic ribbons tether glutamate-containing synaptic vesicles (SVs), ranging between 20-60 vesicles per ribbon (Sobkowicz *et al.*, 1982; Becker *et al.*, 2018; Jean *et al.*, 2018).

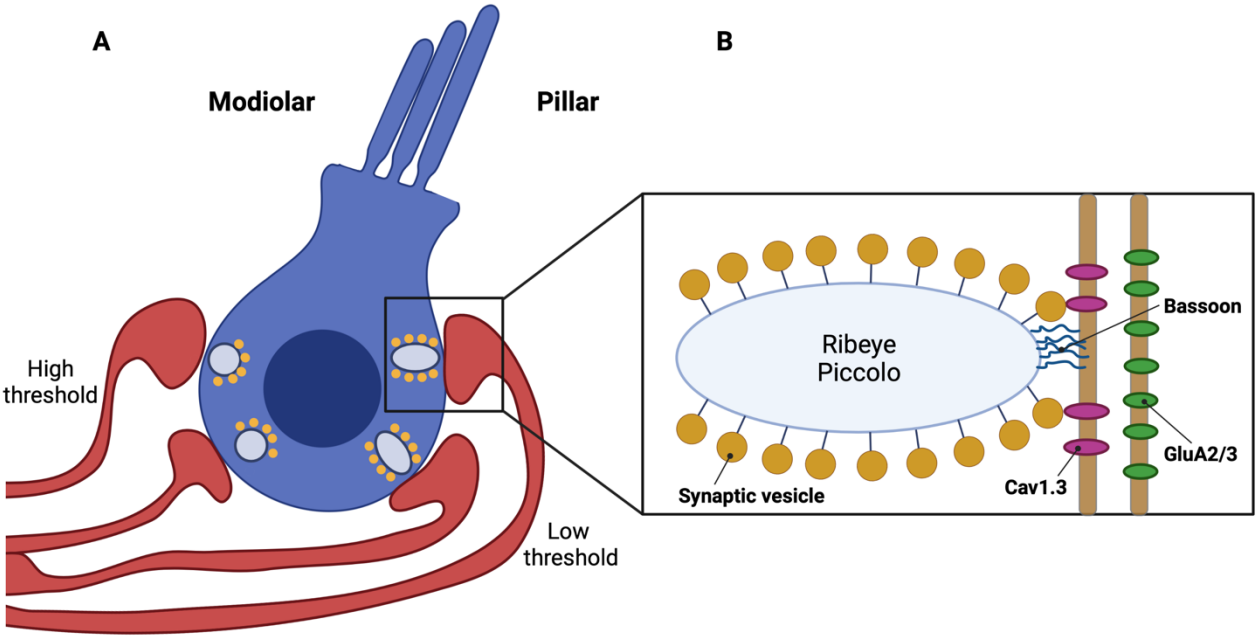

Figure 1.9 General structure of the ribbon synapse

The image shows the general structure of a ribbon synapse in the IHC: Inset: enlarged view of the molecular structure of the ribbon synapse, showing the synaptic ribbon and its anchoring point on the IHC basolateral membrane. A) Each IHC is innervated by multiple afferent neurons (in red) that synapse with a single synaptic ribbon (in blue). Each ribbon tethers multiple vesicles (in yellow) containing neurotransmitter (glutamate). Afferent fibres on the pillar side are low threshold and consequently possess high resting spontaneous discharge. In contrast, afferent fibres on the modiolar side are high threshold and possess low spontaneous firing. B) Enlarged view of a single ribbon synapse. The ribbon is associated with a single layer of synaptic vesicles. The electron-dense ribbon structure is comprised of the proteins ribeye and piccolo. The ribbon is tethered to the release site at the presynaptic membrane by bassoon (blue lines). Ca2+ inflow via the Cav1.3 channels (in purple) causes exocytosis of synaptic vesicles into the synaptic cleft, releasing glutamate. Glutamate then binds to the GluA2/3 receptors (in green), causing firing of the afferent fibre. Figure adapted from Fettiplace, (2017) and redrawn with BioRender.com under academic license.

A group of primed vesicles (around 5-20 vesicles) exist closest to the presynaptic membrane at the base of the ribbon (Meyer *et al.*, 2009; Wong *et al.*, 2014; Jean *et al.*, 2018). These vesicles are called the readily releasable pool (RRP). Synaptic ribbons are specifically located near presynaptic terminals to facilitate vesicle exocytosis and fast release of glutamate (Meyer *et al.,* 2009; Schmitz, 2009). This area is called the active zone (AZ; Pumplin *et al.*, 1981; Burns and Augustine, 1995; Matthews and Fuchs, 2010). The RRP is the most rapid and fast-depleted component of exocytosis and exhibits an exponential reduction with extended stimulation. It is therefore, widely understood to be involved in hair cell synaptic sound coding (Khimich *et al.*, 2005; Schnee *et al.*, 2005).

With increasing distance away from the ribbon, the number of primed vesicles reduces. This indicates that the structure plays a function in priming vesicles for rapid and sustained release (Frank et al. 2010, Chakrabarti et al. 2018). After releasing from the Golgi apparatus, new vesicles are transferred down the ribbon towards the AZ, where they are anchored to the membrane. Newly arrived vesicles are not exocytosis ready or fusion-competent (Jean *et al.*, 2018; Doser *et al.*, 2020). Most vesicles generally need 100-350 ms to initially approach the membrane, and a small subset then become release-ready after 200-500 ms (Doser *et al.*, 2020). Thus, the sustainable release is determined by the rate at which the ribbon can replace the vesicles at the AZ (Moser and Beutner, 2000). The ribbon therefore acts as a conveyer belt to resupply primed, fusion-competent vesicles to the presynaptic release site. The filamentous tethers that bind SVs facilitate a targeted flow of SV to the release site using a mechanism of rapid binding/unbinding of multiple tethers and proximal SVs (Graydon *et al.*, 2014). The molecular nature of these tethers is not completely revealed and continues to be a topic of research (Chakrabarti *et al.*, 2018).

In mature IHCs, each ribbon synapse is associated with a single, myelinated, unbranched, type I afferent fibre, with each fibre maintaining a unique firing threshold. The type I afferent synapses are primary encoders of acoustic signals (Slepecky, 1996; Pujol *et al.*, 1998; Glowatzki and Fuchs, 2002; Huang *et al.*, 2007). In contrast, OHCs contain very few ribbons, and make scarce, *en passant* synapses with unmyelinated, type II afferents (Burda and Branis, 1988; Slepecky, 1996; Pujol *et al.*, 1998). As part of a neuronal control loop inside the central auditory nuclei, type II SGN innervation

is expected to give sensory input from the OHC area. This consists of the inhibitory, efferent olivocochlear innervation of the OHC and the postsynaptic area of the type I SGN at the IHC (Jagger, 2003; Darrow *et al.*, 2006, 2007).

At the synapse associated with each AZ, the afferent terminals express AMPA receptors to detect glutamate release. In IHCs, AMPA receptors are composed of GluR2/3 and GluR4 subunits (Matsubara *et al.*, 1996; Bailey and Sewell, 2000; Glowatzki and Fuchs, 2002). Exocytosis at the presynaptic membrane is mainly controlled by the fast-activating, L-type voltage-dependent Ca^{2+} channels ($Ca_v1.3$), which are clustered around the AZ (Platzer *et al.*, 2000; Wong *et al.*, 2014). The AZ gives the $Ca_v1.3$ channels proximity to the primed vesicles on synaptic ribbons (around 30 nm distance; Neher, 1998).

Even a small influx of calcium through the channel can trigger exocytosis of a nearby vesicle (Kim *et al.*, 2013; Wong *et al.*, 2014). This is because synaptic ribbons (as well as their docked synaptic vesicles) act like a diffusion barrier, which allows the enrichment of Ca^{2+} ions within an area of few hundred square nanometres at the AZ (Graydon *et al.*, 2011). This area is, called the nanodomain, and is responsible for promoting fast and efficient neurotransmitter release. Large EPSC events arising from synchronised multivesicular release might be triggered by the nanodomain (Bucurenciu *et al.*, 2008; Graydon *et al.*, 2011).

It is anticipated that synaptic transmission driven by Ca^{2+} nanodomain regulation is noisier than transmission governed by Ca^{2+} microdomain control. Multiple channels contribute to the Ca^{2+} signal in the microdomain, and the gating of individual channels, to which Ca^{2+} nanodomain control is related, is of less importance (Bucurenciu *et al.*, 2008; Kim *et al.*, 2013; Moser *et al.*, 2020). Conversely, Ca^{2+} nanodomain control provides more linear receptor potential encoding. This serves to expand the dynamic range of synaptic coding. As soon as Ca^{2+} channels open, the nanodomain's high Ca^{2+} concentration quickly saturates the calcium sensor otoferlin, making the temporal accuracy of encoding less stimulus dependent. Consequently, Ca^{2+} nanodomain regulation contributes to lower stimulus-dependent release kinetics (Moser *et al.*, 2020).

Ca^{2+} nanodomains in the cochlea follow a tonotopic gradient. In low-frequency regions, the Ca^{2+} nanodomain is more dominant. However, in high-frequency (30 kHz) cells, exocytosis is dependent on microdomain coupling (Johnson, *et al.*, 2017b). The reason for this tonotopic divergence is still unclear. High-frequency basal cells are unable to phase lock, and therefore rely on small, graded membrane potential changes (Johnson *et al.*, 2008, 2009, 2017b).

The shape and size of synaptic ribbons also vary among the tonotopic axis (Sobkowicz *et al.*, 1982; Khimich *et al.*, 2005). In fact, there is also a considerable difference in ribbons within the same hair cells along various AZs (Merchan-Perez and Liberman, 1996). Ribbons at the apical cochlea are less elliptical in shape than at the basal end. As the frequency regions increase in the cochlea, the ribbons are observed to appear more ellipsoid. Additionally, the number of ribbons per hair cell and afferent innervation along the tonotopic gradient also varies considerably. Depending on their location on the tonotopic axis, IHCs can each have 5-20 afferent synapses. At the cochlear extremes (apex and base), there are fewer than 10 afferent synapses in general (Ehret, 1976). Higher synaptic density is linked to enhanced acoustic acuity at mid-cochlear frequencies (Ehret, 1976).

Within the IHC, the modiolar side contains larger ribbons and afferent synapses, with concurrently larger AZs and $Ca_V1.3$ clusters than the ones on the pillar edge (Meyer *et al.*, 2009; Liberman *et al.*, 2011). The pillar side contains relatively smaller ribbons, and larger postsynaptic glutamate receptor densities (Liberman, 1980; Fettiplace, 2017; Kalluri and Monges-Hernandez, 2017). Spontaneous firing rates in the afferent fibres are higher with a simultaneous low firing threshold towards the pillar side (Merchan-Perez and Liberman, 1996; Meyer *et al.*, 2009; Liberman *et al.*, 2011). This presumably plays a significant role in the ability of IHCs to express a broad dynamic range, since the modiolar fibres will peak at greater volumes and more effectively transmit intensity data to the CNS (Meyer *et al.*, 2009).

1.2.2 Molecular profile and architecture of the ribbon synapse

The composition of ribbon synapses varies considerably from conventional synapses. At the conventional synapse is the SNARE complex (comprising of syntaxin1, VAMP1, VAMP2, and SNAP25). The ribbon synapse mostly does not showcase these proteins (Nouvian *et al.*, 2011). However, SNARE protein mRNA has been observed in hair cells in several studies, suggesting the presence of some redundant constituents (Safieddine and Wenthold, 1999; Sendin *et al.*, 2007; Uthaiah and Hudspeth, 2010; Nouvian *et al.*, 2011). Mature IHC ribbon synapses also lack the conventional vesicle transmembrane proteins such as synaptotagmin 1 and synaptotagmin 2 (Syt1 and Syt2; Safieddine and Wenthold, 1999; Beurg *et al.*, 2010; Bacaj *et al.*, 2013). In conventional synapses in the CNS, synaptotagmins serve as Ca^{2+} sensors for rapid, synchronous neurotransmitter release (Bacaj *et al.*, 2013). Synaptotagmins bind to membrane phospholipids (through their C2-cytoplasmic domains) in a Ca^{2+} dependent fashion (Sutton *et al.*, 1995; Wang *et al.*, 2014). They interact with SNARE complex and complexin to trigger exocytosis (O'Malley *et al.*, 1995; Giraudo *et al.*, 2006; Bacaj *et al.*, 2013).

Syt1 and Syt2 are present in both IHCs and OHCs from P1 to P6. However, they show dissimilar subcellular localisation. At P8, Syt2 is no longer detectable in IHCs, while Syt1 is still present up to P10, but disappears at P15 (Beurg *et al.*, 2010). Since mature IHCs do not contain synaptotagmins (except synaptotagmin 4, Syt4; Johnson *et al.*, 2010), they employ a different Ca^{2+} sensor to initiate exocytosis. This function is performed by the large, Ca^{2+} binding protein, otoferlin (belonging to the ferlin family).

Otoferlin is encoded by the OTOF gene and contains two Fer domains and six C_2 domains (C_2A-F). Otoferlin acts as the primary Ca^{2+} detector for exocytosis at the ribbon presynapse (Safieddine and Wenthold, 1999; Roux *et al.*, 2006; Beurg *et al.*, 2010). Otoferlin knockouts in mice (*Otof* $^{-/-}$) resulted in near elimination of synaptic exocytosis, and consequently led to deafness in the mice (Roux *et al.*, 2006). However, the mice still had an intact mechanoelectric transduction progression (Roux *et*

al., 2006; Santarelli *et al.*, 2015). Additionally, since Syt4 is present in mature IHCs only, it is hypothesised to act as an otoferlin partner. Syt4 is postulated to determine the linearization of the synaptic transfer function (Johnson *et al.*, 2010).

Ribbons are predominantly constituted of the protein RIBEYE, which is exclusive to ribbon synapses. RIBEYE is an alternate splice of the C-terminal binding proteins, which also code for the transcriptional repressors: CtBP1 and CtBP2. RIBEYE consists of an amino-terminal A domain, specific to ribbons as well as a carboxyl-terminal B domain, derived from the identical gene as the 2-hydroxyacid dehydrogenase-associated transcriptional repressor protein CtBP2. The A domain facilitates the aggregation of RIBEYE into bigger structures, while the B domain binds NAD+ with remarkably high affinity, comparable to 2-hydroxyacid dehydrogenases (Schmitz *et al.*, 2000).

Thus, RIBEYE is able to polymerize the A and B domains, resulting in spherical, vesicle-accompanying structures, indicative of synaptic ribbons. NAD+ may also facilitate the formation of synaptic ribbons by promoting homotypic connections and hindering heterotypic connections between RIBEYE-RIBEYE domains (Schmitz *et al.*, 2000; Magupalli *et al.*, 2008). Supplemental proteins may be required to produce ribbons resembling mature ellipsoid structures from these spherical ribbon precursors (Magupalli *et al.*, 2008). Synaptic ribbons are known to be vertebrate-specific as no orthologs of RIBEYE have been observed in non-vertebrate genomes (Fröhlich, 1985; Prokop, 1999; Kawasaki *et al.*, 2004).

The ribbons also contain the cytomatrix proteins such as Piccolo, KIF3A and RIM1. Proteins used for AZ scaffolding (bassoon, munc13-1, ERC2 and RIM2) are used for tethering the synaptic ribbon to the cell membrane (Tom Dieck *et al.*, 2005). Knocking out Bassoon can perturb the attachment of the ribbon from the plasma membrane at the AZ (Dick *et al.*, 2003; Khimich *et al.*, 2005). Consequently, the removal of Bassoon results in the reduction of fast exocytosis, and sound encoding by synaptic afferents is inhibited (Khimich *et al.*, 2005; Buran *et al.*, 2010). In mouse IHCs, Bassoon mutants also show smaller Ca^{2+} currents. This leads to the conclusion that the loss of Bassoon decreases the RRP available at the AZ, due to the detachment of the ribbon (Khimich *et*

al., 2005; Frank *et al.*, 2010). Piccolo is the largest multidomain cytomatrix protein present at the AZ. Its general function is to facilitate the dynamic assembly of the F-actin cytoskeleton within the AZ. Multiple studies in mice show that the absence of Piccolo (i.e., the main isoform- Piccolino), causes severe effects in the retina, but not in the cochlear hair cells. Piccolo knockout mice showed significant defects, wherein the outer nuclear and plexiform layers of the retina were missing (Kim and Koo, 2015). The electroretinograms also showed drastically reduced amplitudes. However, no major abnormalities were observed in cochlear hair cells (Regus-Leidig *et al.*, 2014; Kim and Koo, 2015). It has been hypothesized that the loss of Piccolo disrupts the ultrastructure, development and maturation of ribbons in the photoreceptor (Regus-Leidig *et al.*, 2013, 2014; Kim and Koo, 2015).

1.2.3 Functional maturation of the presynaptic ribbon

In mice, hearing onset is at P12, prior to which, the ribbon synapse undergoes large, structural, and functional development (figure 1.10.). This is also coupled with SV recruitment and priming. Ribbons undergo extensive development, which in mice is continued post birth, and lasts until the onset of hearing. This development is linked closely to the development and functional maturation of the IHC as a whole. Changes occurring at the AZ are paralleled by corresponding changes at the postsynaptic terminal. One of the salient features of ribbon development is the formation and fusion of ribbon precursors.

As early as embryonic day 18 (E18), ribbon precursors are formed within the cytoplasm through the self-aggregation of RIBEYE. These free-floating ribbon precursors are spherical in shape, and already tether some immature, unprimed SVs. Each ribbon precursor tethers ~4-5 SVs, while mature ribbons generally tether 30-40 SVs (Michanski *et al.*, 2019). The ribbon precursors grow in size and are eventually transported to the presynaptic basolateral membrane using KIF1a (Michanski *et al.*, 2019). At the presynapse, the ribbon precursors are progressively anchored to the presynaptic membrane, likely using Bassoon (Khimich *et al.*, 2005).

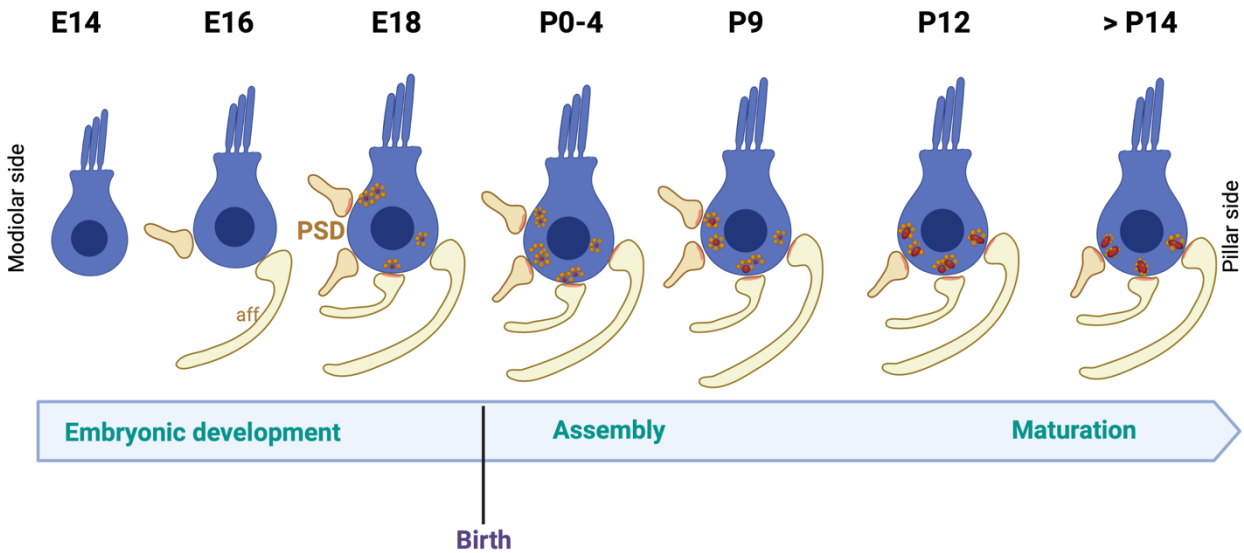

Figure 1.10 Developmental progression of synaptic ribbons in mice

Visual representation of the development of ribbons and maturation of their afferent synapses. Nascent IHCs are visible around E14 and are contacted by synaptic projections from E16 onwards. At E18, ribbon precursors are already visible (in red), tethered to synaptic vesicles (yellow). Some nascent ribbons can be seen to form early synapses with afferent neurons. After birth, ribbon sizes gradually increase, along with ribbon density (P0-P9). Vesicle number per ribbon also increases simultaneously. After the first postnatal week, fusion events of ribbon precursors increase, with the highest rate of fusion events at P12, signalling the onset of hearing in mice. By P14, IHCs have around 5-20 ribbons, each connecting with a single afferent fibre. Some multiribbon synapses can be observed at the modiolar side, which persist during maturity. aff: type I afferent fibre (yellow); PSD: postsynaptic density (orange shading); Figure adapted from Michanski et al., (2019) and redrawn with BioRender.com under academic license.

As more precursor ribbons make their way towards the presynapse, they follow one of three routes; i.e., a) fuse with other spherical, free-floating ribbons, b) fuse with already anchored ribbons, or c) anchor themselves to the presynaptic plasma membrane (Sobkowicz *et al.*, 1982, 1986; Michanski *et al.*, 2019). The largest fusion events are detected to take place around P12, however it is observed to sometimes carry on as far as P14 (Michanski *et al.*, 2019).

Once anchored, the ribbons expand in size and volume until the onset of hearing, after which the size and volume of the ribbon remains stable (Michanski *et al.*, 2019). As the ribbon precursors aggregate, the SV pool of the resultant larger ribbon also increases. SVs mature in parallel to the ribbon, with a comparable time course and shrink in vesicle diameter. This ultimately enables an even greater packing density of the SVs on mature ribbons (Michanski *et al.*, 2019).

At E18, the dense core vesicles (DCV) also appear, which are theorised to help initial synapse assembly (Sobkowicz *et al.*, 1986; Michanski *et al.*, 2019). This indicates that DCVs function to either

transport other components to the presynapse (such as Bassoon and Piccolo; Zhai *et al.*, 2001; Shapira *et al.*, 2003), or storage and release of neurotrophic factors in order to stimulate and maintain connection with the SGNs (Michael *et al.*, 1997; Wu *et al.*, 2004; Kersigo and Fritzsch, 2015; Michanski *et al.*, 2019).

During the first postnatal week, the ribbon number within the IHC increases to up to 30-35. After the first week, the ribbon count decreases progressively, as ribbon-ribbon fusion continues. By the end of the second postnatal week, this number reduces to 5-20 mature ribbons, with one ribbon at each AZ, linked to a single afferent connection. An exception to this is the multi-ribbon synapses predominantly found on the modiolar side of the IHC, thereby indicating a localisation dependence on afferent contact sites (Michanski *et al.*, 2019).

1.2.4 Tuning of Ca^{2+}-dependent exocytosis

The tuning of Ca^{2+}-dependent exocytosis is a defining characteristic of postnatal development of the AZ and a key component to determine the temporal fidelity of the synapse. $Ca_v1.3$ channels situated extrasynaptically are cleared and become tightly localized to patches that correlate with glutamate receptors on the postsynaptic afferent terminal (Frank *et al.*, 2010; Pangšrič *et al.*, 2010; Wong *et al.*, 2014). Additionally, the functional maturation of $Ca_v1.3$ channel properties shows a concurrent increase in the efficacy of excitation/secretion coupling (Johnson *et al.*, 2005, 2009, 2010, 2012; Sendin *et al.*, 2007; Meyer *et al.*, 2009; Pangšrič *et al.*, 2010; Wong *et al.*, 2014).

This is also the period when the microdomain based coupling model between $Ca_v1.3$ channels and primed vesicles transitions to the nanodomain based model (Wong *et al.*, 2014). This close proximity enables a single $Ca_v1.3$ channel to coordinate the release of a specific SV, hence assuring signal transmission with superior accuracy. Otoferlin is visible in immunostains at early development (E16; figure 1.11.) but achieves is highest expression around P6 (Wong *et al.*, 2014). This is shortly before the peak of Cav1.3. expression and consequent calcium current amplitude in the cell. This observation appears to be consistent with the reported switch of the Ca^{2+} sensor during development (Roux *et al.*, 2006; Johnson *et al.*, 2009; Wong *et al.*, 2014). After the increased expression during the first postnatal week, Otoferlin replaces synaptotagmins as the primary Ca^{2+} sensor (Beurg *et al.*, 2010; Michalski *et al.*, 2017; Michanski *et al.*, 2019). Thus, the Ca^{2+} evoked exocytosis mechanism modifies from otoferlin independent to otoferlin dependant at P4 (Beurg *et al.*, 2010). This helps in the development of the high throughput release machinery and is required for vesicle fusion at the presynaptic AZ.

This ensues throughout a critical period for determining presynaptic morphology, decreasing ribbon count and increase volume and size, while also establishing monosynaptic connectivity between IHCs and type I afferents (Sobkowicz *et al.*, 1982; Merchan-Perez and Liberman, 1996; Huang *et al.*, 2012; Wong *et al.*, 2014; Michanski *et al.*, 2019).

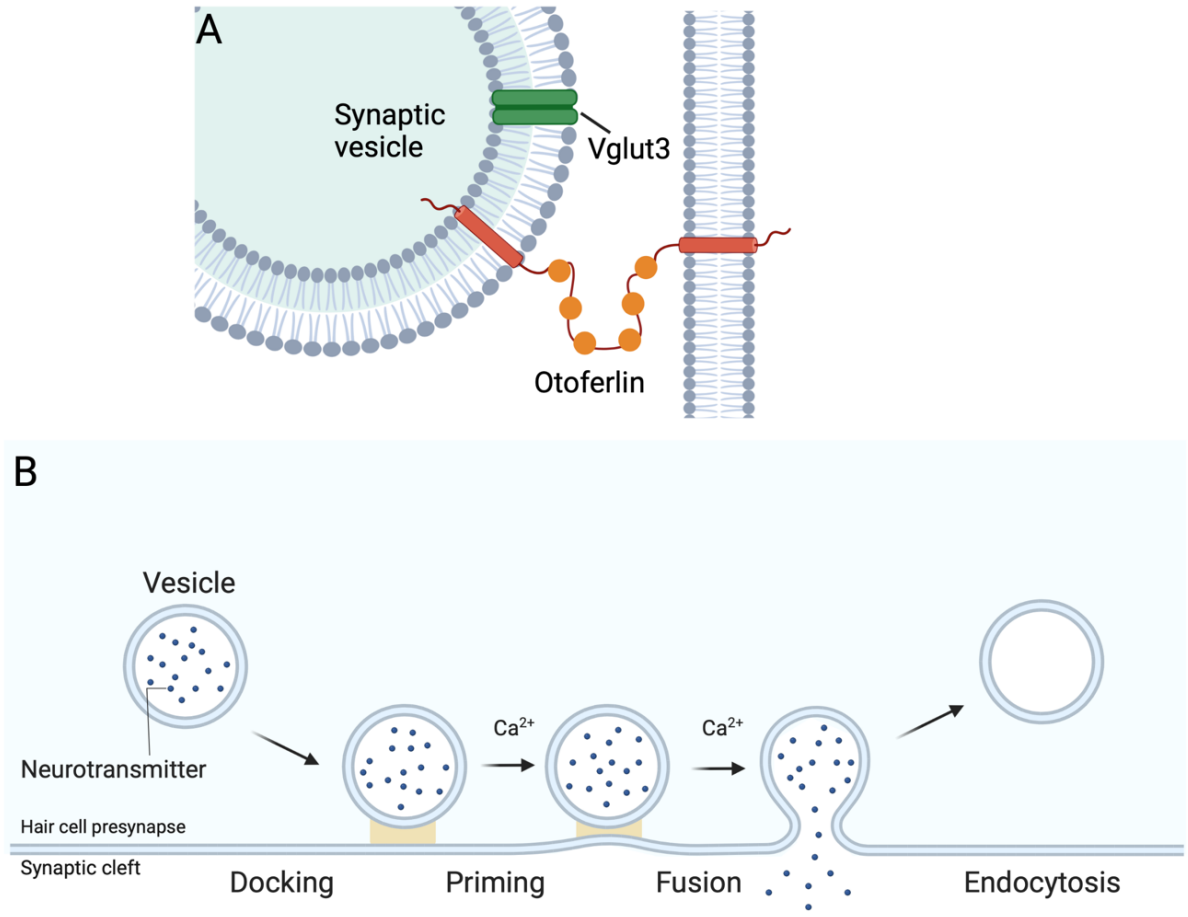

Figure 1.11 General schematic of Ca2+ dependent exocytosis at the ribbon synapse

A) Enlarged view of synaptic vesicle showing the 6 C2-domain protein otoferlin which acts as the primary Ca2+ sensor at the IHC AZ. The glutamate transporter Vglut3 is also visible on the vesicle membrane (green), which is responsible for the active re-uptake of glutamate into the vesicle post exocytosis. B) General process of vesicle fusion and glutamate release during exocytosis. The vesicle containing glutamate (dark blue) is docked and primed for release through the interaction of SNARE proteins (yellow). Vesicle fusion is triggered in a Ca2+ dependent manner. Figure adapted from Fettiplace, (2017) and redrawn with BioRender.com under academic license.

1.3 Spontaneous action potentials in hair cells

1.3.1 Generation of spontaneous action potentials in hair cells

OHCs mature at around P8, the same age when they start displaying electromotility (Marcotti *et al.*, 1999), and IHCs mature at around P12, which coincides with hearing onset in mice (Kros *et al.*, 1998). Preceding hearing onset, the IHC and OHC have very different membrane properties than mature hair cells. During their prehearing period (<P12), immature IHCs generate experience-independent action potentials, called spontaneous action potentials. This activity is Ca^{2+}-dependent, and consequently results in the release of glutamate from ribbon synapses. Spontaneous electrical activity is a common feature in many other developing sensory systems. It is implicated in the development and tuning of neural circuits as it can help to refine and mature synaptic connections (Wang *et al.*, 2015). Spontaneous activity is suggested to similarly play a role in the development of the auditory circuitry and refinement of tonotopic maps (Kros *et al.*, 1998; Moody and Bosma, 2005; Blankenship and Feller, 2010; Johnson *et al.*, 2012; Kirkby *et al.*, 2013). It is suggested that these transient Ca^{2+} action potentials in the IHCs could potentially regulate a number of functions such as gene expression, synaptic maturation and development (Glueckert *et al.*, 2003; McKay and Oleskevich, 2007; Seal *et al.*, 2008).

In mice, spontaneous activity takes place for almost two weeks postnatally, until the onset of hearing. It occurs differently along the length of the mouse cochlea. IHCs at the apical region fire at lower frequencies and in a more irregular, bursting-like pattern than those IHCs at the basal region of the cochlea (Johnson et al., 2011b). The basal region shows a more regular pattern with higher mean frequency (Johnson *et al.*, 2011b).

Spontaneous activity triggers brief periods of electrical activity in the immature type I SGNs (figure 1.12.), which pass through the auditory nuclei in the CNS. Neurons of the auditory pathway present in imminent isofrequency zones sustain associated firing without stimulation of hair cells (Babola *et al.*, 2018). As the activity travels up into the inferior colliculus, populations of neurons linked to the

prospective tonotopic axis display brief bursts of highly coordinated activity. The electrical activity travels sequentially through the dedicated auditory centres of the brainstem, midbrain and finally reaches the auditory cortex. This implies that neurons that will subsequently process similar auditory frequencies are aligned across the auditory pathway throughout this maturational period (Babola *et al.*, 2018). As the spontaneous activity ceases at P12 (hearing onset), the SGN firing pattern also matures to non-bursting, continuous spiking regulated by glutamate release at the IHC synapse.

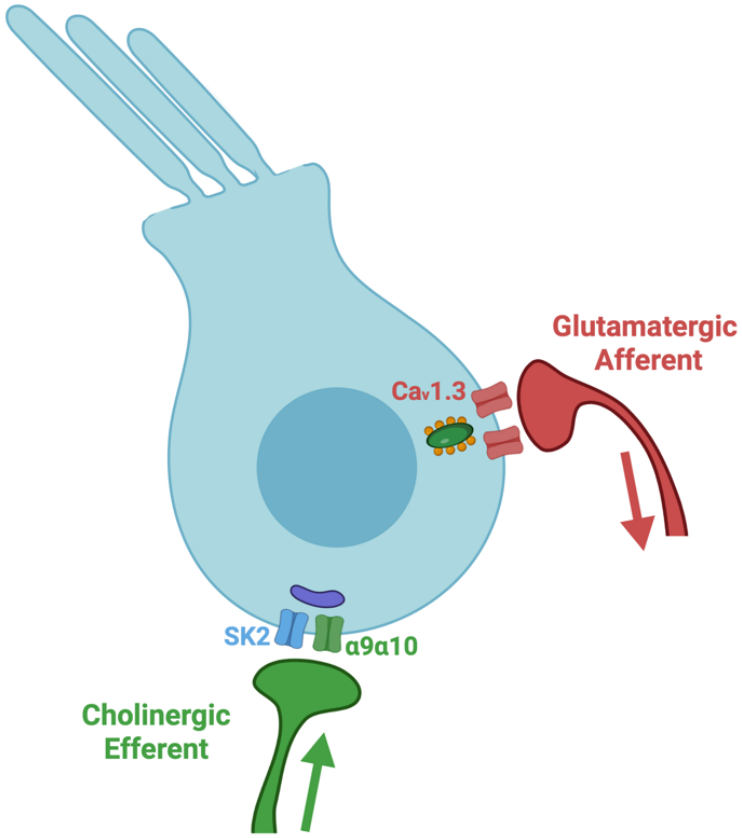

Figure 1.12. Diagrammatic representation of afferent and efferent synapses in immature IHCs during spontaneous activity

During prehearing stages, IHCs make contacts with afferent glutamatergic (red) as well as efferent cholinergic (green) neurons. The firing of Ca2+ based spontaneous activity triggers electrical activity in the afferent neurons, which propagate to the CNS. Cholinergic efferents also act upon the IHC by triggering the influx of Ca2+ by nAChRs (green) and the consequent activity of SK2 channels (blue). Figure adapted from Moglie et al., (2018) and redrawn with BioRender.com under academic license.

An important factor for determining the level of spiking activity in IHCs is the resting membrane potential (V_m). V_m is determined mostly by the interplay between the inward, depolarising, resting mechanotransducer current and the voltage-dependent, outward K^+ current (Johnson *et al.*, 2011b; 2012). Spontaneous activity is shaped by several basolateral ion channels, including the transiently expressed SK2 channels (Johnson *et al.*, 2007). The SK2 channels are activated in response to the opening of Ca^{2+} channels triggered by either membrane depolarisation or the flow of Ca^{2+} through the opening of alpha9-alpha10 AChRs, which are activated by the release of acetylcholine (ACh) from the MOC fibres. This indicates a feedback loop for spontaneous firing regulated from the CNS.

As mentioned previously, spontaneous activity is also controlled by a cholinergic input to the IHC (figure 1.12.). The regions where these fibres synapse with the immature IHCs are intercepted by nicotinic acetylcholine receptors (nAChRs). The nAChRs are composed of two specialised Ca^{2+}-permeable protein subunits; α9 and α10 (Elgoyhen *et al.*, 1994, 2001; Vetter *et al.*, 1999). This produces an inhibitory effect on spontaneous activity. Upon the release of acetylcholine (ACh) by the efferent neurons, the nAChRs allow the influx of Ca^{2+} (Fig 1.4).

Ca^{2+} flow through the nAChRs activates the nearby Ca^{2+}-dependent, small conductance K^+ channels (SK2), producing a hyperpolarisation of the IHC membrane potential (Glowatzki and Fuchs, 2000). This is suggested to effect IHC excitability and modulate the firing pattern of action potential activity (Liberman, 1980; Clause *et al.*, 2014).The efferent fibres thus play an inhibitory role over spontaneous activity through the influence of Ca^{2+} ions.

Mature IHCs exhibit a calcium and voltage-activated current ($I_{K,f}$) that is carried by the potassium channel (BK channel; Kros *et al.*, 1998). Since the modulation of both the efferent and afferent activities are under the influence of intracellular $Ca^{2+}$the IHCs ensure local compartmentalisation of Ca^{2+} ions, thus inhibiting synaptic cross talk. Using subsynaptic cisterns apposed to efferent neurons, the IHC employ a buffering system that prevents the spillover of Ca^{2+} from efferent to afferent synaptic zones. This Ca^{2+} buffering preserves the individual influence of efferent and afferent inputs

into the IHC, and the balance between these inputs aids in the biophysical maturation of IHCs (Moglie *et al.*, 2018).

It was earlier assumed that spontaneous action potential activity in mice was restricted to the first postnatal week (Johnson *et al.*, 2012). However, studies from the past decade have revealed that spontaneous activity is likely to exist in postnatal IHCs until the onset of hearing (Johnson *et al.*, 2011a, 2012). Furthermore, it is postulated that a 'critical period' exists during which Ca^{2+} spiking activity influences IHC maturation (Johnson *et al.*, 2013). This was found to be confined to the second postnatal week. The upper limit of this period is P12 as that is the point of cessation of IHC spiking and consequent onset of hearing (Johnson *et al.*, 2013).

1.3.2 Spontaneous activity in the second postnatal week

What influences the generation of spontaneous action potentials during the second postnatal week has been a matter of debate. Earlier studies theorised that spontaneous activity was intrinsically produced by IHCs only during the first postnatal week, and that the activity observed in the second postnatal week was extrinsically evoked by the extracellular release of ATP by the non-sensory cells from the greater epithelial ridge (GER; Tritsch *et al.*, 2007; Tritsch and Bergles, 2010). The Kölliker's organ arises from the greater epithelial ridge (Lim and Anniko, 1985). It was suggested that Kölliker's organ produced ATP that led to Ca^{2+} transients and caused spontaneous spiking activity in IHCs (Tritsch *et al.*, 2007, 2010). This was further supported by the Kölliker's organ's temporary nature; since it is only present during the critical period of prehearing spiking activity, and subsequently transitions into the inner sulcus of the organ of Corti (Hinojosa, 1977; Lim and Anniko, 1985).

However, separate studies revealed that IHCs produced Ca^{2+} transients intrinsically during the entire postnatal prehearing period, up to the onset of hearing at P12 (Johnson *et al.*, 2012). It was agreed, however, that indeed, the modulation and spontaneous activity is extracellularly influenced by ATP-dependent Ca^{2+} waves made by the cells of the GER (Johnson *et al.*, 2012, 2017a).

OHCs have also shown to fire spontaneous Ca^{2+} spikes in a limited interval during early development (Ceriani *et al.*, 2019). The spiking arose simultaneously in OHCs as well as non-sensory supporting cells of the GER. Ca^{2+} waves from the GER synchronise firing in OHCs through ATP-dependent activation of P2X receptors. Similar to the effect of spiking on IHCs, the spiking activity in OHCs was observed to influence the refining of afferent innervation during development (Ceriani *et al.*, 2019).

As mentioned earlier, spontaneous activity in IHCs is suggested to influence a variety of phenomena, such as gene expression, development of tonotopic maps, synaptic maturation and refinement. If spontaneous activity has a role in cochlear development, then changes in the frequency or pattern

of this spontaneous activity could potentially drive various developmental signals within the developing cochlea. This instructive role for spontaneous activity could occur during the critical period of spontaneous activity (Johnson *et al.*, 2013), similar to that found in the visual system. This could effectively mean that generation of IHCs in culture conditions could be a possibility if one could address the factors influencing IHC development and maturation. Indeed, if their maturation could be controlled *ex vivo* by providing exogenous electrical signals (such as through optogenetic techniques), this could open new avenues for regenerative research for individuals with malfunctional/ damaged hair cells.

1.4 Challenges with culturing the mammalian cochlea, and factors utilised for culture

Culturing the mammalian cochlea has frequently presented challenges in auditory biology. In the context of primary cultures, hair cells are notoriously difficult to maintain (Ogier *et al.*, 2019). Hair cells are few in number in the mammalian cochlea (only one row of around 3500 IHCs and 3 rows of around 12000 OHCs in the humans). They are relatively inaccessible (apart from invasive dissection) and do not proliferate well in *ex vivo environments* (Zhang *et al.*, 2019).

Additionally, the anatomy of the organ of Corti is such that distinct conditions such as the fine separation of the endocochlear fluids cannot yet be reproduced in culture, wherein the hair cell stereocilia are accurately bathed in endolymph and the hair cell bodies are simultaneously bathed in perilymph (Raphael, 2002; Kim *et al.*, 2011). The organ of Corti itself is spiral shaped, which in terms of topography is difficult to maintain in culture in three dimensions. This leads to many culturing protocols to divide the cochlea into separate turns. Most of all, there is no current literature suggesting a reliable technique for maturing hair cells from *ex vivo* conditions, thus limiting the types of functional cells obtained from these methods (Ogier *et al.*, 2019; Zhang *et al.*, 2019). Some studies aim to redirect non-sensory supporting cells (SCs) of the organ of Corti towards sensory cell fates. For example, the transcription factor *Atoh1* was demonstrated to enable hair cell differentiation and regeneration *in vivo* in guinea pigs (Atkinson *et al.*, 2014). However, these cells were found to be in an immature state and did not functionally mature.

Despite these setbacks, culturing hair cells has seen a number of developments in the past few years. A deeper understanding of hair cell culturing would open new avenues to drug development, developmental and regenerative studies (Zhang *et al.*, 2019). Many genes and proteins implicated in cochlear development have been studied closely when culturing IHCs. It is therefore important to note their significance in cultures that aid in prolonging the health of hair cells or their synaptic partners.

1.4.1 Activity of neurotrophins on cultured hair cells

Some growth factors are now employed extensively in neuronal cultures and may also be effective for the successful maintenance and development of long-term cochlear cultures. The neurotrophin family of proteins is exceptionally significant for this purpose. Neurotrophins promote neuronal cell survival and development. It is established that members of this family, including brain-derived neurotrophic factor (BDNF) and neurotrophin-3 (NT3), influence the development of synaptic innervation between IHCs and SGNs (Wan *et al.*, 2014). BDNF and NT3 are essential for the early postnatal development and maintenance of ribbon synapses in the vestibular and cochlear epithelia, respectively NT3 also plays a role in regulating SV density (Wan *et al.*, 2014). BDNF and NT-3 have also demonstrated to improve neuronal survival in monolayer cell cultures (Schwieger *et al.*, 2015). The combination of BDNF and ciliary neurotrophic factor (CNTF) increased SGN survival and neurite outgrowth *in vitro* (Sun and Salvi, 2009; Green *et al.*, 2012; Schwieger *et al.*, 2015; Szobota *et al.*, 2019).

In organotypic cochlear cultures of neonatal deaf mice (Bronx waltzer mice; bv), BDNF and NT-3 alone or in combination enhanced synaptogenesis and IHC survival (by around 10% for cochleae cultivated at ages P0-P3). Eight days in vitro (8DIV) however, the IHCs from these cultures lost their innervation (Sobkowicz *et al.*, 2002). Interestingly, the neurotrophic factor nerve growth factor (NGF) induced more stable innervation of IHCs but also showed similar denervation by 8 days post-culturing (Sobkowicz *et al.*, 2002). Staecker et al. (1996), cultured mouse inner ears (otocyst and cochleovestibular ganglion tissue; CVG) at embryonic day 10.5 (El0.5 stage). NT-3, BDNF, and NGF antisense oligonucleotides were used to treat cultured cells. Then, they were compared to cultures that were sense-treated and to control cultures. It was observed that antisense-treated cells exhibited substantial neuronal cell death, suppression of neuritogenesis, and a reduction in CVG neuron population. Thus, it was proposed that the aforementioned three neurotrophins govern CVG development in vitro (Staecker *et al.*, 1996). This demonstrated their significance in auditory development as well as in cochlear culture techniques.

1.4.2 Activity of thyroid hormone on cultured hair cells

Some hormones have already been known to play a role in IHC development *in vitro*. Hormones such as oestrogen, progesterone, and aldosterone play crucial roles in maintaining auditory function via the maintenance of cochlear neurons, the up/down regulation of key molecular pathways (e.g., IGF-1, BDNF, etc.), and the creation of the endocochlear potential (Coleman *et al.*, 1994; Caruso *et al.*, 2003).

One such hormone is the thyroid hormone (TH). Thyroid hormone is commonly known as triiodothyronine (T3). It influences nearly every physiological system of the body, including that of development and growth, metabolism, core temperature, pulse rate and stem cell proliferation (Contreras-Jurado *et al.*, 2015). Thyroid-stimulating hormone (TSH), that is secreted by the anterior pituitary gland, stimulates the production of triiodothyronine (T3) and its prohormone thyroxine (T4). The two main thyroid-binding nuclear receptor isoforms are TRα1 and TRβ (Contreras-Jurado *et al.*, 2011; García-Serrano *et al.*, 2011). The activity of T3 on target tissues is about fourfold more effective than T4.

The role of TH in hair cell development has been studied comprehensively. IHC pruning and regulation of long-term homeostatic afferent synaptic connection are dependent on TH (Ng *et al.*, 2013; Sundaresan *et al.*, 2016a). It is well established that TH drives ribbon synapse formation, regulates afferent synaptogenesis, and influences hair cell fibroblast growth factor (FGF) receptor expression (Szarama *et al.*, 2013). Additionally, the Kcnq4 gene, which encodes for the voltage-gated K^+ channel $K_v7.4$, is a target for TH in OHCs. In IHCs, TH is also involved in the pruning, function, and long-term preservation of afferent synapses.

Hypothyroidism during the critical period in postnatal mice was observed to cause defects in synaptic pruning and homeostatic maintenance of synapses and resulted in reduced exocytosis efficiency (Rüsch *et al.*, 2001; Sendin *et al.*, 2007; Sundaresan *et al.*, 2016a). Additionally, hypothyroidism not

only disrupted hair cell development but also led to progressive hair cell degeneration and loss of endocochlear potential (Brandt *et al.*, 2007; Szarama *et al.*, 2013; Sharlin *et al.*, 2018). Hypothyroid rat IHCs were discovered to not produce otoferlin mRNA or protein while exhibiting strong capacitance shifts (Yasunaga *et al.*, 1999, 2000). Indeed, this points to the important role of TH in regulating hair cell- and afferent development within the cochlea.

TH and TSH have the ability to influence the metabolic functions of growth hormone and IGF-1 on target organs. Insulin-like growth factor 1 (IGF-1) is a hormonal peptide that is a member of the insulin protein family. The majority of biological functions of IGF-1 are mediated by its high-affinity tyrosine kinase receptors, i.e., IGF-1 receptor IGF1R; and insulin receptor IR (Menting *et al.*, 2013). The IGF system comprises of various receptors, factors, and IGF-binding proteins, and it serves numerous functions in mammalian development, tissue formation, and senescence. IGF-1, in conjunction with Myc (cell-cycle activator) and Notch1 (inner ear progenitor), facilitate the transdifferentiation of adult cochlear supporting cells into hair cell-like fates *in vivo* (Boucher *et al.*, 2010; Yamahara *et al.*, 2019; Gao *et al.*, 2020). Again, this could be further explored *in vitro.* It was also observed that IGF-1 could preserve already established synapses with IHCs. This could prove beneficial for prolonging the life of primary organotypic cultures (Wan *et al.*, 2014; Liberman, 2017; Szobota *et al.*, 2019).

1.5 Aims of the project

The hypothesis for this project is that functional maturity of IHCs can be achieved in *ex vivo* culturing conditions by the application of exogenous electrical activity that mimics Ca^{2+}-dependent spontaneous activity in the developing cochlea.

It was initially observed that immature IHCs, when cultured, lost their spiking activity within 48 hours of culturing and did not mature (unpublished). We therefore utilise an optogenetic mechanism to drive this activity exogenously.

The overall aim of the project, therefore, is to drive IHC maturation in primary cochlear cultures, using optogenetics. The work also aims to determine the extent to which the spontaneous activity regulates the development and maturation synaptic ribbons and its corresponding afferent innervation. Additionally, I intend to check the effect of optogenetic stimulation on the expression of large conductance calcium-activated potassium (BK) channels.

Standardized protocols have already been developed in the lab to culture the mouse cochlea. Postnatal mice at P7 were used for generating cultures. These were ChR2-floxed mice with rapid activation of the channel ChR2 (acquired from Jackson Labs), Expression was driven in the IHCs with a mouse cre-line (otoferlin-cre recombinase). IHC stimulation using the optogenetics setup has been established in the lab by Dr. Federico Ceriani (unpublished).

Therefore, my precise aims are as follows:

1. Investigate the functional maturation of IHCs by means of ribbon synapse maturation using super resolution imaging.
2. To check for the development of IHC innervation in primary cochlear cultures.
3. Investigate the expression of BK channels on cultured IHCs using super-resolution imaging.

It needs to be first determined whether spontaneous activity alone is sufficient to drive IHC maturation. The precise factors driving IHC maturation in the cochlea are still unknown. Therefore, the experimental plan involved a stepwise application of assorted electrical and molecular signals to find the appropriate scope of exogenous signals required to achieve this objective.

The cultures were grown initially for at least 10 days and subsequently checked for functional maturity through imaging. If electrical activity alone is insufficient, the cultures may also be supplied with growth factors to aid with development (as growth factor deficiency is seen to constrain cochlear development; Brandt *et al.,* 2007).

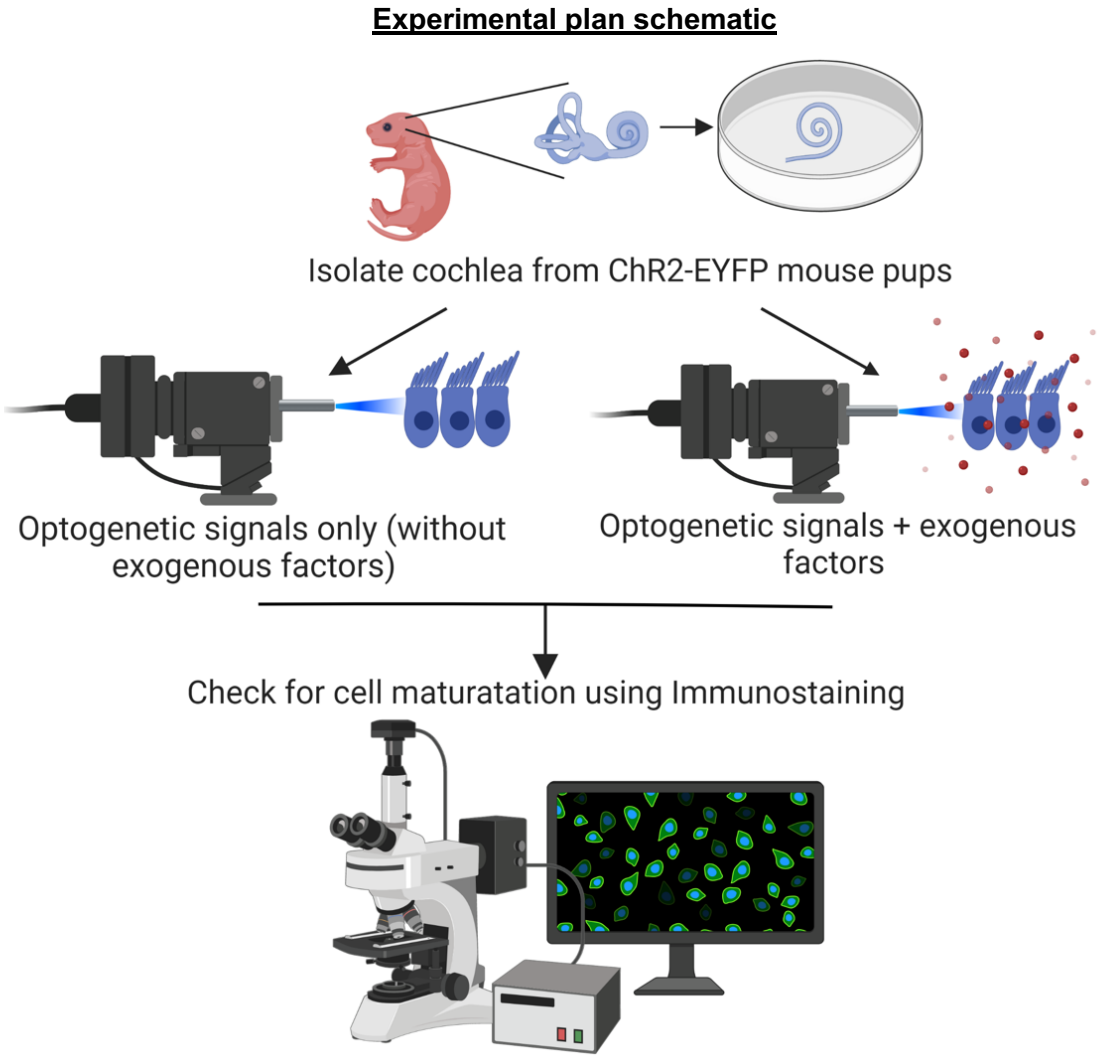

Figure 1.13 Diagrammatic representation of the experimental plan

Figure created with BioRender.com under academic license.

2. General Methods

2.1 Ethics statement

All animal research for this study was conducted in the United Kingdom in compliance with Animals (Scientific Procedures) Act of 1986 permits issued by the Home Office and authorised by the University of Sheffield Ethical Review Committee. For all in vitro research, mice were sacrificed using cervical dislocation, and immediately decapitated.

2.2 Animals

*Otof:*ChR2-EYFP mice were utilized throughout this project. In accordance with Home Office regulations, these mice were housed at the University of Sheffield on a 12-hour light-dark cycle. We used neonatal pups between ages of P3 and P20, where P0 is the day of birth. Postnatal mice at P7 or P10 were used for generating cultures. These were floxed-ChR2 mice with quick activation (obtained from Jackson Laboratories). The expression in the IHCs was driven by a mouse cre-line (otoferlin-cre recombinase).

2.3 Organotypic culture of cochleae

All cultures for this project were generated from the apical coil of the organ of Corti.

2.3.1 Culture protocol

All procedures were carried out in the laminar air flow hood. All surfaces were disinfected with 80% ethanol preceding the culturing procedure. All equipment and instruments used for cultures were sterilized at 200℃ for 4 hours (where applicable) or used new (in sterile condition, such as 6-well tissue culture plates). All other equipment used was sterilised thoroughly with 80% ethanol (such as

the surfaces of the dissecting microscope and pipettes). The microscope used for cochlea dissection was Leica MZ stereo microscope with a transmitted light base.

Coverslip preparation:

Prior to dissection, the coverslips used for culturing the organ of Corti were prepared. In a large glass petri dish (PET1014, SLS), round coverslips (18mm diameter, 71861-030; Deckgläser) were placed on an upturned Maximov slide using offset flat forceps and covered with a drop of rat tail collagen (354236, BD Biosciences) using a curved Pasteur pipette (FB50253, Fisher). The collagen was spread on the surface of the coverslip using a looped Pasteur pipette (both curved and looped pipettes were fashioned from straight glass Pasteur pipettes using a gas Bunsen burner). The coverslips were subsequently treated with ammonia for 20 minutes in a custom assembled chamber in a separate fume hood and transferred back to the sterilised laminar air flow hood after treatment.

Ammonia chamber:

In a second large glass petri dish, a round Whatman filter paper (150mm diameter; 1001150, Whatman) was stuck on the lid using laboratory tape. The filter paper was saturated with ammonia (11309823, Fisher) using a straight glass Pasteur pipette. The lid of the petri dish containing the coverslips was replaced with the ammonia-containing lid, forming in a chamber in which the coverslips would be exposed to ammonia vapours for 20 minutes.

Three Columbia jars were filled with water (dH2O, autoclaved) and one was filled with Hanks' Balanced Salt Solution (HBSS; 14025050, Gibco). 8-10 drops of foetal bovine serum (FBS; S1830-500, Biosera) were added to the HBBS using a curved Pasteur pipette and aspirated 3-4 times to mix the solution as well as coat the pipette with the solution.

Post ammonia treatment, the coverslips were transferred from the large petri dish to the Columbia jars using flat forceps. The coverslips were rinsed thrice in water for 2 minutes each at room temperature, changing Columbia jars between each wash. After the third wash,

the coverslips were transferred into the jar containing the HBSS-serum solution. The coverslips were placed in this solution until they were ready for use.

2.3.2 Tissue preparation

Postnatal mice at either were culled using cervical dislocation and submerged wholly into a beaker containing ethanol (80%). After 2 minutes, the ethanol was poured out and refilled into the beaker. This was repeated twice, for a total of 3 ethanol washes. After the third ethanol wash, the pups were decapitated using standard Metzenbaum surgical scissors and held with a pair of #5 forceps for additional control. The decapitated head was transferred into a petri dish (PET1008, SLS) containing HBSS and shaken gently to rinse off the ethanol. The head was subsequently transferred into a second petri dish containing HBSS. Using curved forceps to hold the oral end of the head, the cranium was bisected using a new, sterile pair of scissors and the brain was removed. The cochleae on the lateral sides of skull were isolated using #5 forceps. Each cochlea was transferred to a new 35mm plastic culture dish (430165, Corning) containing HBSS.

Using a new set of fine forceps, each cochlea was dissected under a transmitted light dissecting microscope (Leica) to obtain the organ of Corti. Using a 30G hypodermic needle and syringe (304000, BD Microlance), the apical coil was separated from the rest of the organ of Corti, whilst ensuring the apical modiolus is attached at the apical coil. The tectorial membrane was then removed. Subsequently, the isolated apical coil was transferred from the 35mm petri dish onto the collagen-coated coverslip using a curved serum-coated Pasteur pipette. Care was taken to prevent excessive movements of the organ of Corti in the pipette to minimise tissue damage. Any excess HBSS was pipetted out, and two to three drops of DMEM-F12 media (containing 7% FBS; recipe below) was added to the coverslip, ensuring enough liquid to cover the tissue, but not enough to cause it to detach and float. It was confirmed under the dissecting microscope that the organ of Corti was affixed into the collagen and facing upwards (such that the hair cell stereocilia face upwards). A Maximov slide was then dotted with sterile Vaseline on four outer edges of the circular cavity. The slide was then turned over, such that the cavity would face the culture. The Maximov slide cavity was gently

positioned on top of the coverslip, making sure that the culture was in the centre of the cavity. Gentle pressure was applied on the Maximov slide to so that the Vaseline glued the square coverslip and Maximov slide together. The edges of the coverslips were carefully sealed onto the Maximov slides using a combination of paraffin wax (76243, Sigma) and Vaseline (1:1 by weight), heated at 90℃ in a glass beaker in a water bath. The mixture was carefully applied using a paintbrush (round, size 3-5), and immediately solidified upon application, creating a water and airtight seal around the coverslip. This step was repeated for all the cochleae used for the experiment. The Maximov slides were carefully placed on a sterile metal slide holder. The metal slide holder was then placed in an incubator (at 37℃ and 5% CO_2) for 24 hours.

2.3.3 Changing culture media and initiating optogenetic stimulation

After 24 hours, the Maximov slides were removed from the incubator and placed in the laminar air flow hood. Using the back of sterile flat forceps, the coverslips were dislodged from the wax seal, and removed from the Maximov slide. Using sterile flat forceps, the coverslip containing the cultured organ of Corti was picked up and placed in a 6-well tissue culture plate (657160, Cellstar), which contained 2 ml of the appropriate culture medium (recipe below). The 6-well tissue culture plate was then placed on top of the optogenetics setup (figure 2.1) within the incubator (at 37℃ and 5% CO_2), and the setup was switched on.

Each experimental set was divided into cultured cochleae that were either optogenetically stimulated, or not stimulated (controls). The control cultures were placed in a separate incubator that lacked the optogenetic setup, with the same media, and at the exact same temperature and pressure conditions (at 37℃ and 5% CO_2). One cochlea from each animal was used for optogenetically stimulated (OS) cultures, and the contralateral cochlea from the same animal was used as control. Media was changed in all cultures every 48 hours. The cultures were maintained for the specified amount of time for each respective experimental condition.

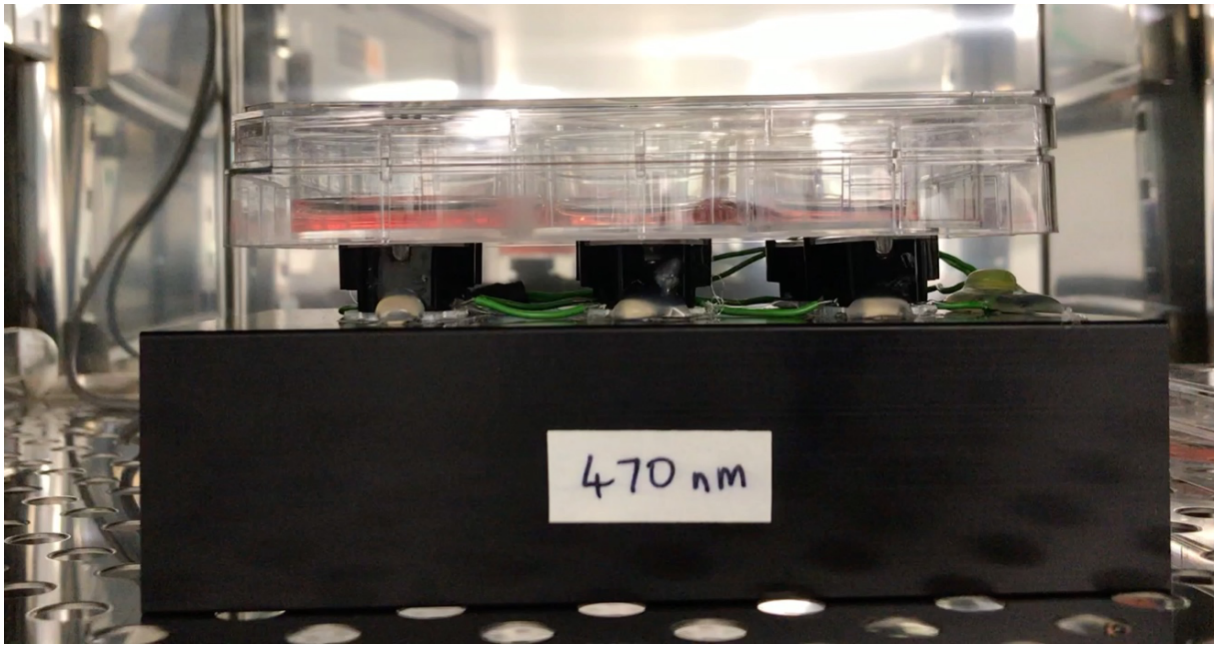

Figure 2.1 LED setup within the incubator with cultures

The 6-well tissue culture plate containing the organotypic cultures are placed on top of the LED setup within the incubator, ensuring that the plates are balanced not titled. Image acquired on iPhone7.

2.3.4 Culture media and experimental solutions

Dissection of cochleae was performed in Hanks' Balanced Salt Solution (HBSS; 14025050, Gibco), buffered with HEPES (concentration in HBSS-10mM; H0887, Sigma).

For culturing, two separate types of culture media were prepared. Media for the first 24 hours of culturing was prepared with 93% DMEM/F12 (D8062, Sigma), 7% FBS (heat inactivated, S1830-500, Biosera) and 0.1% ampicillin (10µg/ml, A9518, Sigma). After 24 hours, the cultures were transferred into media without FBS, containing DMEM/F12, 0.1% ampicillin and antioxidants (Catalase, C9322, Sigma; Superoxide dismutase, S5395, Sigma; Trolox, 238813, Sigma;

Glutathione G4251, Sigma; Vitamin C, A4403, Sigma) to prevent damage from phototoxicity (table 2.1). DMEM/F12 is already supplemented with $CaCl_2$ • 2H2O (1.05mM) and KCl (4.18mM). The media was additionally appended with additional 1M $CaCl_2$ and 1M KCl to bring up the concentration to perilymph (extracellular solution) levels of 1.3mM (for Ca^{2+}) and 5.8mM (for K^+). Additional supplementary factors were added according to the respective experiments.

Component	**Concentration in culture media**
Catalase	10 nM
Trolox	100 μM
Superoxide dismutase	77 nM
Glutathione	3.2 μM
Vitamin C (L-Ascorbic acid)	110 μM

Table 2.1 Composition antioxidants in culture media

The antioxidants were added to all the culture media, regardless of whether they were exposed to optogenetic stimulation (to maintain consistency in culture conditions between optogenetic and control cultures). All antioxidant stock solutions were prepared prior to culturing and added to the total media immediately preceding each media change.

For cultures supplemented with growth factors:

The following growth factors were added to DMEM/F12 + 0.1% ampicillin + antioxidants. The concentrations of NT-3 (Zhou *et al.*, 2005), BDNF (Adamson *et al.*, 2002) and TH (He *et al.*, 2003) were rereferred from established protocols.

Component	Concentration in culture media
NT-3	10ng/ml
BDNF	10 ng/ml
TH	1.8ng/ml

Table 2.2 Growth factors used in the culture media surrounding the cochlea

Experiments with different concentrations of extracellular Ca^{2+}:

For experiments using the endolymphatic concentration of Ca^{2+} (0.3mM) in culture, the media (containing DMEM/F12 + 0.1% ampicillin + antioxidants) was supplemented with trisodium HEDTA (pH 7.4; H8126, Sigma) to quench the available Ca^{2+} ions already present in the DMEM/F12 media (1.05mM Ca^{2+}), leaving a free Ca^{2+} concentration of 0.3 mM. The concentration of HEDTA was specifically calculated using Maxchelator (maxchelator.stanford.edu, Schoenmakers *et al.*, 1992).

Component	Concentration in culture media
HEDTA	0.758mM

Table 2.3 Composition of HEDTA in media

For experiments using 5 mM Ca^{2+}, the media was supplemented with a solution of 1 M $CaCl_2$ (21115, Sigma) to reach the final concentration of 5 mM Ca^{2+}. As the amount of Ca^{2+} already present in the DMEM/F12 media was 1.05mM Ca^{2+}, additional 3.95µl/ml (for each ml of media) of 1 M $CaCl_2$ was added to the media to reach 5mM Ca^{2+}.

Component	Concentration in culture media
1M CaCl2	5mM

Table 2.4 Supplementation of $CaCl_2$ in media

2.4 Optogenetics protocol: LED setup

The LED setup for optogenetics used in this project was setup with collaboration with and courtesy of Dr. Federico Ceriani, based on previous established protocol.

The setup was built using 6 blue LED lights (figure 2.2; emission at 470nm; 20mm, Star LED MR-B0040-20S Luxeonstar), glued to a standard extruded aluminium heatsink (SK92 150SA, Fischer Elektronik). 6, wide-angle beam LED lenses (35° Spot; 10196, Carclo) were placed on top of the LEDs using 20mm hex optic holders (10431, Carclo) and carefully glued using a hot glue-gun at the periphery of the lens. The LEDs were wired into cable-mount subminiature circular connectors (99-0972-100-02; 99-0971-02-02, Binder) and led into a junction box (COMBI 607/5, Wiska). The LED setup was modulated using an LED driver (RCD-24-1.00/W, Recom).

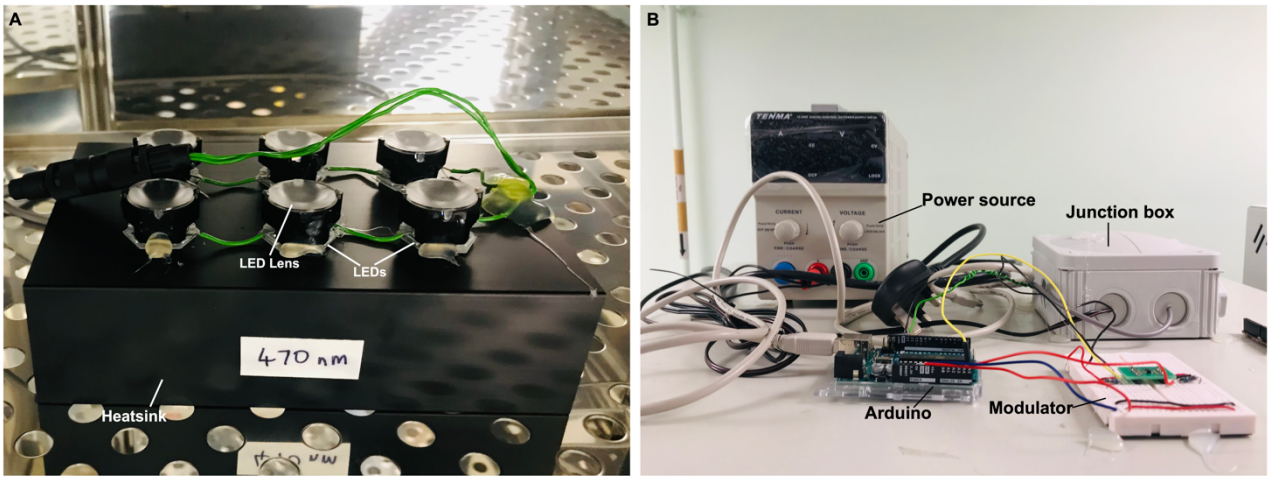

Figure 2.2 Complete optogenetics setup showing the LED setup within the incubator and the external setup placed on top of the incubator

.A) The LED setup within the incubator consists of the LEDs attached to the heatsink and connected with cables that are connected externally to the programming setup Care is taken to ensure that the setup is disinfected using 80% ethanol prior to use. B) The setup outside the incubator, which is responsible for modulating the LED spikes. The LED setup inside the incubator leads into the junction box, which connects to the external setup. The setup includes the Arduino board that contains the sketch to run the LED spikes, the modulator for the spiking and the power source. Image acquired on iPhone7.

The LED spiking signal was controlled using a sketch uploaded on an Arduino board (A000066, Arduino). The entire setup was attached to a 24V battery (8921, Mascot) for constant power supply (figure 2.3.). The Arduino was programmed using python (pyRhodopsin software).

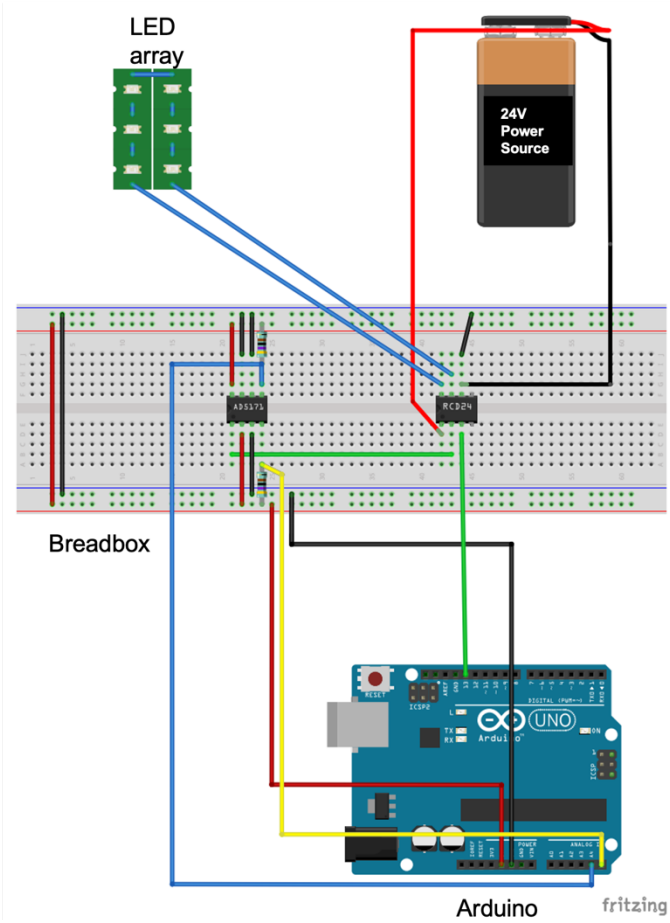

Figure 2.3 Circuit assembly for the LED setup

Image obtained by courtesy of Dr. Federico Ceriani (unpublished).

The LED, lens, heatsink and connector cable were wiped using 80% ethanol prior to placement in the incubator. The rest of the components were placed on top of the incubator. After placement inside the incubator, the LED setup was wiped with 80% again, carefully ensuring nothing is dislodged from the setup and no ethanol comes in contact with exposed electrical/wiring.

The spiking protocol used for the LED setup was (figure 2.4.):

Duration of the light step: 5 ms

Interspike interval (ISI): 1000 ms

Burst: no (chosen for continuous spiking of LED)

Pretrigger duration (i.e., duration of the light step during pretrigger): 40 ms

Pretrigger power: 8/63

Power: 45-52/63

(Note: 0 is for LED off, and 63 is full power)

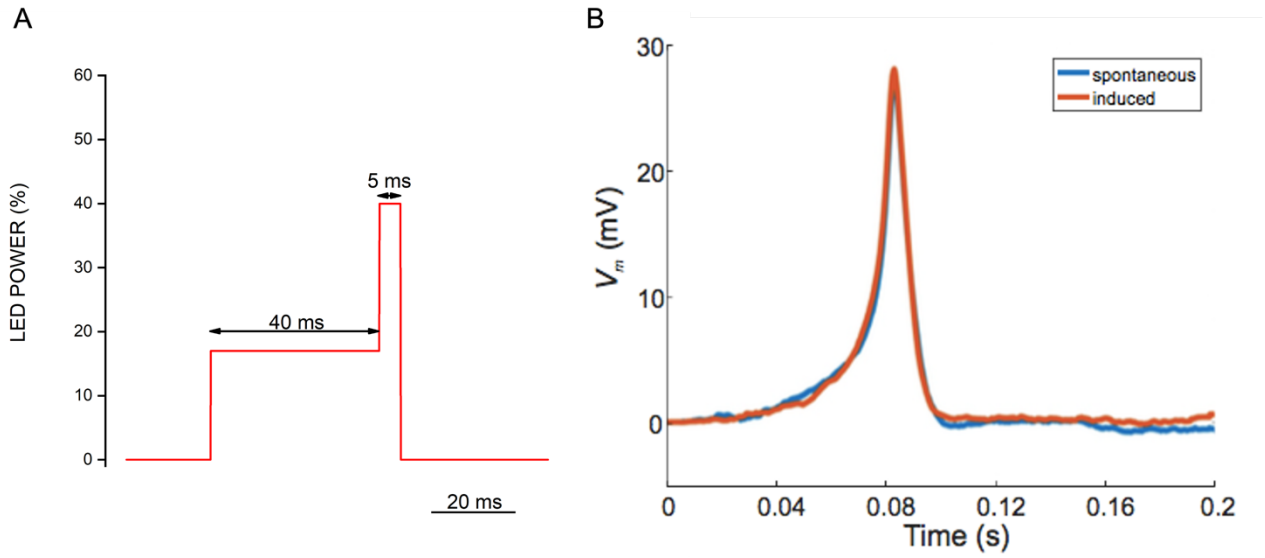

Figure 2.4 Waveform of optogenetics protocol

A) Diagram showing the waveform of optogenetics protocol provided to the cultures. B) Shows that light stimulus using this protocol can accurately mimic the shape of the spontaneous activity. Image obtained by courtesy of Dr. Federico Ceriani (unpublished).

2.5 Immunofluorescence staining and microscopy

All imaging for this project was performed on the apical coil of the organ of Corti at the 9-12 kHz region.

This project used both wholemount cochlea and organotypic cochlea cultures for immunofluorescence microscopy. The cultures and wholemount cochleae were fixed individually but blocked and immunostained simultaneously. In case of wholemount cochleae, the tissue from pups between ages P3 to P20 were washed with HBSS three times for two minutes each and fixed directly using 4% paraformaldehyde (PFA; prepared in phosphate buffered saline; PBS; pH 7.4) for one hour at room temperature. The PFA was washed using PBS three times for 10 minutes each. The organs of Corti were dissected from the cochleae in PBS for further use. In case of organotypic cultures; after the required period of incubation, the coverslips containing the respective cultures were washed with HBSS three times for 2 minutes each and fixed using 4% PFA for 30 minutes at room temperature. The cultures were then washed with PBS three times for 10 minutes each. Organotypic cultures as well as wholemount cochleae were both incubated in blocking solution (PBS with 0.5% TritonX-100. i.e., PBST; containing either 5% normal horse serum; H0146, Sigma-Aldrich; or normal goat serum; # 31873, Invitrogen) at room temperature for 1 hour.

Primary antibodies (prepared with PBST with 1% either goat or horse serum respectively) were added to the samples and incubated overnight at 37 ˚C. The primary antibodies used were; mouse anti-CtBP2 for synaptic ribbons, mouse anti-GluR2 for postsynaptic afferents, mouse anti-BK for BK channels (as listed below).

After overnight incubation, the samples were washed thrice with PBS for 10 minutes at room temperature. Secondary antibodies (similarly diluted in PBST with 1% either goat or horse serum respectively) were then added to with respect to the individual primary antibodies and incubated for one hour at 37 ˚C. The secondary antibodies used were; goat anti-mouse IgG1 Alexa Fluor 647 (far red), goat anti-mouse IgG2a Alexa Fluor 568 (red), goat anti-mouse IgG1 Alexa Fluor 568 (red; all antibodies as listed below).

The samples were washed with PBS thrice for 10 minutes each at room temperature. The environment was maintained dark during the washes. The samples were subsequently mounted in Vectashield® antifade mounting medium (H-1000-10, Vector Laboratories). Care was taken to ensure that the hair cells were facing the correct orientation, such that the apical poles of the hair cells were pointing upwards, perpendicular to the slide. The samples were covered with coverslips and sealed using clear nail varnish.

Primary antibody	**Host-Isotype**	**Concentration**	**Catalogue number**	**Company**
CtBP2	Mouse-IgG1	1:500	612044	BD
GluR2	Mouse-IgG2a	1:500	MAB397	Millipore
BK	Mouse-IgG1	1:200	75-408	Antibodies incorporated

Table 2.5 List of primary antibodies used for immunofluoresnce microscopy

Secondary antibody	**Host-Isotype**	**Concentration**	**Excitation (nm)**	**Emission (nm)**	**Catalogue number**	**Company**
For CtBP2	Goat anti-mouse IgG1	1:1000	650	665	A21240	Invitrogen
For GluR2	Goat anti-mouse IgG2a	1:1000	578	603	A21134	Invitrogen
For BK	Goat anti-mouse IgG1	1:1000	578	603	A21124	Invitrogen

Table 2.6 List of secondary antibodies used for immunofluoresnce microscopy

Since the mice express EYFP (*Otof:*ChR2-EYFP), the plasma membrane of the IHCs appeared fluorescent, and a cellular/nuclear counterstain was not required. However, since the resultant EYFP (yellow; excitation at 513nm; emission at 527nm) resulted in crosstalk with Alexa Fluor 488 (green), we chose to not use the Alexa Fluor 488 secondary antibody for immunofluorescence microscopy.

Super-resolution images were obtained using a Zeiss LSM 880 Airyscan microscope (Zeiss, Germany). The airyscan feature was used as it aids to 1.7x higher resolution in 3D, with up to 140 nm lateral resolution and 400 nm axial resolution with a 4x signal to noise ratio. Fitted with Plan-Apochromatic 63x oil objective and 1x zoom level, z-stack images were captured using Zeiss software (Zeiss, Germany).

Images were first processed using airyscan processing. Processed images were then analysed through Arivis Vision4D (Arivis AG, Germany). Figures were composed using Fiji ImageJ software (Schindelin *et al.*, 2012)and compiled in Microsoft PowerPoint (Microsoft, USA). The IHCs appeared yellow (EYFP), CtBP2 positive puncta appeared magenta (647, far red; false coloured), the GluR2 positive puncta appeared red (568), and the BK positive puncta appeared red (568). For better visibility between the CtBP2 and GluR2 positive puncta in images presented in this thesis, the GluR2 positive puncta were false coloured to green using FIJI lookup tables.

All imaging was carried out at Wolfson Light Microscope Facility at the University of Sheffield.

2.6 Image analysis and statistics

After airyscan processing, image stacks were analysed on Arivis Vision4D software. Individual channels for CtBP2, GluR2 and BK positive puncta were thresholded and single puncta were counted using “blob finder” (size: 0.5 µm, split sensitivity: 65%). To obtain counts of puncta per IHC, total counts for each positive puncta was divided by the total number of IHCs in the ROI, giving an average value of number of puncta per IHC. Volumes of individual CtBP2 and GluR2 positive puncta were calculated by Arivis using the “volume” setting for each channel and averaged by dividing the number by total number of puncta within the respective channel. Thus, it would yield the average volume of a single puncta per IHC.

In images with CtBP2 and GluR2 positive puncta, blob finder was employed for colocalization analysis using “distance measurement”. Distances between CtBP2 and GluR2 positive puncta were measured using CtBP2 positive puncta as reference points, with the maximum distance between any two points kept at 0.05µm (to provide indications of colocalizations). The resultant numbers indicated the number of GluR2 puncta associated in close proximity with CtBP2 puncta, indicating colocalization. The number of colocalizations were divided by the total number of CtBP2 positive puncta (as CtBP2 was the reference to measure colocalization towards) and multiplied by 100 to obtain colocalization as a percentage.

The ratio between the number of CtBP2 and GluR2 positive puncta was calculated by dividing the total number of GluR2 puncta per IHC by the total number of CtBP2 puncta per IHC (with CtBP2 as the reference) and presented as a number. A resultant ratio of 1 would suggest equivalent numbers of CtBP2 and GluR2 positive puncta, while a ratio higher than 1 would suggest more GluR2 positive puncta than CtBP2 and a ratio less than 1 would suggest more CtBP2 positive puncta than GluR2.

Statistical analyses were performed on GraphPad Prism version 9.0 (GraphPad Software, USA). Multiple data sets were analysed and compared using T-test or two-way ANOVA accompanied by Welch correction. T-test with Welch correction was applied to compare optogenetically stimulated

and control cultures from the same days in culture, while two-way ANOVA was utilised to compare optogenetically stimulated and control cultures from different days in cultures. The p-value for statistical significance was 0.05. Data are presented as mean +/- SD.

3. Investigating the Maturation of Hair Cell Cultures *in vitro*

3.1. Introduction

For this experiment we used transgenic mice that expressed ChR2-EYFP using an otoferlin-cre promoter. Following dissection, cochleae from neonatal mouse pups at 7 days following birth (P7) were cultured and maintained for a maximum of 10 days *in vitro* (10 DIV). The cultures were provided with extrinsic optogenetic stimulation using an LED setup (λ=470 nm; refer methods chapter 2.4). Cochleae from the contralateral ear of the same pup were cultured without optogenetic stimulation (control).

Cultures were then fixed and immunostained at three intervals; P7+3 DIV, P7+7 DIV and P7+10 DIV (henceforth referred to as 3DIV, 7DIV and 10DIV), giving the cochlea a total age of P10, P14 and P17. Cochlea from pups undergoing normal development were also utilised to act as references for normal maturation (positive control). Cochleae from pups at ages between P3 and P20 were fixed and immunostained for CtBP2 and GluR2 at regular intervals.

The readouts considered for this experiment were the presynaptic ribbon marker; CtBP2 and postsynaptic marker GluR2. The broad, overall morphology of cultures was also evaluated, especially for cultures that were grown for 10 DIV.

Figure 3.1 shows the normal progression of synaptic ribbons as well as afferent synapses in the developing cochlea. Preceding hearing onset (<P12), ribbon synapses of IHCs undergo substantial structural and functional development (Michanski *et al.*, 2019). As early as embryonic stage 16-18 (E16-18), precursors for synaptic ribbons (including RIBEYE and piccolino) aggregate at the presynaptic active zones (AZs; as described in introduction chapter 1.2.1).

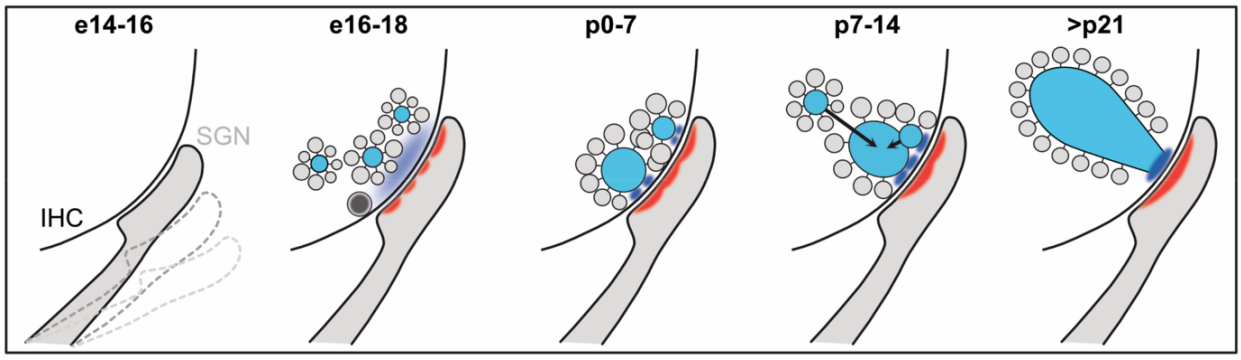

Figure 3. 1 Shows the normal maturation of synaptic ribbons during development.

Synaptic ribbon precursors aggregate around the active zone at E16-E18. Development continues after birth where smaller ribbons aggregate into larger ribbons. At age P20 and upwards, ribbons are fully mature, acquiring their characteristic ribbon shape. The mature ribbon forms a synapse with a singular type I SGN. Dark grey: SGN (spiral ganglion neuron); Light grey: SV (synaptic vesicle); blue: synaptic ribbons; red: PSD (postsynaptic density); black circles: DCVs (Dense core vesicle) (Figure adapted from Voorn et al., 2020).

The normal number of ribbons generally increases from around P4 until P7 or P8. Around this time, the number of synaptic ribbons per IHC is approximately 30 to 35. Smaller precursor ribbons are gradually fused into larger ribbons at the AZ, thus acquiring their characteristic ribbon shape. This occurs the most approaching P12, which coincides with hearing onset in mice. With further development, this number falls until hearing onset at P12. By P15-P20, the ribbon stabilizes to approximately 5-20 ribbons per IHC.

After hearing onset, the volume of ribbons remains consistent. This process is considered to consequently parallel morphological and functional maturation of the AZ.

Postsynaptic type I SGNs undergo similar refining in conjunction with the presynaptic development (as described in introduction chapter 1.1.2). Type I SGN numbers increase considerably between P3 to P7. At the age of P7-P8, there are at least twice as many type I synapses associated with each

IHC as there are ribbons. Consequently, the SGNs undergo synaptic pruning, paralleled by neurite retraction, leading to a 50% decrease of ribbon synapse number in mice between P7 and P14. At maturity, each IHC is innervated by a total of 6 to 20 type I SGNs (Kalluri and Monges-Hernandez, 2017), almost the same number as the synaptic ribbons.

Due to the changes occurring in synaptic ribbons during postnatal development and their importance in maturation, we believed that immunostaining for synaptic ribbons would provide us with an accurate representation for maturation. We used the ribbon marker CtBP2- which is a transcriptional co-repressor transcribed from independent promoters in the same gene as RIBEYE(Schmitz *et al.*, 2000; Jeong *et al.*, 2018). For type I afferents, we used anti-GluR2, which is a component of the postsynaptic AMPA receptor.

We expected that if the optogenetic stimulation is enough to drive maturation, the cultures would show an initial decline in the number of ribbons in the P7+3 DIV cultures and then maintain that number throughout the P7+7 DIV and P7+10 DIV cultures. We also anticipated a sequential rise in ribbon volume, indicating the aggregation of smaller ribbons into larger ribbons. In addition, we would expect to observe a decrease in SGN numbers with a corresponding increase in the amount of colocalization between the ribbons and afferent SGN boutons. To visualise this through immunohistochemistry we used anti-CtBP2 antibody for synaptic ribbons, anti-GluR2 antibody for the postsynaptic afferents.

If optogenetic stimulation was insufficient to induce maturation, exogenous growth factors would be administered to the cultures. The objective was to investigate if the introduction of growth factors in conjunction with optogenetics would promote IHC maturation in the cultures. We added BDNF (Brain-derived neurotrophic factor; 10ng/ml), NT-3 (Neurotrophin-3; 10ng/ml), and T3 (Thyroid hormone -Triiodothyronine; 1.8ng/ml) to the culture media to examine the impact of exogenous growth factor supplementation on immature IHCs undergoing optogenetic stimulation *in vitro.*

Cultures were prepared at P7. Culture media was supplemented with 10ng/ml BDNF, 10ng/ml NT-3 and 1.8ng/ml T3. Cultures were then fixed and immunostained for CtBP2 and GluR2 at P7+3DIV

and P7+7DIV. Cochleae from the contralateral ear of the same pup were cultures without optogenetic stimulation (control).

3.2. Results

3.2.1. Wholemount immunostaining of cochleae for visualising progression of synaptic ribbons during normal development

Cochlea from pups undergoing normal development were utilised as references for normal maturation (positive control). Cochleae from pups at ages between P3 and P20 were fixed and immunostained for CtBP2 and GluR2 at regular intervals (i.e., P3, P5, P7, P8, P10, P12, P15, and P20) to visualise the synaptic ribbons and postsynaptic afferents respectively (as shown in figure 3.2.). Images of the apical coil were acquired at the 9–12kHz region for each condition.

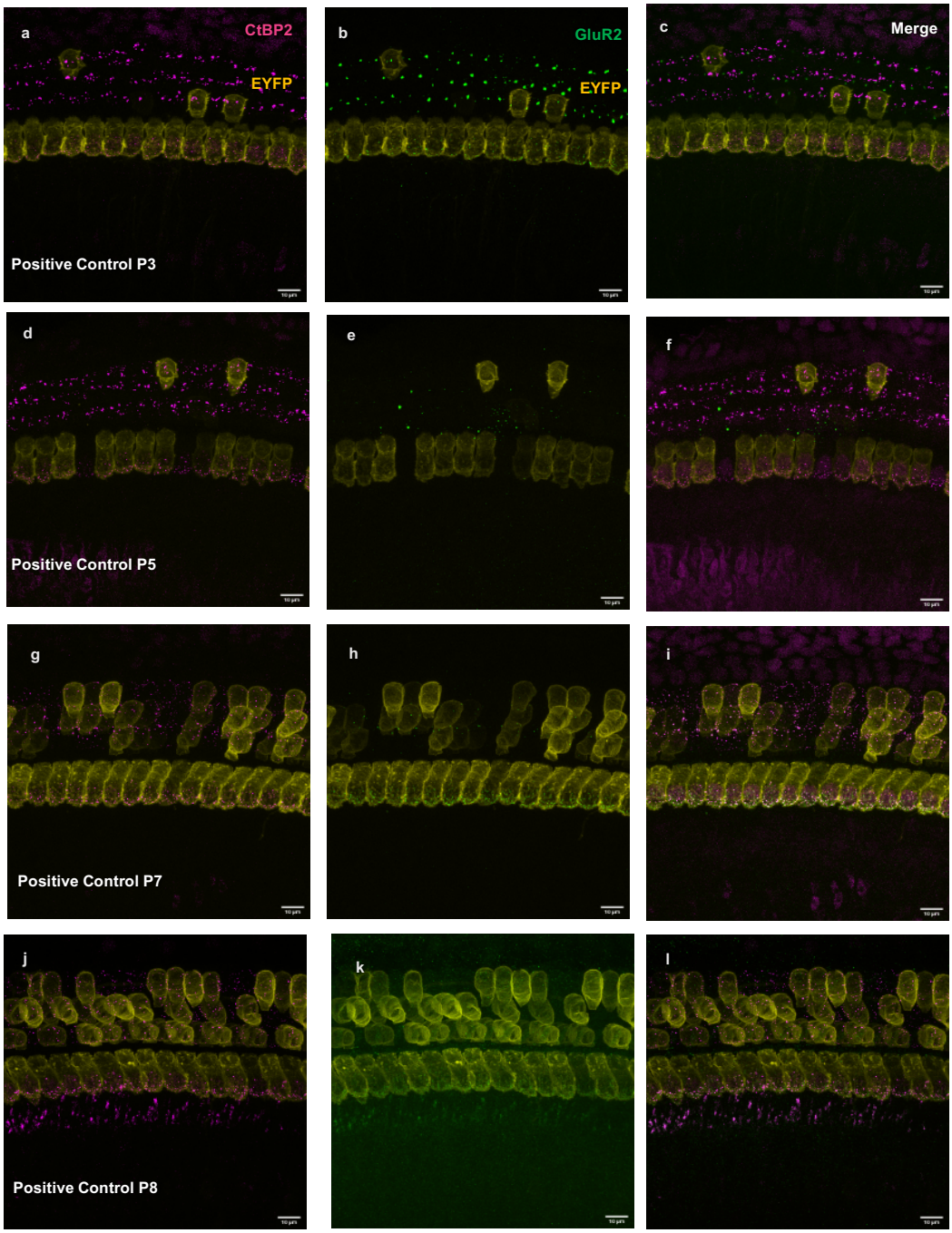

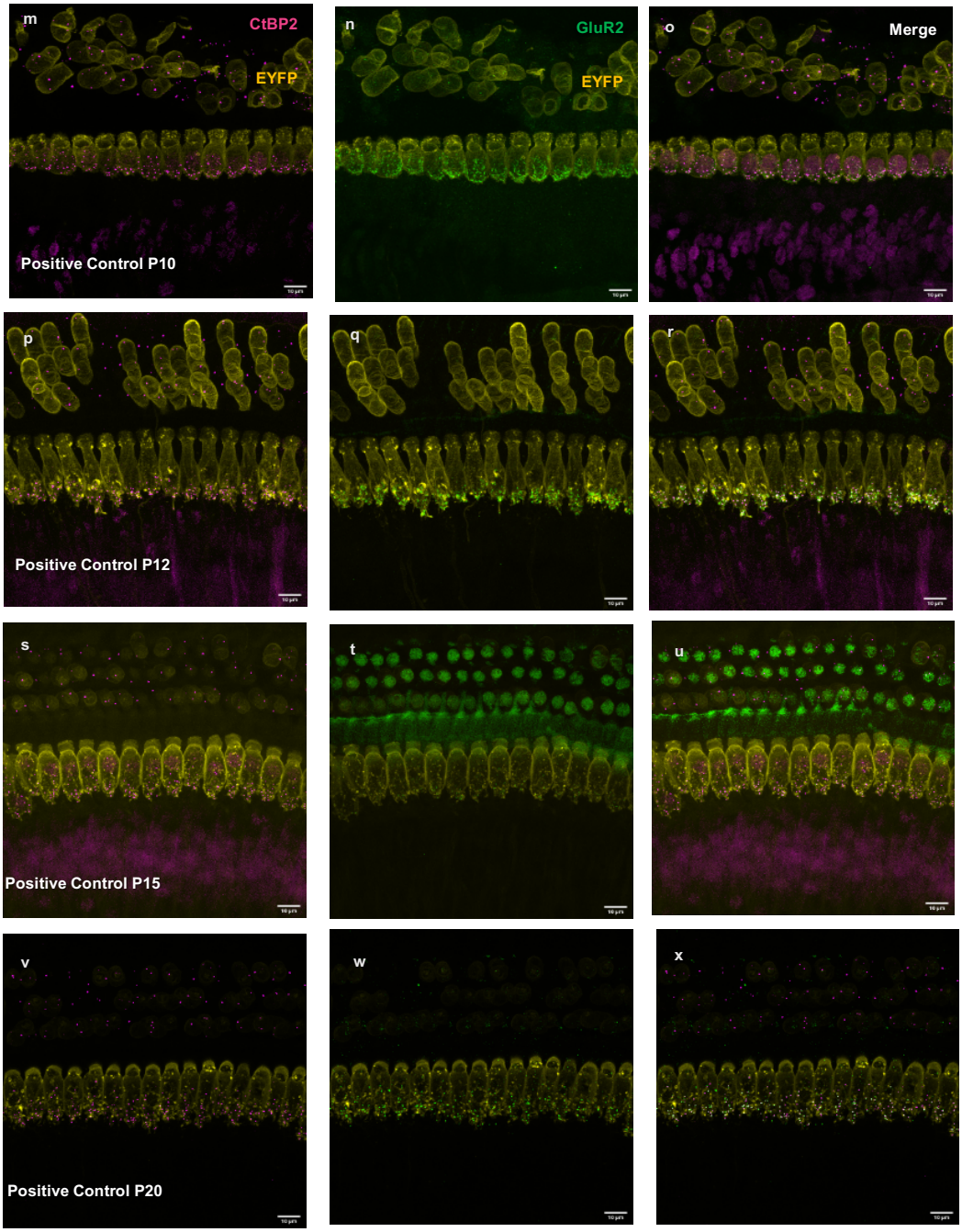

Figure 3.2 Shows wholemount immunostaining of cochleae at different age intervals between P3 to P20 with CtBP2 and GluR2.

All images taken at the 9–12kHz region for each condition; Images for each age show CtBP2 positive puncta and EYFP, GluR2 positive puncta and EYFP, and merged images for CtBP2 and GluR2 positive puncta with EYFP. a, d, g, j, m, p, s, v: CtBP2 positive puncta with EYFP; b, e, h, k, n, q, t, w: GluR2 positive puncta with EYFP.: c, f, i, l, o, r, u, x: Merge of CtBP2 and GluR2 positive puncta with EYFP. Images at 63x. Magenta: CtBP2; Green: GluR2; Yellow: EYFP. Scale bar: 10*μm*. n= number of cochleae used for

wholemount immunostaining. For P3, n=4; P5, n=2; P7, n=4; P8, n=4; P10, n=2; P12, n=4; P15, n=2; P20, n=2.

CtBP2- and GluR2-positive puncta were quantified and plotted for each age (graph 3.1.). Figure 3.2. a-x shows confocal images of the immunostained cochleae. CtBP2 and GluR2 positive puncta were observed and quantified for number of CtBP2/GluR2 puncta, volumes of CtBP2/ GluR2 puncta, ratio of CtBP2 vs GluR2 puncta numbers and colocalization of the two signals as a percentage.

The number of CtBP2 positive puncta for the immunostained cochleae from P3 to P20 were as follows (graph 3.1.a); P3; 11.0 (±7.0, n=4), P5; 24.0(±2.0, n=2), P7; 34.0(±3.0, n=4), P8; 21.0(±7.0, n=4), P10; 18.0(±3.0, n=2), P12; 17.0(±2.0, n=4), P15; 17.0(±0.1, n=2), P20; 15.0 (±1.0, n=2).

The number of GluR2 positive puncta for the immunostained cochleae was also quantified from P3 to P20 as follows (graph 3.1.b): P3; 0.0(±0.0, n=4), P5; 0.0(±0.0, n=2), P7; 34.4 (±21.5, n=4), P8; 27.0(±22.0, n=4), P10; 56.0(±13.0, n=2), P12; 33.0(±8.0, n=4), P15; 17.0(±3.0, n=2), P20; 15.0(±0.1, n=2).

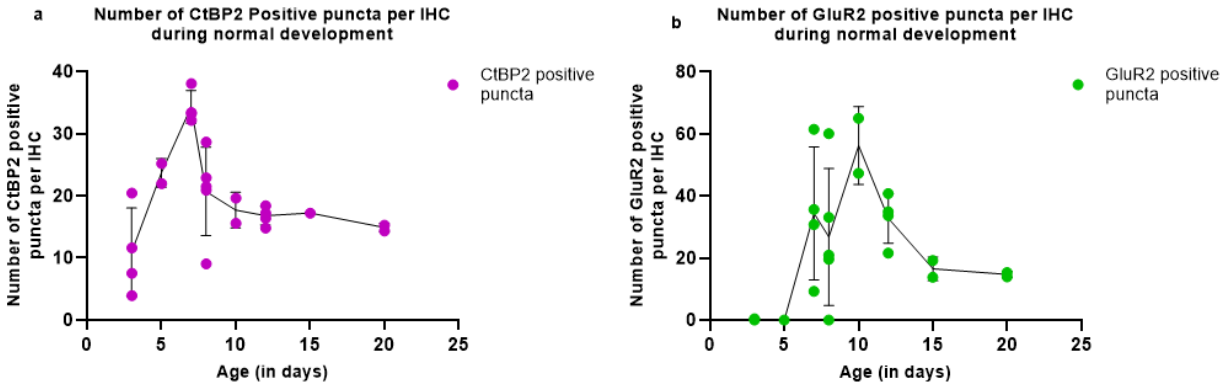

Graph 3.1 Shows number of CtBP2 and GluR2 positive puncta positive puncta in wholemount cochlea for different age intervals between P3 to P20.

a: Number of CtBP2 positive puncta per IHC in mice at ages P3, P5, P7, P8, P10, P12, P15 and P20. Magenta dots represent individual values of CtBP2 positive puncta from each cochlea. The number of CtBP2 positive puncta is low during the first postnatal week

(11.0±7.0, n=4; at P3), but increases rapidly around P7 (34.0±3.0, n=4). In the second postnatal week, it decreases to around 15-20 per IHC (17.0±2.0, n=4; at P12) and remains constant in later ages (15.0±1.0, n=2; for P20). **b:** Number of GluR2 positive puncta per IHC in mice at ages P3, P5, P7, P8, P10, P12, P15 and P20. Green dots represent individual values of GluR2 positive puncta from each cochlea. The number of GluR2 positive puncta shows a sharp increase in the first postnatal week followed by a sharp decline due to synaptic pruning in the second postnatal week. N= number of cochleae used for wholemount immunostaining. For P3, n=4; P5, n=2; P7, n=4; P8, n=4; P10, n=2; P12, n=4; P15, n=2; P20, n=2.

During maturation, the volume of synaptic ribbons increases progressively, and stabilises during maturation. The volumes of CtBP2- positive puncta were calculated and plotted (graph 3.2.a). The volume of CtBP2 positive puncta for the immunostained cochleae are as follows; P3; 0.05 μm^3 (±0.02, n=4), P5; 0.07 μm^3 (± 0.01, n=2), P7; 0.13 μm^3 (± 0.03, n=4), P8; 0.09 μm^3 (±0.03, n=4), P10; 0.12 μm^3 (±0.04, n=2), P12; 0.15 μm^3 (±0.02, n=4), P15; 0.16 μm^3 (±0.01, n=2), P20; 0.13 μm^3 (±0.04, n=2).

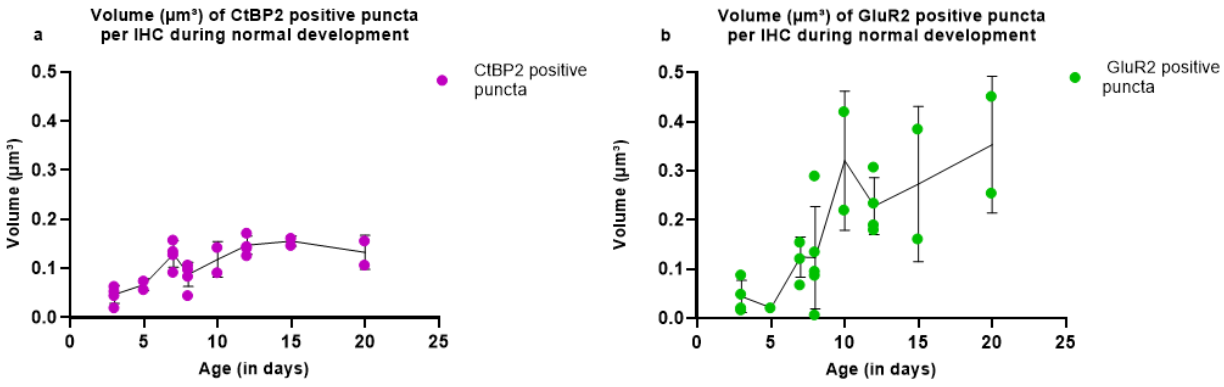

Graph 3.2 Shows the volume (μm^3) of CtBP2 and GluR2 positive puncta in wholemount cochlea for different age intervals between P3 to P20.

a: Volume (μm^3) of CtBP2 positive puncta per IHC in mice at ages P3, P5, P7, P8, P10, P12, P15 and P20. Magenta dots represent individual volumes of CtBP2 puncta from

each cochlea. The volume of CtBP2 is low in the first postnatal week (0.05μm^3±0.02 at P3) and increases with age (0.13 μm^3 ±0.04, n=2; at P20). This is due to the coalescence of smaller ribbon precursors into larger ribbons around the active zone. **b:** Volume (μm^3) of GluR2 positive puncta per IHC in mice at ages P3, P5, P7, P8, P10, P12, P15 and P20. Green dots represent individual volumes of GluR2 puncta from each cochlea. The volume of GluR2 is also low during the first postnatal week (0.04 μm3 ±0.03, n=4; at P3) and steadily shows an increase with normal maturation after which, it becomes consistent (0.35μm3 ±0.14, n=2; at P20). This is due to the maturation of the synaptic site where the type I SGN forms the synapse with the ribbon. N= number of cochleae used for wholemount immunostaining. For P3, n=4; P5, n=2; P7, n=4; P8, n=4; P10, n=2; P12, n=4; P15, n=2; P20, n=2.

The volume of GluR2 positive puncta during imaging was also calculated for positive controls. The positive controls can show that the volume of each postsynapse increases with maturation. As a postsynaptic marker, Glur2 highlights the relatively minute size of the postsynapse during early days after birth (P3-P5). There is a sharp incline in volume during postnatal development and a subsequent plateau following hearing onset (graph 3.2.b). For GluR2 positive puncta, the volumes were as follows; P3; 0.04 μm^3 (±0.03, n=4), P5; 0.02 μm^3 (± 0.0, n=1), P7; 0.13 μm^3 (± 0.04, n=4), P8; 0.12 μm^3 (±0.1, n=4), P10; 0.32 μm^3 (±0.14, n=2), P12; 0.23 μm^3 (±0.06, n=4), P15; 0.27 μm^3 (±0.16, n=2), P20; 0.35μm^3 (±0.14, n=2).

During early development, the number of type I afferents innervating IHCs outnumber synaptic ribbons by twice or thrice. However, after hearing onset, it drastically drops and the average ratio of synaptic ribbon to afferents is one to one (i.e., 1:1).

To calculate this ratio, we divided the total number of GluR2 positive puncta per IHC by the number of CtBP2 positive puncta per IHC for each image (graph 3.3.a). On a scale of 0 to 1, a ratio of 1 would indicate equal number of ribbons to afferents. A ratio higher than 1 would indicate more afferents than ribbons, and a ratio lower than 1 would indicate fewer afferents than ribbons.

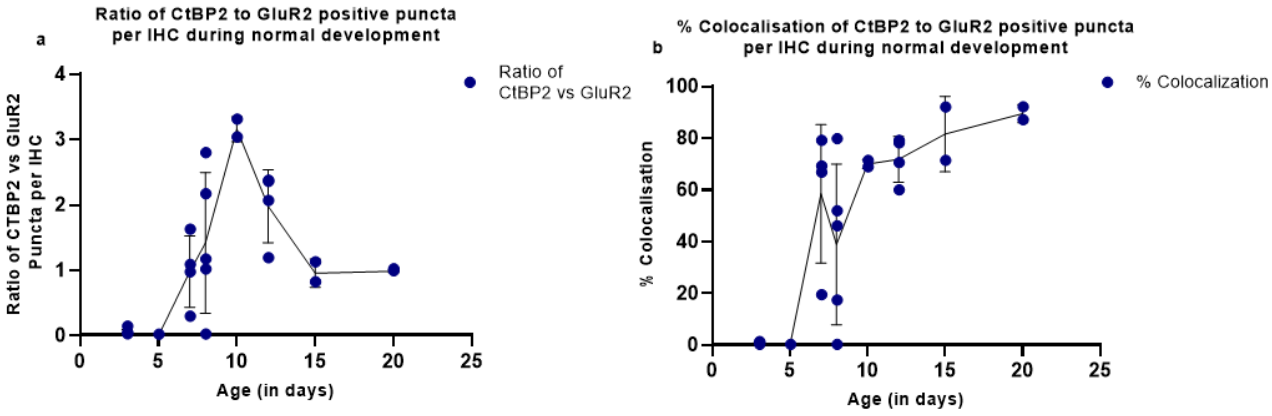

<u>Graph 3.3</u> Shows the ratio and colocalization of CtBP2 and GluR2 positive puncta in wholemount cochlea for different age intervals between P3 to P20.

a: Ratio of CtBP2 with GluR2 positive puncta per IHC in mice at ages P3, P5, P7, P8, P10, P12, P15 and P20. The ratio of CtBP2 vs. GluR2 puncta increases drastically during the prehearing stage, owing to twice or thrice as many postsynaptic afferents at each IHC terminal. By the end of the second postnatal week, the ratio becomes closer to 1:1. **b:** Colocalization percentage of CtBP2 with GluR2 positive puncta per IHC in mice at ages P3, P5, P7, P8, P10, P12, P15 and P20. The colocalization of CtBP2 and GluR2 signal is lower for younger ages and increases with age. At P20, the colocalization of CtBP2 with GluR2 is seen to be 90.0%±4.0; n=2, indicating maturation of most ribbon synapses in the IHC. Dark blue dots represent individual values from each cochlea. n= number of cochleae used for wholemount immunostaining. For P3, n=4; P5, n=2; P7, n=4; P8, n=4; P10, n=2; P12, n=4; P15, n=2; P20, n=2.

The ratio of CtBP2 to GluR2 positive puncta for the immunostained cochleae were as follows (graph 3.3.a): P3; 0.0(±0.0, n=4), P5; 0.0(±0.0, n=2), P7; 1.0(±0.6, n=4), P8; 1.0(±1.1, n=4), P10; 3.0(±0.2, n=2), P12; 2.0(±0.6, n=4), P15; 1.0(±0.2, n=2), P20; 1.0(±0.0, n=2).

At the time of IHC maturation, each synaptic ribbon is affiliated with a single type I afferent terminal (Liberman et al., 1990; Liberman, 1980). To check the amount of mature ribbon synapses in IHCs, we utilised this hallmark. When immunostained with presynaptic ribbon (CtBP2) and postsynaptic afferent (GluR2) markers, colocalization between the two signals would indicate the presence of mature ribbon synapses. With increase in IHC maturation, the percentage of colocalization would consequently increase. We calculated colocalization between CtBP2 positive and GluR2 positive puncta using ARIVIS software (refer to materials and methods). This was then plotted as a percentage of colocalization, with 0% indicating no colocalization and 100% indicating complete colocalization of each GluR2 puncta with each CtBP2 puncta (graph 3.3.b).

The colocalization of CtBP2 and GluR2 for the immunostained cochleae were as follows (graph 3.3.b): P3; 1.0%(±0.6, n=4), P5; 0.0%(± 0.0, n=2), P7; 59.0%(±27.0, n=4), P8; 40.0%(±31.0, n=4), P10; 70.0%(±2.0, n=2), P12; 72.0%(±9.0, n=4), P15; 82.0%(±15.0, n=2), P20; 90.0%(±4.0, n=2).

3.2.2. Culturing cochlea with optogenetic stimulation for 10 days does not show IHC maturation

CtBP2- and GluR2- positive puncta were immunostained and quantified for each condition over three varying time intervals for OS (optogenetically stimulated) and control cultures (figure 3.3. a-x). Images of the apical coil were acquired at the 9–12kHz region for each condition.

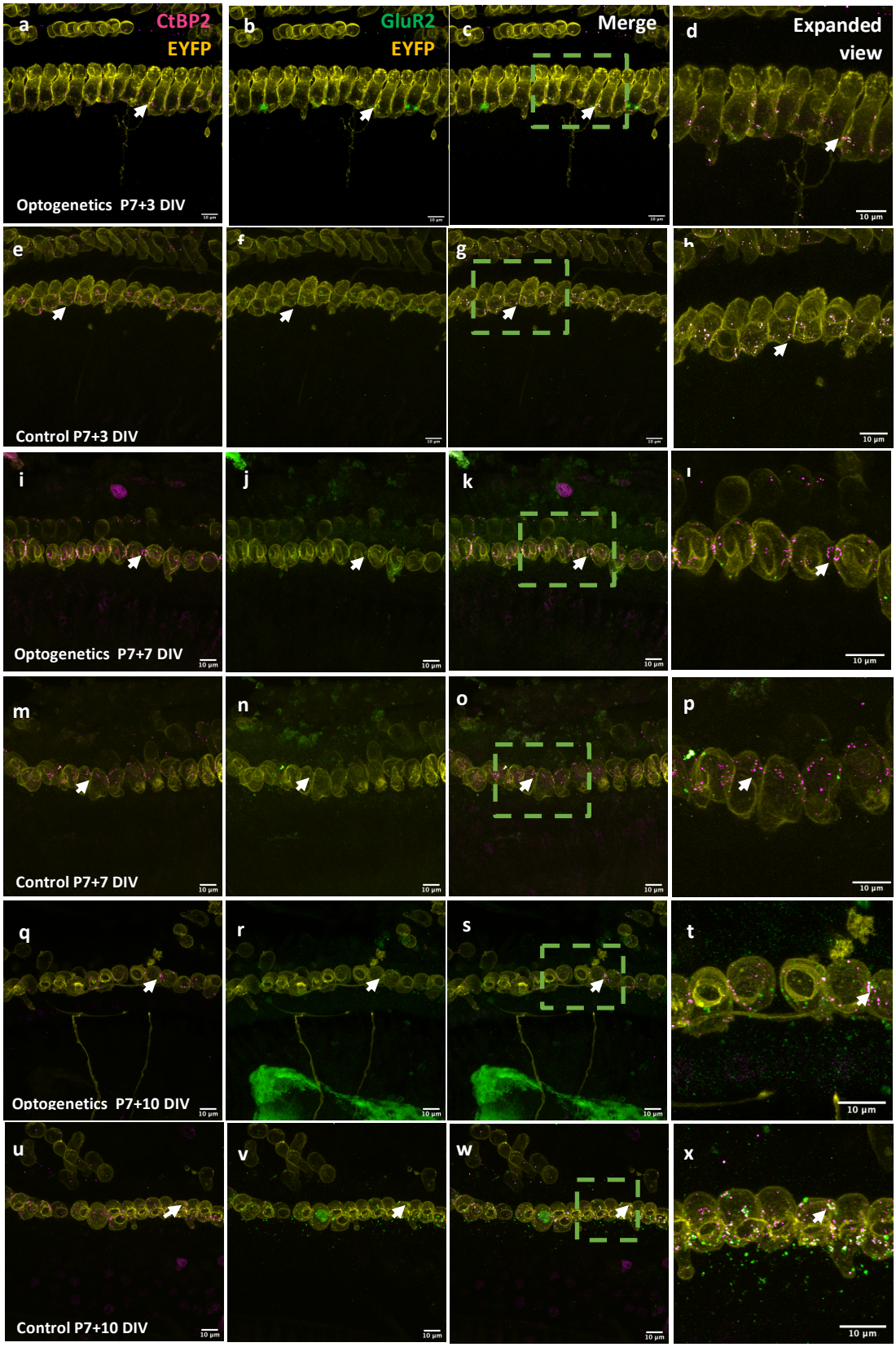
a
CtBP2
EYFP
b
GluR2
EYFP
c
Merge
d
Expanded
view
Optogenetics P7+3 DIV
e
f
g
h
Control P7+3 DIV
i
j
k
l
Optogenetics P7+7 DIV
m
n
o
p
Control P7+7 DIV
q
r
s
t
Optogenetics P7+10 DIV
u
v
w
x
Control P7+10 DIV
10 µm

<u>Figure 3.3</u> Shows immunostaining for cultures stimulated by optogenetics (OS cultures) and controls (with no optogenetic stimulation applied) at P7+3 DIV, P7+7 DIV and P7+10 DIV.

All images taken at the 9–12kHz region for each condition; Images for each day in culture show CtBP2 positive puncta and EYFP, GluR2 positive puncta and EYFP, and merged images for CtBP2 and GluR2 positive puncta with EYFP. The cultures were imaged at 3-, 7- and 10-days *in vitro*, after either being optogenetically stimulated (OS) or maintained without optogenetic stimulation (control). a, e, i, m, q, u: CtBP2 positive puncta with EYFP; b, f, j, n, r, v: GluR2 positive puncta with EYFP: c, g, k, o, s, w: Merged image showing CtBP2 and GluR2 positive puncta with EYFP; d, h, l, p, t, x: expanded view of merged image. Images at 63x. Magenta: CtBP2; Green: GluR2; Yellow: EYFP. Green box indicates expanded area; Arrows point to CtBP2/GluR2 puncta; DIV; Days *in vitro*; All cultures prepared at P7; Scale bar: 10*μm*.

The number of CtBP2 positive puncta in cultures show interesting results (graph 3.4.a). For cultures at 3 DIV, the number of puncta was 11.0 (±3.0, n=2) for OS cultures and for 12.0(±4.0, n=2) controls. At 7 DIV, the number of puncta remained fairly consistent, at 12.0(±7.0, n=6) for OS cultures and 12.0(±7.0 n=8) for controls. At 10 DIV, the number of CtBP2 positive puncta for OS cultures was 9.0(± 2.0, n=5) and 12.0(± 12.0, n=4) for controls.

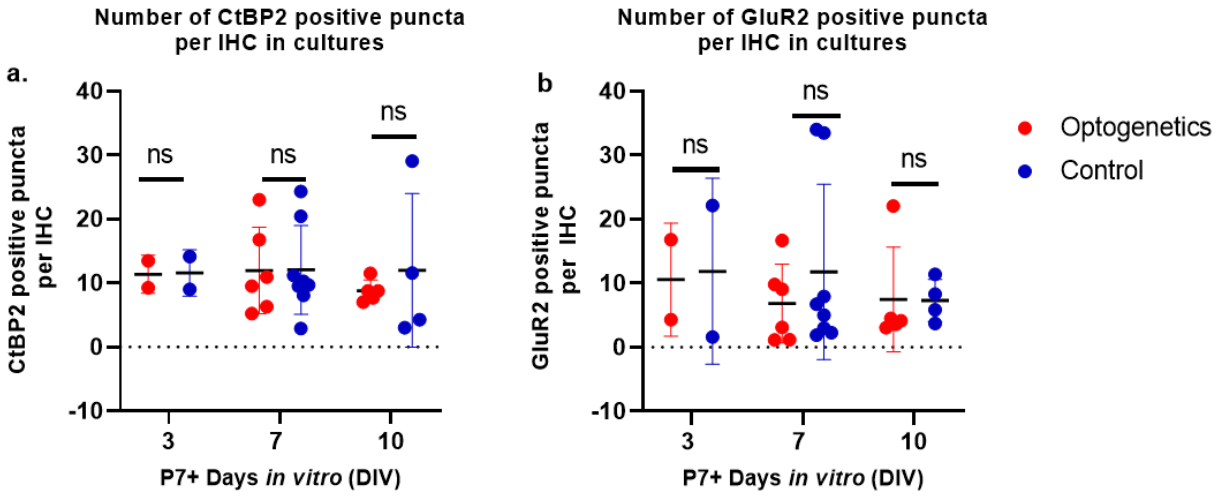

Graph 3.4 Shows number of CtBP2 and GluR2 positive puncta in cultures stimulated by either optogenetics (OS cultures) or controls (no optogenetic stimulation applied) at P7+3 DIV, P7+7 DIV and P7+10 DIV.

a: Number of CtBP2 positive puncta per IHC in 3DIV, 7DIV and 10DIV cultures; (p=0.96 for 3DIV, n=2; p= 0.98 for 7DIV, n=6, p=0.63 for 10DIV, n=4). **b:** Number of GluR2 positive puncta per IHC in 3DIV, 7DIV and 10DIV cultures; (p=0.93 for 3DIV, n=2; p=0.39 for 7DIV, n=8; 0.97 for 10DIV, n=4). There was no significance in the number of CtBP2 or GluR2 puncta at 3DIV, 7DIV or 10DIV between OS and control cultures. Red; Cultures stimulated by optogenetics, Blue: Controls. DIV; Days *in vitro*; All cultures prepared at P7. n number signifies the number of cochleae used for culturing.

Two-way ANOVA with Welch correction showed no statistical significance for CtBP2 positive puncta numbers for each stage of culturing respectively, i.e., 3 days, 7 days and 10 days in culture.

For 3 days, the p value was 0.96 between OS and control cultures; for 7 days, the p value was 0.98 between OS and control cultures; for 7 days, the p value was 0.63 between OS and control cultures. It is important to note that there was large deviation in the readings for the control cultures at 10DIV, which could have affected these statistics.

Similarly, GluR2-positive puncta were quantified and the count per IHCs was calculated (graph 3.4.b). The mean number of GluR2-positive puncta for 3DIV cultures was 11.0(±9.0, n=2) for OS cultures and 12.0(±15.0, n=2) for controls. For the 7DIV, the number of GluR2 positive puncta for OS cultures were 7.0 (±7.0, n=6) and 12.0(±14.0, n=8) for controls. For 10DIV, the number of GluR2 puncta for OS cultures was 8.0(±8.0, n=5) and 7.0(±3.0, n=4) for controls. Unsurprisingly, two-way ANOVA with Welch correction did not suggest any significant difference between OS and control numbers for each stage of culturing respectively. For 3 days, the p value was 0.93 between OS and control cultures; for 7 days, the p value was0.39 between OS and control cultures; for 10 days the p value was 0.97 between OS and control cultures.

Additionally, OS and control cultures at 10DIV showed a slightly diffused appearance in images (figure 3.3.q-x). At first glance, the puncta appeared to be present normally, but upon inspection using ARIVIS analysis software, they were relatively difficult to quantify and properly evaluate. In some cases, the GluR2-positive puncta appeared slightly 'diffused' and not fully punctate in appearance. However, the comparative ratio of diffused to punctate GluR2 positive puncta was not calculated at this point.

To gain further insight into ribbon synapse development during optogenetic stimulation, the volume of CtBP2, and Glur2 positive puncta was calculated (graph 3.5.). If cultures were driven towards maturation, then the volume of CtBP2 positive puncta would progressively increase, signifying active fusion of smaller ribbons into bigger, membrane attached ribbons at the AZ.

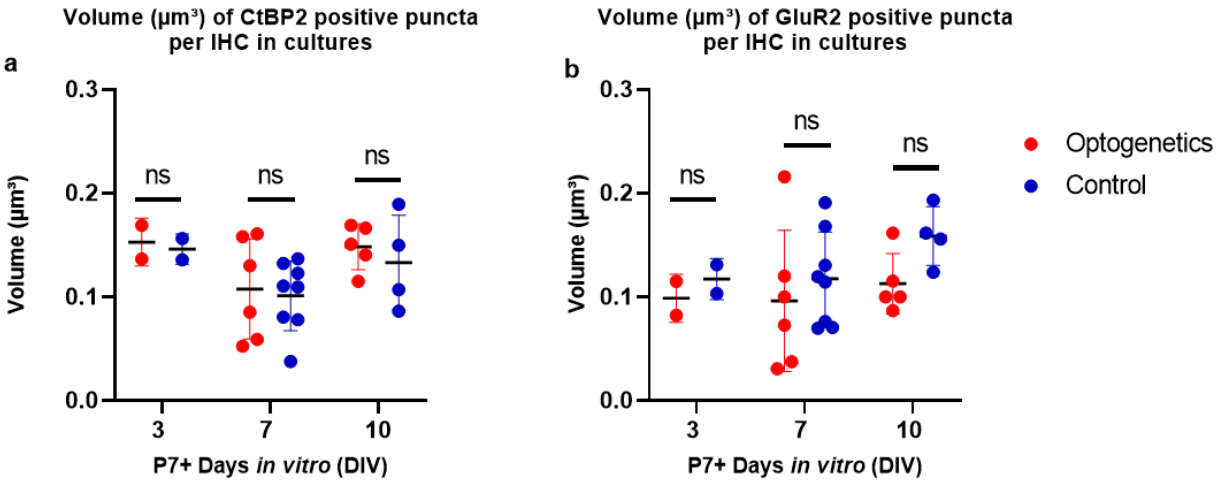

Graph 3.5 Shows volume (in µm^3) of CtBP2 and GluR2 positive puncta in cultures stimulated by either optogenetics (OS cultures) or controls (no optogenetic stimulation applied) at P7+3 DIV, P7+7 DIV and P7+10 DIV.

a: Volume (in µm^3) of CtBP2 positive puncta per IHC in 3 DIV, 7 DIV and 10 DIV cultures (p=0.77 for 3DIV, n=2; p=0.78 for 7DIV, n=6; p=0.57 for 10DIV, n=4).; **b:** Volume (in µm^3) of GluR2 positive per IHC in 3 DIV, 7 DIV and 10 DIV cultures p=0.48 for 3DIV, p=0.52 for 7DIV, p=0.05 for 10DIV). There was no significance in the volumes of CtBP2 or GluR2 positive puncta between OS and control cultures. Red; Cultures stimulated by

optogenetics, Blue: Controls. DIV; Days *in vitro*; All cultures prepared at P7. n number signifies the number of cochleae used for culturing.

The volume of CtBP2 positive puncta was measured in μm^3 for both OS cultures and controls (graph 3.5.a). For OS cultures, the volume at 3DIV was 0.15μm^3 (±0.02, n=2), and for controls was 0.15μm^3(±0.01, n=2). At 7DIV, the volume for OS cultures was 0.11 μm^3(±0.05, n=6) and for controls was 0.10μm^3(±0.03, n=8). At 10DIV, the volume was 0.15μm^3(±0.02, n=5) for OS cultures and 0.13μm^3(±0.05, n=4) for controls. Again, two-way ANOVA with Welch correction to compare the volume of CtBP2 positive puncta for OS cultures with controls respectively for each stage of culturing separately (i.e., 3 days, 7 days and 10 days in culture) did not illustrate a significant difference between the volumes of OS cultures and controls. For 3 days, the p value was 0.77 between OS and control cultures; at 7 days in culture, the p value was 0.78 for OS and control cultures; at 10 days, the p value was 0.57 between OS and control cultures. We could postulate that, since the individual volumes of ribbons did not increase significantly, it suggests that ribbon fusion likely did not take place in cultures the way that it would during normal development.

Similarly, the volume of GluR2 positive puncta was also calculated (graph 3.5.b). As mentioned previously, the volume of GluR2 positive puncta increases in the first postnatal week and stabilizes around hearing onset. For 3DIV, the volume for GluR2 positive puncta was 0.10μm^3 (±0.02, n=2) for OS cultures and 0.12μm^3 (±0.02, n=2) for controls. At 7 DIV, the volume was 0.10μm^3 (±0.07, n=6) for OS cultures and 0.12μm^3 (±0.05, n=8) for controls. At 10 DIV, the volume was 0.11μm^3 (±0.03, n=5) for OS cultures and 0.16μm^3 (±0.03, n=4) for controls. For both, OS and control cultures, the volumes of GluR2 positive puncta appeared consistent in all three different time intervals. In contrast to these values, the mean volume of GluR2 positive puncta per IHC at P7 was 0.13μm^3(± 0.04), and at P15, was 0.27μm^3 (±0.16). Predictably, two-way ANOVA with Welch correction did not show a significant difference between the OS and control conditions for this experiment for each stage respectively. For 3 days in culture, p value was 0.48 between OS and controls; for 7 days in culture, the p value was 0.52 between OS and controls; for 10 days in cultures, the p value was 0.05 between OS and control cultures.

The ratio of CtBP2 and GluR2 puncta was also calculated. As explained in 3.1, we would expect that if the cultures were driven towards maturation, the ratio of ribbons vs afferents would be higher in 3DIV cultures, and progressively decrease in 7DIV and 10DIV cultures, trending towards a ratio of closer to 1.0.

For 3DIV (graph 3.6.a.), the ratio of CtBP2 vs. GluR2 positive puncta was 1.1 (±1.1, n=2) for OS cultures and 0.9(±1.0, n=2) for controls. For 7 DIV, the ration was 0.6(±0.4, n=6) for OS cultures and 0.8(±0.5, n=8) for controls. For 10 DIV, the ratio was 1.0(±1.2, n=5) for OS cultures and 1.5(±1.6, n=4) for controls. Two-way ANOVA with Welch correction did not reveal any significance between the OS and control conditions for each time stage respectively. For 3 days in culture, the p value was 0.9 between OS and control; for 7 days in culture the p value was 0.5; for 10 days in culture, the p value was 0.61 between OS and control cultures.

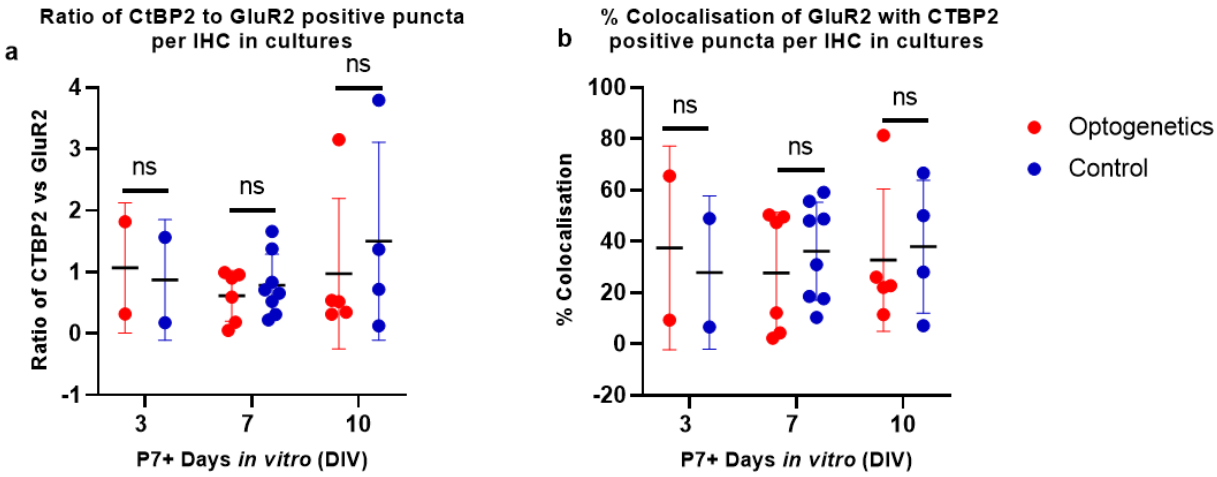

Graph 3.6 Shows the ratio and colocalization of CtBP2 and GluR2 positive puncta in cultures stimulated by either optogenetics (OS cultures) or controls (no optogenetic stimulation applied) at P7+3 DIV, P7+7 DIV and P7+10 DIV.

a: Ratio of CtBP2 and GluR2 positive puncta per IHC in 3 DIV, 7 DIV and 10 DIV cultures (p=0.87 for 3DIV, n=2; p=0.49 for 7DIV, n=6; p=0.61 for 10DIV, n=4).; **b:** Colocalization

percentage of CtBP2 and GluR2 positive puncta per IHC in 3 DIV, 7DIV and 10 DIV cultures (p=0.81 for 3DIV, n=2; p=0.49 for 7DIV, n=6; p=0.78 for 10DIV, n=4). There was no significance in the ratio or colocalization of CtBP2 and GluR2 positive puncta between OS and control cultures. Red; Cultures stimulated by optogenetics, Blue: Controls. DIV; Days *in vitro*; All cultures prepared at P7. n number signifies the number of cochleae used for culturing.

The colocalization between CtBP2 and Glur2 positive puncta was also calculated (graph 3.6.b.). As mentioned previously, the percentage of colocalization is low in the first postnatal week and increases consistently until it stabilizes around hearing onset. We would expect that if IHCs in culture were driven towards maturation due to optogenetics, the colocalization between the CtBP2 and GluR2 positive puncta would be lower at first in the 3DIV cultures, and increase in 7DIV and 10DIV cultures, indicating the maturation of synaptic connections between ribbons and type I afferents.

For 3DIV, the colocalization was 37.5% (±39.7, n=2) for OS cultures and 27.8% (±30.0, n=2) for controls. At 7DIV, the colocalization was 27.6% (±23.7, n=6) for OS cultures and 36.0% (±19.0, n=8) for controls. For 10DIV, it was 32.7% (±27.7, n=5) for OS cultures and 38.0% (±26.0, n=4) for controls. Although the values between OS and controls between 3DIV and 7DIV appeared distinct, two-way ANOVA with Welch correction did not show any significance between the OS and control conditions for either time interval respectively. For 3 days in culture, the p value was 0.81 between OS and control cultures; for 7 days, the p value was 0.49 between OS and control cultures; for 10 days, the p value was 0.78 between OS and control cultures. This indicates that the application of optogenetics in the presence of normal media without additional supplementation of growth factors did not showcase any significant developments within the IHCs.

3.2.3. Supplementation of growth factors in cultures with optogenetic stimulation

Cultures were prepared from mice cochleae at P7 were placed in media supplemented with NT-3 (10ng/ml), BDNF (10ng/ml) and T3(1.8ng/ml). The cultures were provided with extrinsic optogenetic stimulation. Cochleae from the contralateral ear were placed in culture without optogenetic stimulation (control). Cultures were fixed with paraformaldehyde and immunostained at two intervals: P7+3DIV and P7+7DIV (3DIV and 7DIV, giving the cochleae a total age of P10 and P14). Cultures were immunostained for CtBP2 and GluR2 to visualise the synaptic ribbons and postsynaptic afferents respectively. CtBP2- and GluR2-positive puncta were quantified for each condition. Images of the apical coil were acquired at the 9–12kHz region for each condition. Figure 3.4. shows confocal images of the immunostained cultures. CtBP2 and GluR2 positive puncta were observed and quantified for number of CtBP2/GluR2 puncta, volumes of CtBP2/GluR2 puncta, ratio of CtBP2 vs GluR2 puncta numbers and percentage colocalization of CtBP2/GluR2 positive puncta.

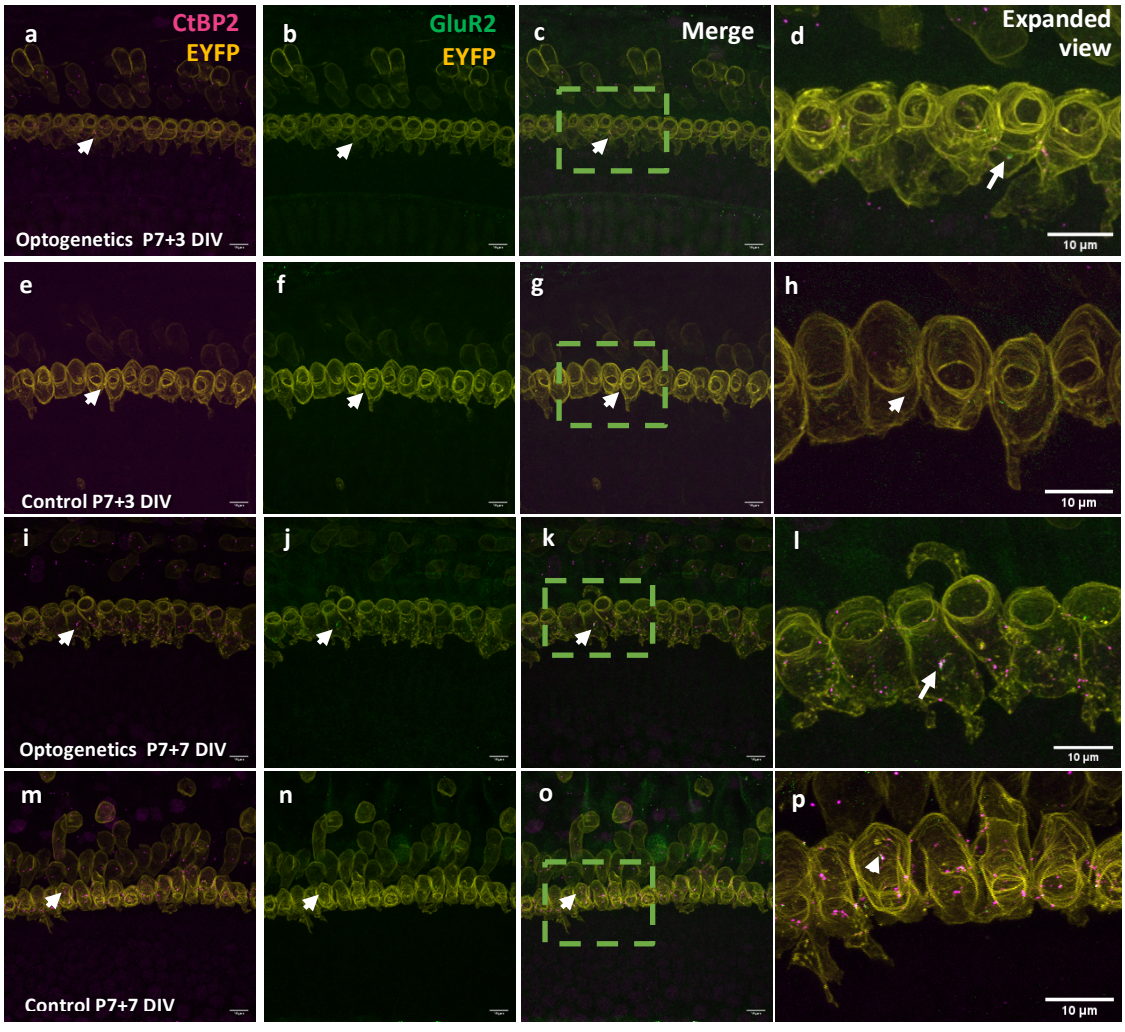

Figure 3. 4 **Shows the staining of CtBP2 and GluR2 positive puncta in cultures at P7+3 DIV and P7+7 DIV supplemented with growth factors provided with optogenetic stimulation and controls (with no optogenetic stimulation applied).**

Growth factors used were: NT-3 (10ng/ml), BDNF (10ng/ml) and T3(1.8ng/ml). All images taken at the 9–12kHz region for each condition; Graphs show the quantification of CtBP2 and GluR2 per IHC for each condition. Images for each day in culture show CtBP2 positive puncta and EYFP, GluR2 positive puncta and EYFP, and merged images for CtBP2 and GluR2 positive puncta with EYFP. The cultures were imaged at 3- and 7 days *in vitro*, after either being optogenetically stimulated (OS) or maintained without optogenetic stimulation (control). a, e, i, m: CtBP2 positive puncta with EYFP; b, f, j, n: GluR2 positive puncta with EYFP: c, g, k, o: Merged image showing CtBP2 and GluR2 positive puncta with EYFP; d, h, l, p: expanded view of merged image; Images at 63x. Magenta: CtBP2; Green: GluR2; Yellow: EYFP. Green box indicates expanded area; Arrows point to CtBP2/GluR2 puncta; DIV; Days *in vitro*; All cultures prepared at P7; Scale bar: 10*μm*. n=2 for P7+3; n=3 for P7+7.

The number of CtBP2 positive puncta for OS cultures (graph 3.7.a.) at 3 DIV was 3.0 (± 4.0, n=2) per IHC and for control cultures was 10.0 (± 11.0, n=2). For 7 DIV cultures, the number of CtBP2 positive puncta for OS cultures is 9.0 (± 3.0, n=3) per IHC and control culture was 11.0 (± 4.0, n=3). Two-way ANOVA with Welch correction did not show any significance between the OS and control cultures for each stage of culture respectively. For 3 days, the p value was 0.53 between OS and control cultures; for 7 days, the p value was 0.69 between OS and control cultures.

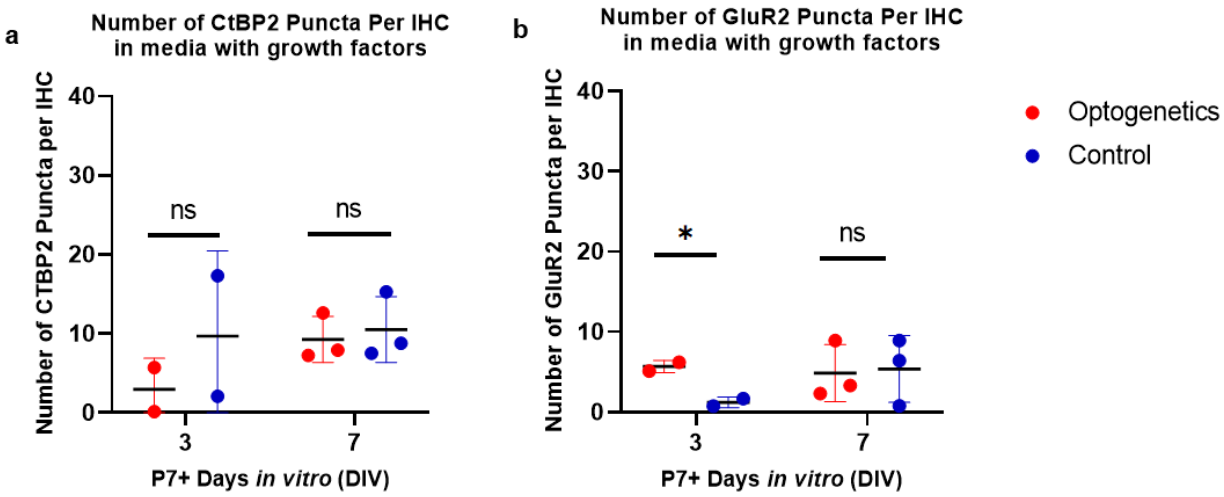

Graph 3.7 Number of CtBP2 and GluR2 positive puncta in media supplemented with growth factors provided with optogenetic stimulation and controls (with no optogenetic stimulation applied) at P7+3 DIV and P7+7 DIV;

a: Number of CtBP2 positive puncta per IHC in 3 DIV and 7 DIV cultures; (p=0.53 for 3 DIV cultures, n=2; p=0.69 for 7 DIV cultures, n=4). **b:** Number of GluR2 positive puncta per IHC in 3 DIV and 7 DIV cultures; (p=0.03 for 3 DIV cultures, n=2 p=0.88, n=3). (*****) Is significant at $p<0.05$; There was no significance in the number of CtBP2 puncta at 3DIV and 7 DIV. There was a significant difference between GluR2 positive puncta between OS and control cultures at 3 DIV ($p<0.05$), but not at 7 DIV; DIV; Red; Cultures stimulated by optogenetics, Blue: Controls; Days *in vitro*; All cultures prepared at P7. n number signifies the number of cochleae used for culturing.

GluR2 positive puncta values were also quantified for these cultures (graph 3.7.b). For OS cultures, there were 7.0 (±0.8, n=2) puncta per IHC for 3 DIV. For controls, there are 1.0(±0.7, n=2) puncta per IHC. For 7 DIV, there were 5.0 (±3.6, n=3) puncta per IHC for OS cultures and 5.0(±4.0, n=3) for control cultures. Two-way ANOVA with Welch correction at 3 DIV cultures showed significant difference between OS and control values (p=0.03), but not for 7 DIV (p=0.88 between OS and controls).

The volume of CtBP2 positive puncta (graph 3.8.a) in 3DIV cultures was 0.08µm^3 (±0.11, n=2) for OS cultures and 0.10(±0.04, n=2) for controls. For 7 DIV cultures, the volume was 0.12µm^3 (±0.03, n=3) for OS cultures and 0.10µm^3 (±0.04, n=3) for control cultures. Two-way ANOVA with Welch correction found no significant difference between the OS and control cultures for respective stages of cultures. For 3 days, the p value was 0.88 between OS and control cultures; for 7 days the p value was 0.59 between OS and control cultures. This suggests that the addition of growth factors on cultured IHCs has no effect on the quantity of synaptic ribbons or their size.

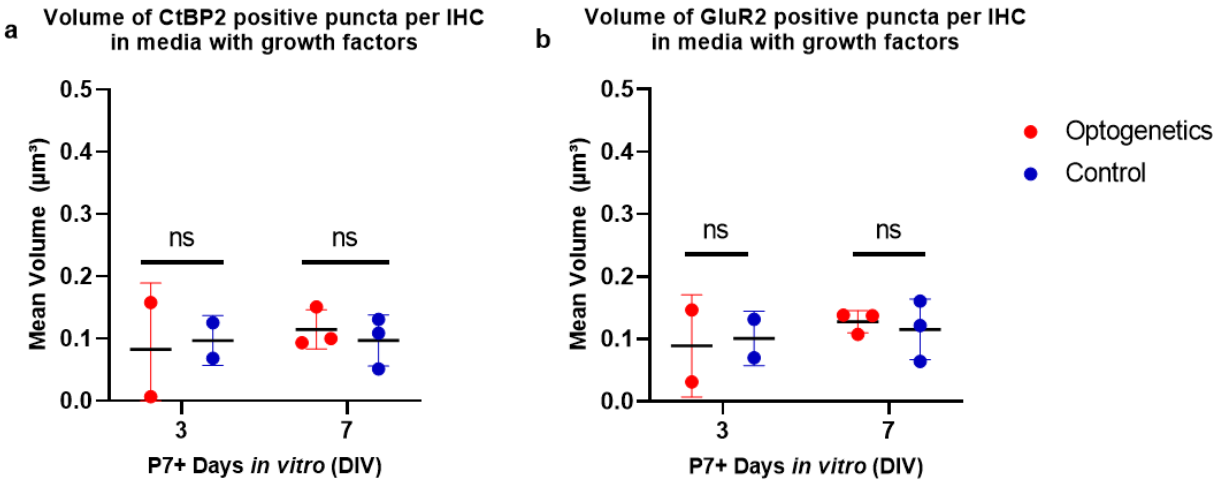

Graph 3.8 Volume (µm^3) of CtBP2 and GluR2 positive puncta in media supplemented with growth factors provided with optogenetic stimulation and controls (with no optogenetic stimulation applied) at P7+3 DIV and P7+7 DIV.

a: Volume (µm^3) of CtBP2 positive puncta per IHC in 3DIV and 7DIV cultures (p=0.88 for 3 DIV, n=2; p= 0.59 for 7 DIV, n=3).; **b:** Volume (µm^3) of GluR2 positive puncta per IHC in 3DIV and 7 DIV cultures (p=0.88 for 3 DIV, n=2; p= 0.72 for 7 DIV, n=3); There was no significance in the volume of CtBP2 with GluR2 positive puncta between OS and control cultures. Red; Cultures stimulated by optogenetics, Blue: Controls; DIV; Days *in vitro*; All cultures prepared at P7. n number signifies the number of cochleae used for culturing.

The volume of GluR2 positive puncta (graph 3.8.b) in 3DIV cultures was 0.10μm^3 (±0.08, n=2) for OS cultures, and 0.10μm^3 (±0.04, n=2) for controls. For 7 DIV cultures, the volume was 0.13μm^3 (±0.02, n=3) for OS cultures and 0.12μm^3 (±0.05, n=3) for controls. Two-way ANOVA with Welch correction found no significant difference between the OS and control cultures within each respective stage of culturing. The p value for cultures between OS and controls at 3 days was 0.88; and for 7 days, the p value was 0.72 between OS and control cultures.

The ratio of CtBP2 puncta to GluR2 puncta (graph 3.9.a) on 3 DIV is 20.7 (±28.0, n=2) for OS cultures and 0.2 (±0.2, n=2) for controls. For 7 DIV cultures, the ratio is 0.6 (±0.5, n=3) for OS cultures and 0.5 (±0.4, n=3) for controls. Two-way ANOVA with Welch correction found no significant difference between the OS and control cultures within each stage of culturing. For 3 days, the p value was 0.5 between OS and control cultures: for 7 days, the p 0.83 between OS and control cultures.

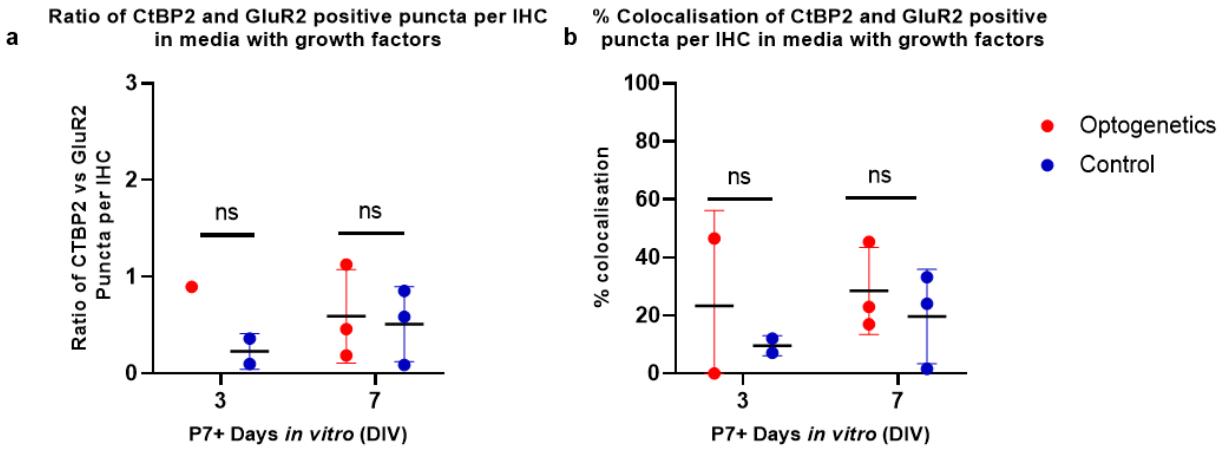

Graph 3.9 Ratio and colocalization of CtBP2 and GluR2 positive puncta in media supplemented with growth factors at P7+3DIV and P7+7DIV for optogenetically stimulated cultures and controls (not stimulated by optogenetics).

a: Ratio of CtBP2 with GluR2 positive puncta per IHC in 3DIV and 7DIV cultures (p=0.50 for 3DIV, n=2; p= 0.83 for 7DIV, n=3); **b:** Colocalization of CtBP2 with GluR2 positive puncta per IHC in 3DIV and 7 DIV cultures (p=0.66 for 3DIV, n=2; p= 0.53 for 7DIV, n=3).

There was no significance in the ratio or colocalization of CtBP2 with GluR2 positive puncta between OS and control cultures. Red; Cultures stimulated by optogenetics, Blue: Controls; DIV; Days *in vitro*; All cultures prepared at P7. n number signifies the number of cochleae used for culturing.

In longer cultures, they were predicted to have twice as many synapses as ribbons. As hearing onset approaches, this would then decrease to 1:1. At P7+7 DIV (P14 correlate), the was expected to reduce in the OS cultures. However, this was not the case in these cultures. Although the mean values shown here indicating some very slight reduction in the amount of GluR2 puncta over time. It has not yet been determined, though, if this can be called development per se or is merely the maintenance of SGNs.

Although there were slight variances in the colocalization percentages between the 3 DIV and 7DIV cultures, these differences were not statistically significant (graph 3.9.b). In the 3DIV cultures, the colocalization percentage was 23.0%(±33.0, n=2) for OS cultures and 10.0%(±3.5, n=2). For 7DIV cultures, the colocalization percentage was 28.0%(±15.0, n=3) for OS cultures and 20.0%(±16.0, n=3) for control cultures. Two-way ANOVA with Welch correction found no significant difference between the OS and control cultures when comparing colocalization between CtBP2 and GluR2 positive puncta between the respective stages of culturing. For 3 days, the p value was 0.66 between OS and control cultures; for 7 days, the p value was 0.53 between OS and control cultures.

This is an intriguing finding since, despite literature that makes it clear that growth factors are essential for maintaining cultures(He *et al.*, 2003; Wang and Green, 2011; Wan *et al.*, 2014). When we examined the cultures' development, we were unable to detect any signs of developmental maturation. It is significant to notice that the cultures did not exhibit morphological distress or symptoms of degeneration, as was the case with 10 DIV cultures, for instance.

3.3. Discussion

In this chapter, we explored the effect of optogenetic stimulation of neonatal cochlea cultures over the period of 10 days without the addition of any supplemental factors to the growth media. The cultures were then investigated for readouts of maturation against cultures that did not receive any stimulation (controls). We aimed to establish a baseline for these readouts to assess any changes that the cultures would exhibit without any supplemental factors in the growth media (Normal growth media; NM).

We therefore initially cultured cochleae under only two specific conditions – with optogenetic stimulation (OS) and without optogenetic stimulation (control). We aimed to observe the cultures at intervals of 3 days (P7+3DIV), 7 days (P7+7DIV), and 10 days (P7+10DIV).

After culturing for 10 days, we expected to observe a decrease in the number of ribbons per IHC. However, this was not observed. We also did not see any differences in the volume of ribbons after 10DIV. Similarly, there was no significant change in the number of GluR2 positive puncta in both, OS and control cultures. GluR2 puncta volume remained consistent in both OS and control cultures, with no difference between the two conditions. This was confirmed with two-way ANOVA with Welch correction, which showed no significant difference between OS and controls in either condition within the specified stages of culturing respectively.

Therefore, it might be hypothesised that the cultures were "stuck" on fundamental cellular maintenance (or housekeeping) and lacked the physiological or molecular signalling to develop any further. We can speculate that prolonged culturing without the addition of exogenous factors such as growth factors could have a negative effect on the overall health of the cultured tissue (Brandt *et al.*, 2007; Ubaidah *et al.*, 2015; Sharlin *et al.*, 2018; Gao *et al.*, 2020).

According to the results of these experiments, optogenetics alone, when applied to the cultures, was insufficient to produce any discernible IHC maturation indicators. Evidently, we acknowledged that the cultures might require additional components supplemented into the growth media to facilitate maturation. Consequently, this is indeed established for us, a baseline for cultures that were grown

without supplementary factors. Any following experiments could be compared to these data to provide a more accurate picture of any effect the supplemental factors would have on the cultures.

It was also decided that, for the interest of tissue morphology, we would only grow cultures until P7+7DIV, due to the diffused appearance of GluR2 puncta at 10 DIV. It was seen morphologically that cultures kept for 10 days (10DIV) were morphologically deformed and the hair bundles on the cells were not clearly visible. This indicated that we look at cultures only until 7 DIV as keeping them for 10 days was not conducive to IHC health overall, even if they remain alive.

Since optogenetic stimulation alone was insufficient to promote IHC maturation, we incorporated exogenous growth factors in conjunction with optogenetics to the cultures, as a means of facilitating hair cell maturation.

Cultures were supplemented with the growth factors NT-3 (10ng/ml), BDNF (10ng/ml), and T3(1.8ng/ml), which have been well-documented for their roles in neurodevelopment (He *et al.*, 2003; Wang and Green, 2011; Wan *et al.*, 2014; Schwieger *et al.*, 2015; Sharlin *et al.*, 2018; Williamson *et al.*, 2020), and checked whether they would contribute to hair cell maturation in the cultures. Specifically, the preservation of synaptic contacts between IHCs and type I afferents was assessed.

We postulated that the utilisation of these growth factors would assist the long-term maintenance of afferent synapses in the cultured cochleae. We also wanted to evaluate whether there would be an increase in the total volume of ribbons in older cultures (10DIV). However, we did not observe any significant hallmarks of maturation in either OS or control cultures. Given the outcomes of these experiments, the application of optogenetics with exogenous growth factors in the cultures was inadequate to elicit any identifiable characteristics of IHC maturation.

4. Investigating the Role of Ca^{2+} in IHC Development Using Optogenetics

3.4. Introduction

Following dissection, cochleae from neonatal mouse pups at P7 were cultured and maintained for a maximum of 7 days *in vitro* (7DIV). The cultures were provided with extrinsic optogenetic stimulation using an LED setup (λ=470 nm; refer methods chapter 2.4). Cochleae from the contralateral ear of the same pup were cultured without optogenetic stimulation (control). Cultures were then fixed and immunostained for CtBP2 and GluR2 at regular intervals. The readouts considered for this experiment were similar to the previous chapter i.e., the quantification of CtBP2-and GluR2-positive puncta.

Spontaneous action potential (AP) activity in the developing cochlea is Ca^{2+} driven. IHCs generate Ca^{2+} spikes mediated by L-type Ca^{2+} channels ($Ca_v 1.3$), which result in the release of glutamate at the IHC ribbon synapse (as explained in the introduction chapter 1.3). Ca^{2+} has multiple essential functions in IHCs. It regulates neurotransmitter release at the hair cell synapse as well as frequency selectivity. Ca^{2+} signalling is also essential for the normal development of the cochlea, in both, sensory and non-sensory cells.

The concentration of Ca^{2+} in the endolymph during postnatal development differs greatly from the adult endolymph. In the prehearing stages (<P12), the endolymphatic concentration of Ca^{2+} has been estimated to be around 0.3mM (Johnson *et al.*, 2012), whereas the Ca^{2+} concentration in the adult endolymph is 0.02 mM (Bosher *et al.*, 1978). The low Ca^{2+} concentration in the endolymph increases the resting mechanotransducer current, which causes the membrane potential to depolarise, causing the generation of spontaneous APs in inner hair cells. The activity lasts until the fast activating large conductance Ca^{2+} activated K^+ (BK) current and delayed rectifier $I_{K,n}$ takes over (Kros *et al.*, 1998; Marcotti *et al.*, 2003).

In contrast, the perilymph, has a constant Ca^{2+} concentration of at 1.3mM. Extracellular Ca^{2+} is known as a blocker of the mechanotransducer channel (Marcotti *et al.*, 2005). The growth media generally used for culturing cochleae usually maintains the perilymphatic concentration.

We therefore wanted to evaluate the effect of optogenetic stimulation on cultures grown in media using the physiological endolymphatic concentration of Ca^{2+} (0.3mM). We expected the low Ca^{2+}

concentration to mimic the *in vivo* endolymphatic environment, and indirectly drive functional maturation. Culture media was supplemented with HEDTA (hydroxyethyl ethylenediamine triacetic acid trisodium salt), to chelate Ca^{2+} ions (as stated in materials and methods; Durham, 1983).

As extracellular Ca^{2+} is known to be a blocker of the mechanotransducer channel, we also wanted to evaluate the effect of higher concentration of Ca^{2+} on the cultures. We therefore supplemented the growth medium with $CaCl_2$ to increase the total concentration of the media to 5mM Ca^{2+}. We then evaluated the same criteria for the cultures (CtBP2 and GluR2 puncta).

4.2. Results

4.2.1. Investigating the effect of 0.3mM Ca^{2+} in growth media on cultures

For investigating the possible direct role of Ca^{2+} in cochlear IHC development in vitro, we used HEDTA to chelate the Ca^{2+} ions in the media, resulting in the final free Ca^{2+} concentration of 0.3mM. Cochleae from postnatal mice (P7) were cultured and maintained for a maximum of 7days (7DIV). Cultures were provided with optogenetic stimulation (OS). Contralateral cochleae from the same pup were cultured without optogenetic stimulation (control). Cultures were fixed at P7+3DIV and P7+7DIV and immunostained for CtBP2 and GluR2. Images of the apical coil were acquired at the 9–12kHz region for each condition (Figure 4.1).

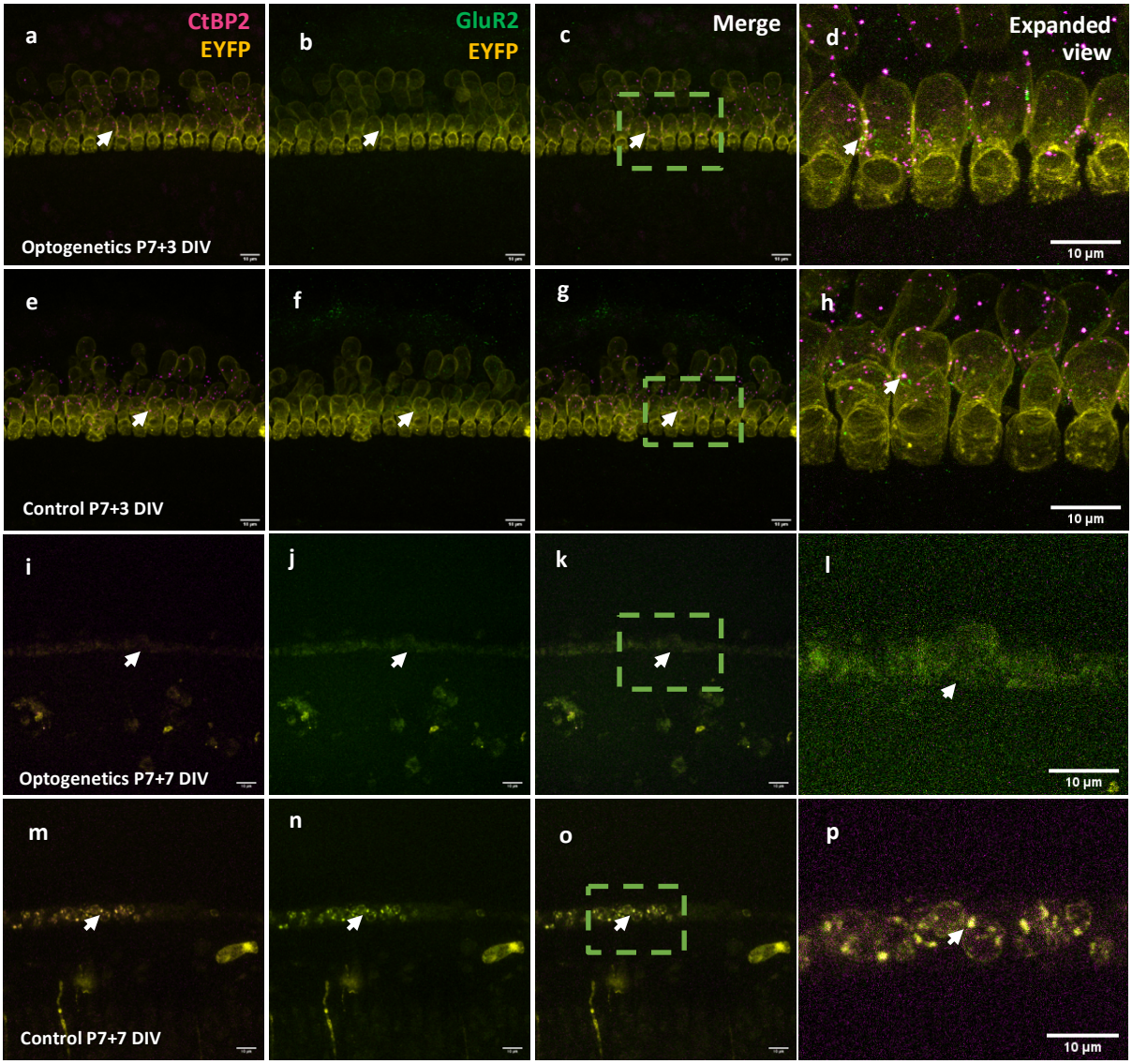

Figure 4.1 Shows the staining of CtBP2 and GluR2 puncta in cultures with 0.3mM Ca^{2+} at P7+3 DIV and P7+7 DIV provided with optogenetic stimulation and controls (with no optogenetic stimulation applied).

All images taken at the 9–12kHz region. Graphs show the quantification of CtBP2 and GluR2 per IHC for each condition. Images for each day in culture show CtBP2 positive puncta and EYFP, GluR2 positive puncta and EYFP, and merged images for CtBP2 and GluR2 positive puncta with EYFP. The cultures were imaged at 3- and 7 days *in vitro*, after either being optogenetically stimulated (OS) or maintained without optogenetic stimulation (control). a, e, i, m: CtBP2 positive puncta with EYFP; b, f, j, n: GluR2 positive puncta with EYFP: c, g, k, o: Merged image showing CtBP2 and GluR2 positive puncta with EYFP; d, h, l, p: expanded view of merged image; Images at 63x. Magenta: CtBP2; Green: GluR2; Yellow: EYFP. Green box indicates expanded area; Arrows point to CtBP2/GluR2 puncta; DIV; Days *in vitro*; All cultures prepared at P7; Scale bar: 10*μm*. n=5 for P7+3.

We found that for cultures grown in media containing the physiological equivalent concentration of calcium (0.3mM), the number of CtBP2 puncta at 3 DIV was comparable in both, OS and control cultures, at an average value of 16.9(± 8.2, n=5) puncta per IHC for OS cultures and 18.6(± 12.2 n=5) puncta per IHC for controls. There was a large standard deviation in the individual puncta values for cultures in both OS and control conditions. The p value for 3 day cultures was 0.81 between OS and controls for CtBP2 positive puncta.

The number of GluR2 positive puncta at 3 DIV was 7.5(±5.7, n=5) puncta per IHC for OS cultures and 7.2 (± 5.8, n=5) puncta per IHC for controls. The p value for GluR2 positive puncta at 3 days was 0.93 between OS and control cultures. T-test with Welch correction found no significant difference between the OS and control values respectfully for both CtBP2 and GluR2 puncta for 3DIV cultures.

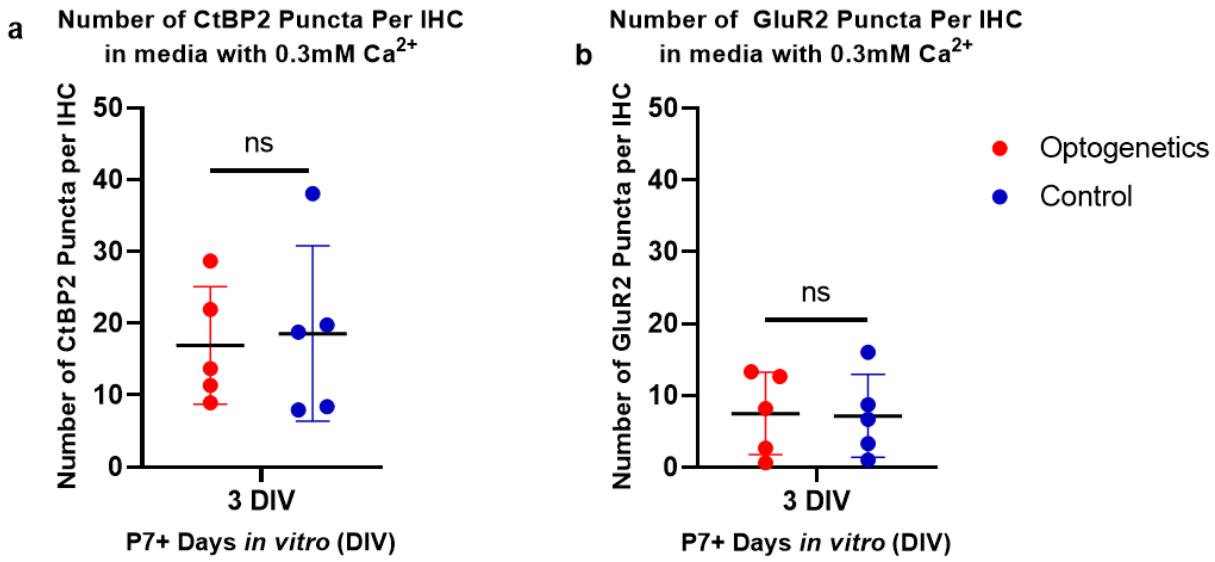

Graphs 4.1 Number of CtBP2 and GluR2 positive puncta in cultures with 0.3mM Ca^{2+} provided with optogenetic stimulation and controls (with no optogenetic stimulation applied) at P7+3 DIV;

a: Number of CtBP2 positive puncta per IHC in 3 DIV cultures (p=0.81, n=5); **b:** Number of GluR2 positive puncta per IHC in 3 DIV cultures (p=0.93, n=5). There was no significance in the number of CtBP2 or GluR2 positive puncta between OS and control cultures. Red; Cultures stimulated by optogenetics, Blue: Controls; DIV; Days *in vitro*; All cultures prepared at P7. n number signifies the number of cochleae used for culturing.

The volume of CtBP2 puncta also remained similar for OS and control cultures, averaging 0.17μm^3 (± 0.01, n=5) for OS cultures and 0.16μm^3 (±0.05, n=5) for controls. The volume of GluR2 puncta was 0.11μm^3(±0.05, n=5) for OS and 0.14μm^3 (±0.06, n=5) for control cultures. T-test with Welch correction found no significant difference between the OS and control volumes for both CtBP2 and GluR2 puncta at 3DIV. The p value for 3-day cultures was 0.68 for CtBP2 puncta; the p value for GluR2 positive puncta at 3 days was p=0.34 between OS and control cultures.

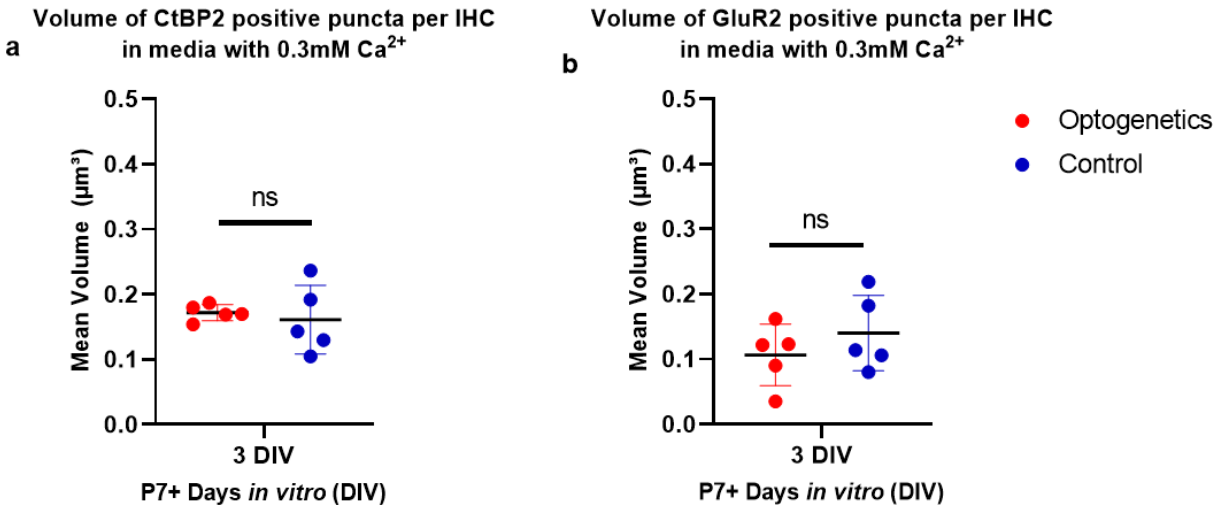

Graphs 4.2 Volume of CtBP2 and GluR2 positive puncta in cultures with 0.3mM Ca^{2+} provided with optogenetic stimulation and controls (with no optogenetic stimulation applied) at P7+3DIV;

a: Volume (μm^3) of CtBP2 positive puncta per IHC in 3DIV cultures (p=0.68, n=5); **b:** Volume (μm^3) of GluR2 positive puncta per IHC in 3DIV cultures (p=0.34, n=5). There was no significance in the volumes of CtBP2 or GluR2 positive puncta between OS and control cultures. Red; Cultures stimulated by optogenetics, Blue: Controls; DIV; Days *in vitro*; All cultures prepared at P7. n number signifies the number of cochleae used for culturing.

The ratio between CtBP2 and GluR2 puncta in the 3 DIV cultures was 0.4(± 0.2, n=5) for OS cultures and 0.5 (± 0.5, n=5) for controls. T-test with Welch correction found no difference between the OS and controls for CtBP2 and GluR2 positive puncta (p=0.75).

The percentage colocalization between CtBP2 positive puncta and GluR2 positive puncta was 27.5% (±18.0, n=5) for OS cultures and 27.5% (± 24.8, n=5) for control cultures. T-test with Welch correction found no difference between the OS and control cultures at 3DIV (p= 0.83).

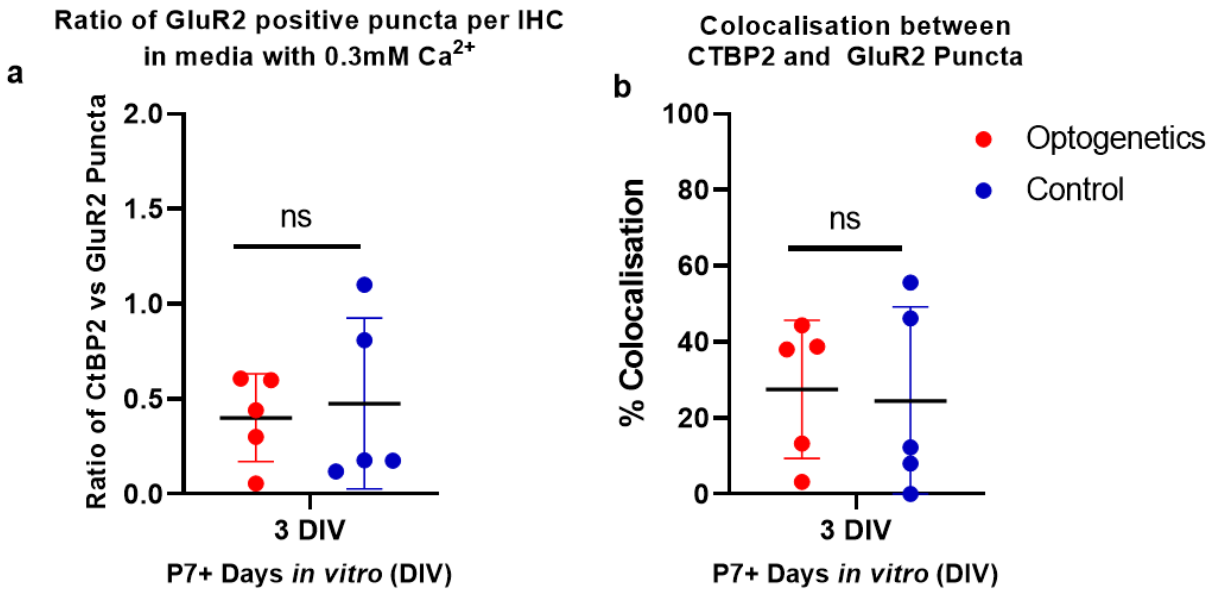

Graphs 4.3 Ratio and colocalization of CtBP2 and GluR2 positive puncta in cultures with 0.3mM Ca^{2+} provided with optogenetic stimulation and controls (with no optogenetic stimulation applied) at P7+3 DIV;

a: Ratio of CtBP2 with GluR2 positive puncta per IHC in 3DIV cultures (p=0.75, n=5); **b:** Colocalization of CtBP2 with GluR2 positive puncta per IHC in 3DIV cultures (p=0.83, n=5). There was no significance in the ratio or colocalization of CtBP2 with GluR2 positive puncta between OS and control cultures. Red; Cultures stimulated by optogenetics, Blue: Controls; DIV; Days *in vitro*; All cultures prepared at P7. n number signifies the number of cochleae used for culturing.

For the 7 DIV cultures, the morphology looked degenerated (**figure 4.1. i-p).** Figure 4.2. a-h shows additional images of P7+7DIV cultures at the 12–16kHz frequency region, with adjacent expanded views. The cultures showed no discernible IHCs. The supporting cells were visibly indistinguishable. Peculiarly, some CtBP2 and GluR2 puncta were still detectable in the images.

However, these puncta were not quantified, as the cell membranes themselves were not clear, so it was not possible to distinguish whether the puncta being counted were present inside or outside the cells. This has not been previously observed in literature. Previous attempts at mimicking the physiological concentration of calcium for evoking spontaneous APs have either used ex vivo preparations with extracellular media containing 0.3mM Ca^{2+} or have cultured adult IHCs with the media containing 0.3mM Ca^{2+}. Thus, this is a novel finding for the activity of immature IHCs *in vitro* with 0.3mM Ca^{2+} in media.

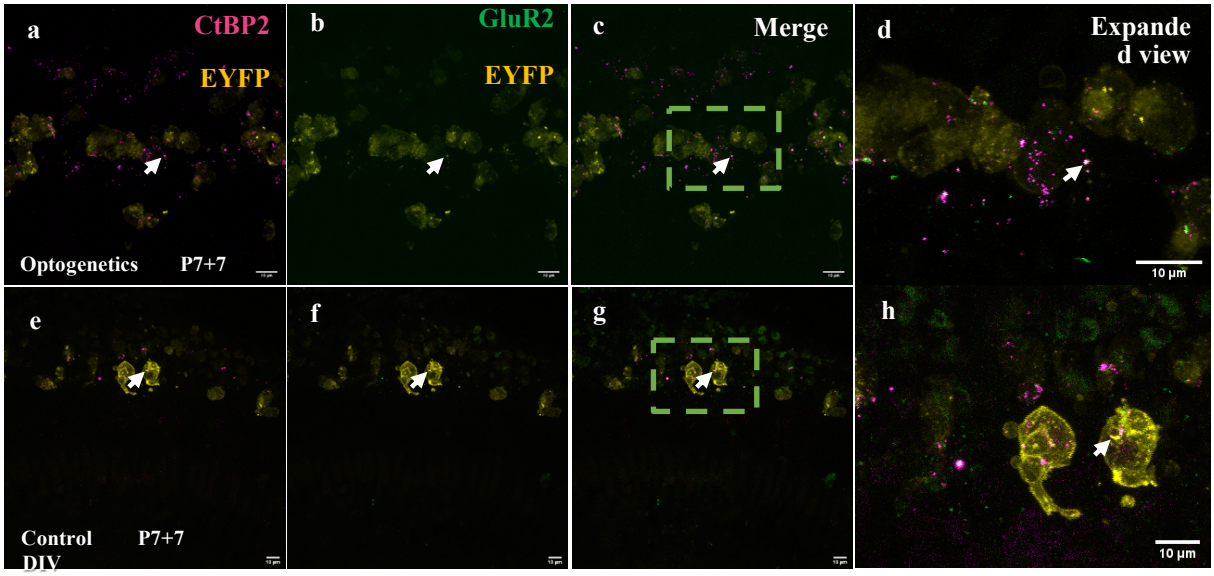

Figure 4.2 Shows the staining of CtBP2 and GluR2 puncta in cultures with 0.3mM Ca^{2+} at P7+7 DIV provided with optogenetic stimulation and controls (with no optogenetic stimulation applied).

Images show complete destruction of IHCs at P7+7DIV. Although some puncta are still visible, the tissue morphology is completely disrupted. All images taken at the 12–16kHz region. Images show CtBP2 positive puncta and EYFP, GluR2 positive puncta and EYFP,

and merged images for CtBP2 and GluR2 positive puncta with EYFP. a, e: CtBP2 positive puncta with EYFP; b, f: GluR2 positive puncta with EYFP: c, g: Merged image showing CtBP2 and GluR2 positive puncta with EYFP; d, h: expanded view of merged image; Images at 40x. Magenta: CtBP2; Green: GluR2; Yellow: EYFP. Green box indicates expanded area; Arrows point to CtBP2/GluR2 puncta; DIV; Days *in vitro*; All cultures prepared at P7; Scale bar: 10*μm*.

4.2.2. Blocking mechanotransducer current using 5mM Ca^{2+} shows no maturation in IHCs *in vitro*

We, wanted to evaluate whether reducing the open probability of the mechanoelectrical transducer channel through to prolonged exposure to a high concentration of Ca^{2+} in the growth media would cease the spontaneous AP firing, and whether it would show the similar results as observed in chapter 4.2.1. (with 0.3mM Ca^{2+}).

Cochleae from postnatal mice (P7) were cultured and maintained for a maximum of 7days (7DIV). Cultures were supplemented with 3.95µl/ml (for each ml of media) of 1M $CaCl_2$ to raise the total concentration of Ca^{2+} to 5mM *in vitro.* Cultures were provided with optogenetic stimulation (OS). Contralateral cochleae from the same pup were cultured without optogenetic stimulation (control). Cultures were fixed at P7+3 DIV, P7+5 DIV and P7+7DIV and immunostained for CtBP2 and GluR2. Images of the apical coil were acquired at the 9–12kHz region for each condition (figure 4.3.). Due to the results from the previous experiments (chapter 4.1.), which showed rapid degeneration of cultures at 7 DIV, we decided to use an additional time point at 5 DIV between the time points 3 DIV and 7 DIV for imaging and analysis.

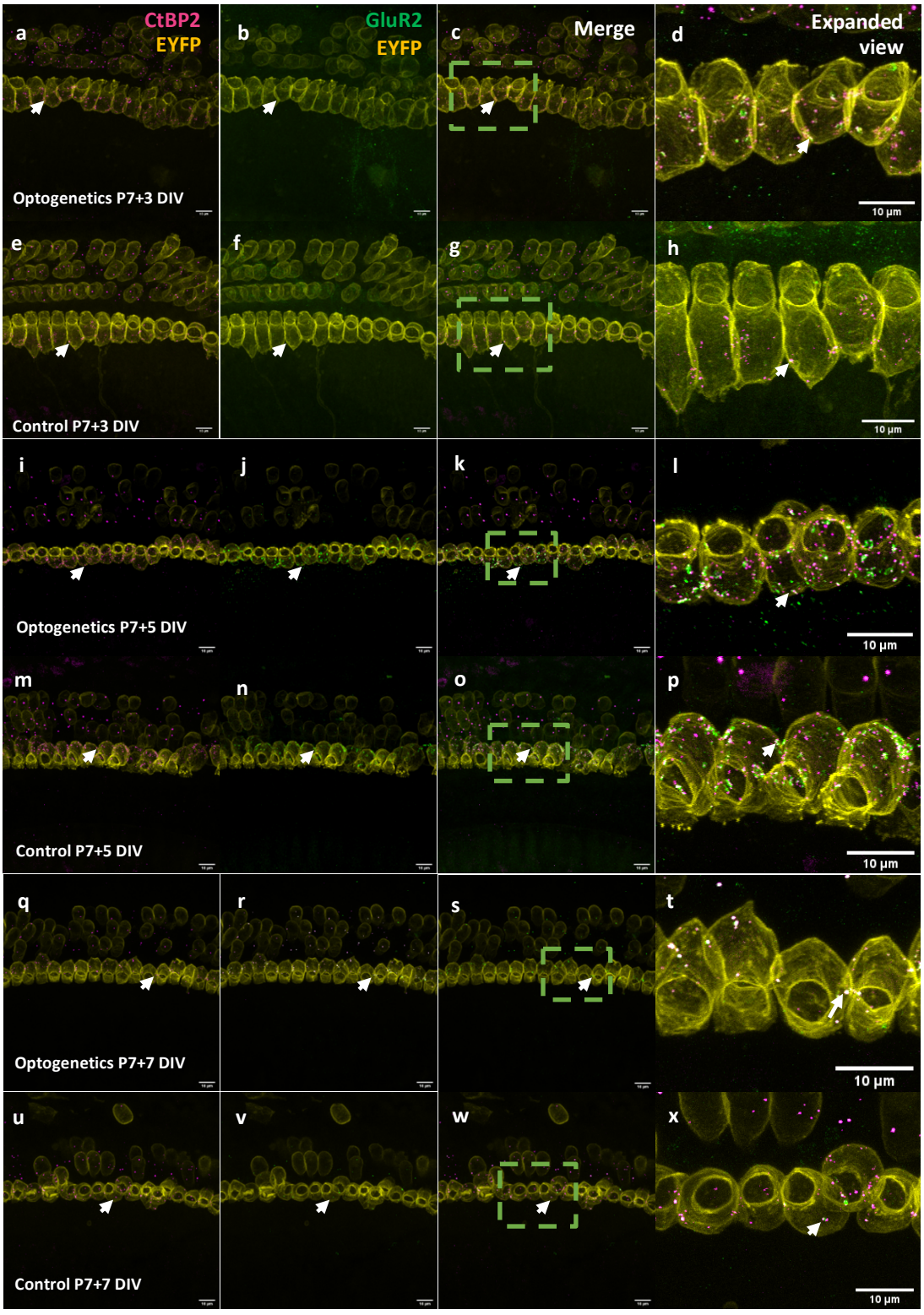

Figure 4.3 Shows the staining of CtBP2 and GluR2 puncta in cultures with 5mM Ca^{2+} at P7+3DIV, P7+5DIV and P7+7DIV provided with optogenetic stimulation and controls (with no optogenetic stimulation applied).

All images taken at the 9–12kHz region. Graphs show the quantification of CtBP2 and GluR2 per IHC for each condition. Images for each day in culture show CtBP2 positive

puncta and EYFP, GluR2 positive puncta and EYFP, and merged images for CtBP2 and GluR2 positive puncta with EYFP. The cultures were imaged at 3-, 5- and 7-days *in vitro*, after either being grown in 5mM Ca^{2+} with optogenetic stimulated (OS) or maintained without optogenetic stimulation (control). a, e, i, m, q, u: CtBP2 positive puncta with EYFP; b, f, j, n, r, v: GluR2 positive puncta with EYFP: c, g, k, o, s, w: Merged image showing CtBP2 and GluR2 positive puncta with EYFP; d, h, l, p, t, x: expanded view of merged image. Images at 63x. Magenta: CtBP2; Green: GluR2; Yellow: EYFP. Green box indicates expanded area; Arrows point to CtBP2/GluR2 puncta; DIV; Days *in vitro*; All cultures prepared at P7; Scale bar: 10*μm*.

The number of CtBP2 puncta in 3 DIV cultures is 28.0(±20.0, n=3) per IHC for OS and 9.0(±4.0, n=4) per IHC for controls. It is important to note that there was a large deviation in the individual values. For 5 DIV, the CtBP2 positive puncta number was 9.0 (±2.0, n= 3) for OS cultures and 7.0 for controls (±2.0, n=3). For 7 DIV the number of CtBP2 puncta was 11.0(±5.0, n=4) for OS and 7.0 (±3.0, n=4) for control cultures. Two-way ANOVA with Welch correction found no difference between the OS and controls for CtBP2 positive puncta for 3-, 5- and 7- days respectively. The p value for 3 days was 0.23 between OS and control cultures; the p value for 5 days was 0.48 between OS and control cultures; the p value for 7 days was 0.24 between OS and control cultures.

The number of GluR2 puncta at 3 DIV was 5.0(±5.0, n=3) per IHC for OS cultures and 3.0(±2.0, n=4) for controls. At 5 DIV, the number of GluR2 positive puncta for OS cultures was 7.0(±5.0, n=3) puncta per IHC and for control was 7.0 (±5.0, n=3) per IHC. For 7 DIV, the number of GluR2 puncta for OS at 7.0 (±1.0, n=4) and for controls was at 5.0(±6.0, n=4) per IHC. Two-way ANOVA with Welch correction did not show any significant difference between the OS and control numbers for each culture stage respectively. For 3 days, the p values is 0.50 between OS and control cultures; for 5 days, the p value is 0.97 between OS and control cultures; for 7 days, the p value is 0.60 between OS and control cultures.

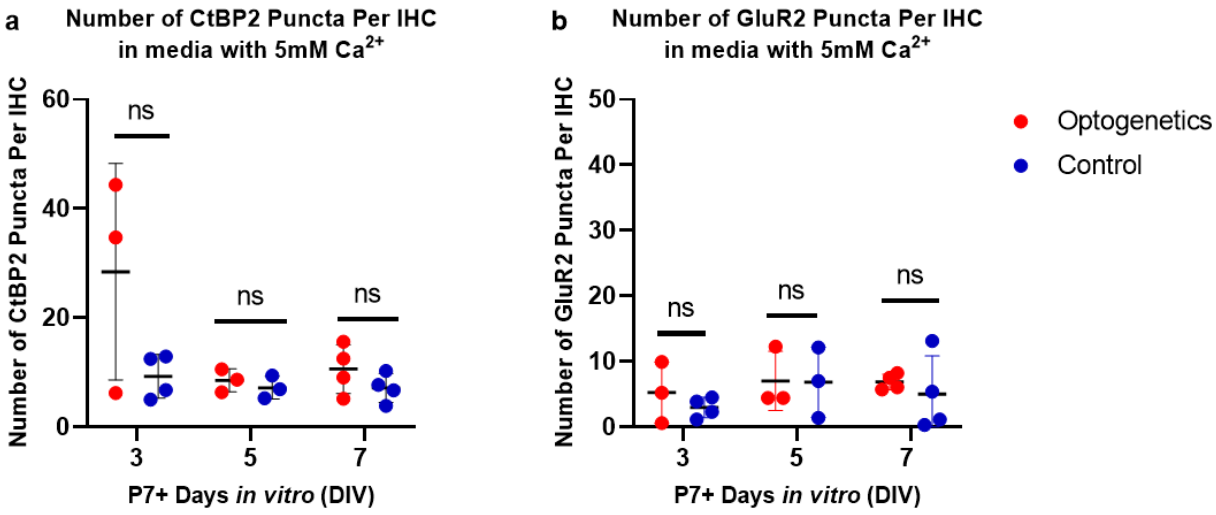

Graphs 4.4 Number of CtBP2 and GluR2 positive puncta in cultures with 5mM Ca^{2+} at P7+3 DIV, P7+5 DIV and P7+7 DIV; for optogenetically stimulated cultures and controls (not stimulated by optogenetics).

a: Number of CtBP2 positive puncta per IHC in 3 DIV, 5 DIV and 7 DIV cultures (p= 0.23 for 3 DIV, n= 3; p= 0.48 for 5 DIV, n=3; p= 0.24 for 7 DIV, n=4); **b:** Number of GluR2 positive puncta per IHC in 3 DIV, 5 DIV and 7 DIV cultures p= 0.50 for 3 DIV, n= 3; p= 0.97 for 5 DIV, n= 3; p= 0.60 for 7 DIV, n=4); There was no significance in the number of CtBP2 or GluR2 positive puncta between OS and control cultures. Red; Cultures stimulated by optogenetics, Blue: Controls; DIV; Days *in vitro*; All cultures prepared at P7. n number signifies the number of cochleae used for culturing.

The volume of CtBP2 per IHC for 3 DIV cultures was 0.14μm^3 (±0.01, n=2) for OS cultures and 0.13μm^3 (±0.02, n=2) for controls. For 5 DIV cultures, it was 0.08μm^3 (±0.02, n=3) for OS cultures, whereas the controls were at 0.09μm^3 (±0.04, n=3). At 7 DIV, the volume of CtBP2 puncta was similar, at 0.11μm^3 (±0.04, n=4) for OS cultures and 0.07μm^3 (±0.02, n=4) for controls.

Although we expected a statistical difference in the values presented, two-way ANOVA with Welch correction showed that there was no difference between the OS and controls within the same stage

of cultures respectively. At 3 days, the p value was 0.50 between OS and control cultures; at 5 days, the p value was 0.54 between OS and control cultures; at 7 days, the p value was 0.25 between OS and control cultures. This could be attributed to the large deviation from the mean for the individual CtBP2 puncta values.

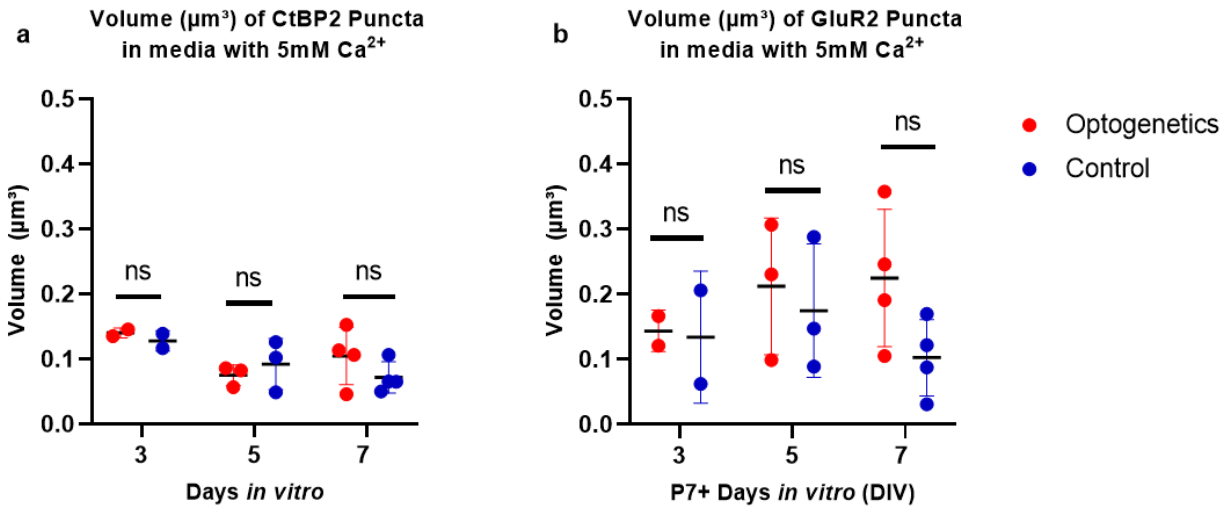

<u>Graphs 4.5</u> Shows volume (in µm^3) of CtBP2 and GluR2 positive puncta in cultures with 5mM Ca^{2+} at P7+3 DIV, P7+5 DIV and P7+7 DIV for optogenetically stimulated cultures and controls (not stimulated by optogenetics).

a: Volume (in µm^3) of CtBP2 positive puncta per IHC in 3 DIV, 5 DIV and 7 DIV cultures (p= 0.50 for 3 DIV, n= 2; p= 0.54 for 5 DIV, n= 3; p= 0.25 for 7 DIV, n=4); **b:** Volume (in µm^3) of GluR2 positive puncta per IHC in 3 DIV, 5 DIV and 7 DIV cultures (p= 0.92 for 3 DIV, n=2; p= 0.68 for 5 DIV, n=3; p= 0.10 for 7 DIV, n=4); There was no significance in the volumes of CtBP2 or GluR2 positive puncta between OS and control cultures. Red; Cultures stimulated by optogenetics, Blue: Controls; DIV; Days *in vitro*; All cultures prepared at P7. n number signifies the number of cochleae used for culturing.

The volume of GluR2 for the 3 DIV cultures was similar, at 0.14μm^3 (±0.03, n=2) for OS and 0.13μm^3 (±0.10, n=2) for control. At 5 DIV, it was 0.21μm^3 (±0.10, n=3) for OS and 0.18μm^3 (±0.10, n=3) for control cultures. For 7 DIV it was 0.23μm^3 (±0.11, n=4) for OS and 0.10μm^3 (±0.06, n=4) for control cultures. Two-way ANOVA with Welch correction did not show any significant difference between the OS and control numbers for each DIV ($p= 0.916$ for 3 DIV, $p= 0.682$ for 5 DIV, $p= 0.102$ for 7 DIV).

The ratio between CtBP2 and GluR2 for this condition at 3 DIV for OS cultures was 0.2 (±0.1, n=3) and 0.4(±0.3, n=4) for controls. For 5 DIV, this number was slightly higher, 0.8(±0.5, n=3) for OS cultures and 1.2 (±1.1, n=3) for controls. At 7 DIV, the number was fairly similar for both OS and controls at 0.7 (±0.3, n=4) for OS cultures and 0.6 (±0.6, n=4) for controls. Two-way ANOVA with Welch correction did not show any significant difference between the OS and control numbers for each DIV analysed ($p= 0.22$ for 3 DIV, $p= 0.68$ for 5 DIV, $p= 0.60$ for 7 DIV).

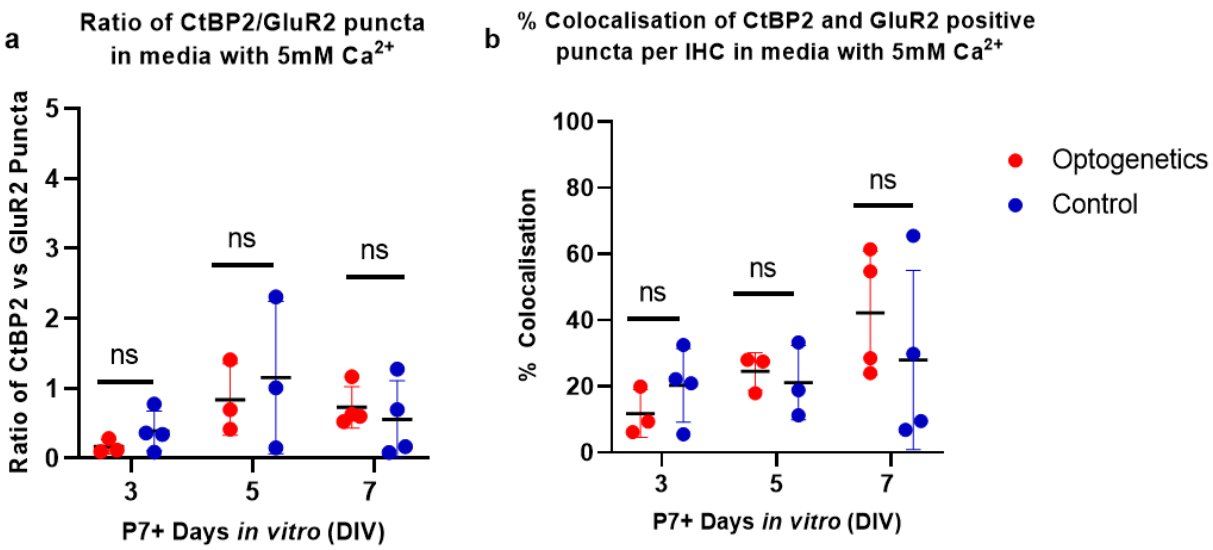

<u>Graphs 4.6</u> Shows the ratio and colocalization of CtBP2 and GluR2 positive puncta in cultures with 5mM Ca^{2+} at P7+3 DIV, P7+5 DIV and P7+7 DIV for optogenetically stimulated cultures and controls (not stimulated by optogenetics).;

a: Ratio of CtBP2 and GluR2 positive puncta per IHC in 3 DIV, 5 DIV and 7 DIV cultures (p= 0.22 for 3 DIV, n=3; p= 0.68 for 5 DIV, n=3; p= 0.60 for 7 DIV, n=4); **b:** Colocalization of CtBP2 and GluR2 positive puncta per IHC in 3 DIV, 5 DIV and 7 DIV cultures (p= 0.28 for 3 DIV, n=3; p=0.67 for 5 DIV, n=3 p=0.42 for 7 DIV, n=4). There was no significance in the ratio or colocalization of CtBP2 with GluR2 positive puncta between OS and control cultures. Red; Cultures stimulated by optogenetics, Blue: Controls; DIV; Days *in vitro*; All cultures prepared at P7. n number signifies the number of cochleae used for culturing.

For colocalization between the CtBP2 and GluR2, at 3 DIV, the percentage colocalization was 12.0% (±7.0, n=3) for OS cultures. For control cultures at 3 DIV, it was 20.0% (±11.0, n=4). At 5 DIV, the colocalization percentage for OS cultures was 25.0% (±6.0, n=3) and for control cultures was at 21.0% (±11.0, n=3). For 7 DIV, colocalization percentages for OS cultures was 42.0% (±19.0, n=4) and for controls it was 30.0% (±27.0, n=4). However, two-way ANOVA with Welch correction did not show

any significant difference between the OS and control numbers for each DIV (p= 0.28 for 3 DIV, p=0.67 for 5 DIV, p=0.42 for 7 DIV).

The mechanotransducer channel is partially blocked with a high influx of calcium concentration. This generally is causes the IHC to no longer depolarise. However, since the mice used here express channelrhodopsin, we expected to bypass this block and we anticipated that the IHCs would fire upon light activation. We therefore still expected that optogenetic stimulation would drive the IHC towards maturation. However, we did not see any significant maturation of the IHCs. Although there was some change observed in the volume of SGNs, there was no strong indication that this was consistent in results.

4.3. Discussion

This chapter explores the application of optogenetics on cultures containing differing levels of Ca^{2+}. For cultures grown in media with 0.3mM Ca^{2+}, there was no significant difference between the CtBP2 and GluR2 puncta evaluated for OS and controls conditions. However, the most interesting result was the disappearance of the IHCs in cultures at 7 DIV. Very few experiments have been performed looking at the effect of physiologically accurate levels of Ca^{2+} on IHCs *in vitro*, or even a high concentration of Ca^{2+} (5mM Ca^{2+}, as we used) for that matter (Vélez-Ortega *et al.*, 2017). In our cultures, it was clear that although there were differences that we observed in gross morphologically, such as that observed in 7DIV cultures for 0.3mM Ca^{2+}, we were unable to find quantifiable differences.

For cultures grown in media containing 5mM Ca^{2+}, there were no statistically significant results between OS and controls in 3DIV, 5DIV and 7DIV intervals. We aimed to obstruct the mechanotransducer current through a large supplementation of Ca^{2+} in the cultures (5mM). However, since we used *Otof*:ChR2-EYFP mice, we expected to circumvent the activity of the MET channel. We speculated that the IHCs would still be activated through optogenetics and be driven towards maturation. Although the subsequent cultures did not show the same disruption in overall tissue morphology or individual IHCs that we saw from cultures in 0.3mM Ca^{2+}, we also did not observe any significant data that would indicate hair cell maturation. Future studies involving electrophysiological recordings of individual IHCs could be conducted to obtain a clearer perspective for IHC activity in media containing 5mM Ca^{2+}.

Ca^{2+} drives the spontaneous activity in the IHCs (refer to introduction chapter 1.3; Johnson *et al.*, 2012). At hearing onset around P12, the APs cease due to the expression of large-conductance K^+ (BK; $I_{K,f}$) currents. The concentration of Ca^{2+} in the endolymph and perilymph are similar during birth and change vastly during postnatal development. The concentration of Ca^{2+} in the endolymph of prehearing mice is 0.3mM. In mature cochleae, the endolymphatic Ca^{2+} concentration is 0.02mM. In contrast, the ionic concentration of Ca^{2+} in the perilymph is constant during development, at 1.3mM.

The reticular lamina separates the IHC hair bundles at the apical pole from the basolateral membrane, maintaining the separation between the endolymph and perilymph. During spontaneous firing *in vivo,* hair bundles are exposed to the endolymph (0.3mM Ca^{2+}), while still maintaining the ionic gradient across the basolateral membrane. Therefore, we hypothesise that, to evoke true spontaneous APs *in vitro*, we would need to present physiologically accurate ionic conditions for the IHCs and the channels. We speculated that this could perhaps help to stimulate the IHCs towards maturation.

But, due to the dissection process for culture preparation, this ionic division is destroyed, and leads to the entire sensory epithelia tissue being exposed to the 0.3mM Ca^{2+} culture media. It is, therefore, impossible to maintain the positional ionic separation within culture, which could explain the lack of IHC development with 0.3mM Ca^{2+} media.

It is important to note that the Ca^{2+} influences several developmental pathways. Additionally, Ca^{2+} is also important for the integrity of the cochlear tissue, as adherens junctions between cells are Ca^{2+} dependent. Consequently, exposing the entire tissue to changes in Ca^{2+} concentration could negatively impact the normal tissue integrity and developmental pathways of hair cells, as well as surrounding cells. We suggest that the large change in Ca^{2+} concentration and lack of ionic gradient in culture could play a role in the large-scale changes observed in the morphology of the cultured IHCs, and the entire observed sensory epithelium.

4.4. The effect of optogenetic stimulation on potassium (BK) channel development.

4.4.1. Introduction

Cochleae from neonatal mouse pups expressing ChR2-EYFP were cultured at 10 days following birth (P10) and maintained for 5 days *in vitro* (5 DIV). The cultures were stimulated extrinsically using optogenetics (λ=470 nm; refer methods chapter 2.4). Cochleae from the contralateral ear of the same pup were cultured as negative controls (without optogenetic stimulation). Cultures were fixed at P10+5DIV (henceforth referred to as 5DIV), giving the cultures a total age of P15. The readout considered for this experiment was the large-conductance Ca^{2+}-activated K^+ current (BK), called $I_{K,f.}$ In addition to this, the general morphology of the cultures was analysed as well. Cochleae from normally developing pups were used as maturational reference points (positive controls). Cochleae from pups aged between P3 and P20 were fixed at regular intervals and immunostained for BK channels.

In the mature organ of Corti, BK channels are found in clusters localized to the neck of the cell of IHCs (pericuticular region) and conspicuously distant from ribbon active zones (Pyott *et al.*, 2004). The average number of BK channels per IHC generally correlates to the average number of synaptic active zones, suggesting a tight correlation between these two critical Ca^{2+} signalling domains (Pyott *et al.*, 2004). The expression of BK channels on IHCs is one of the hallmarks of IHC maturation. We therefore evaluate whether optogenetic stimulation would drive the expression of BK channels in the P10+5DIV cultures and push the IHCs towards maturation. We used mice at later age (P10) rather than P7, as we thought that P7 was too early to expect to drive gene expression of the BK channel. We hoped to give the IHCs less time between the culturing and appearance of BK channels. To visualise this through immunostaining, we used anti-BK antibody.

4.4.2. Results

4.4.2.1. Wholemount immunostaining to show the appearance of BK channels with development

We initially conducted immunostaining for BK positive puncta to show the progression of the BK channel appearance during normal development and quantified the number of BK positive puncta. Confocal images of the apical coil were taken at the 9–12kHz region.

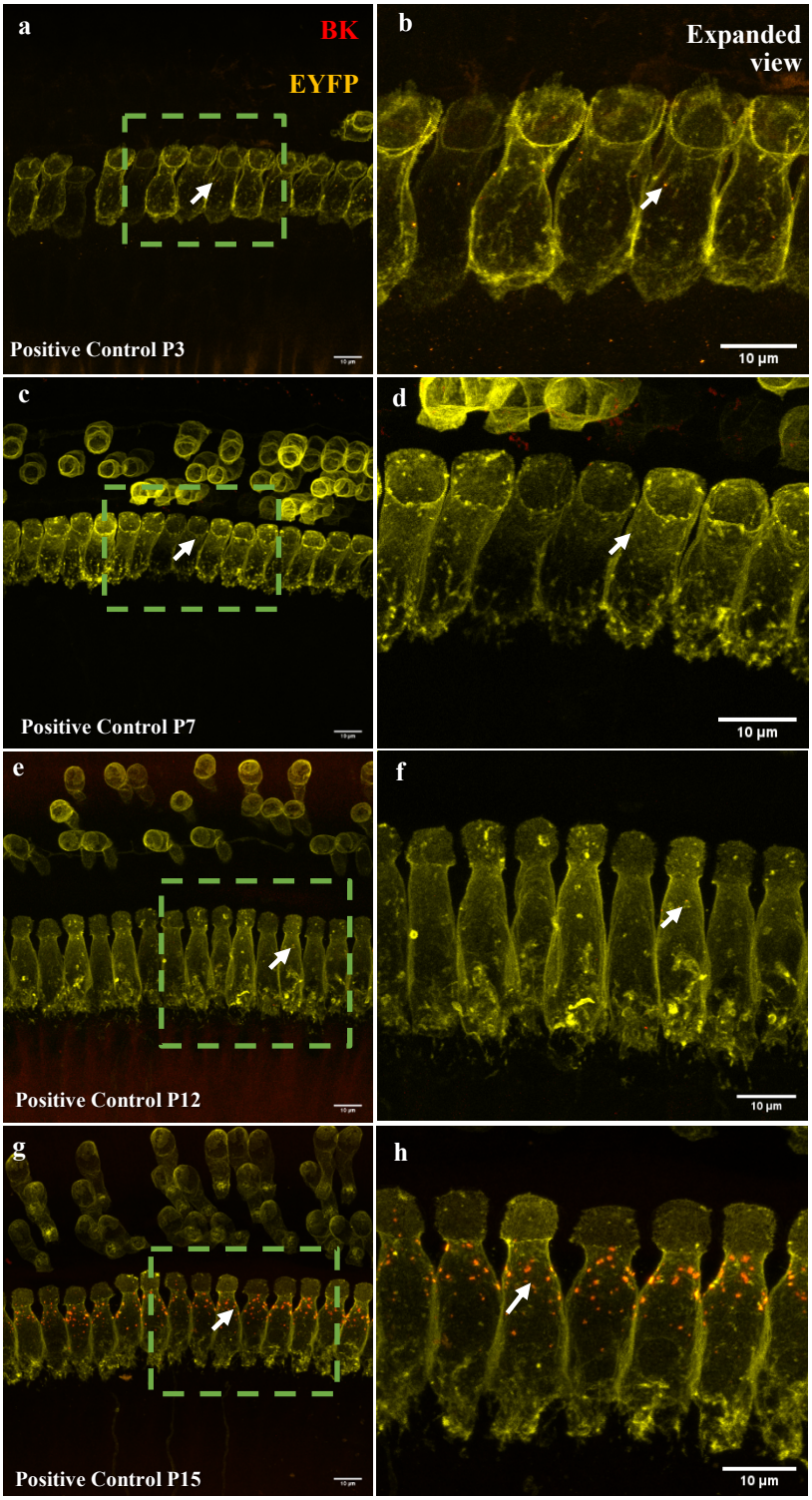

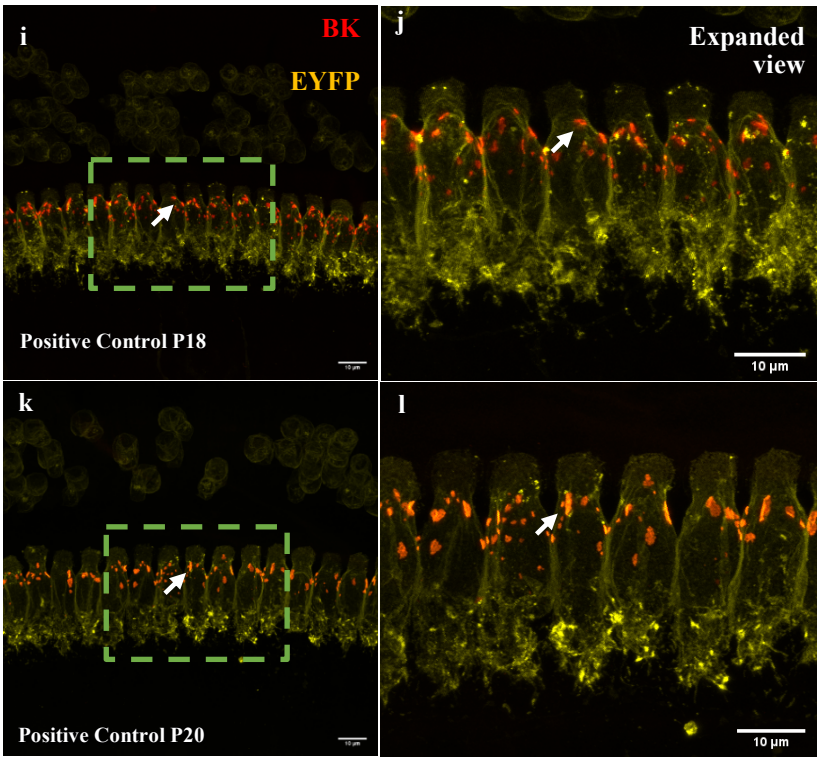

Figure 4.4 Shows wholemount immunostaining of cochleae for BK channels at different age intervals between P3 to P20.

All images taken at the 9–12kHz region; Graphs show the quantification of BK positive puncta per IHC for each condition. Images for each age show BK positive puncta and EYFP, and an expanded view of the image. a, c, e, g, i, k: BK positive puncta with EYFP; b, d, f, h, j, l: Expanded view; Images at 63x. Red: BK; Yellow: EYFP. Green box indicates expanded area; Arrows point to BK positive puncta; Scale bar:10*µm*; n=4 for each age; n number signifies the number of cochleae used for wholemount immunostaining.

The mean number of BK positive puncta at P3 were 0.3(±0.5, n=4), at P7 was 0.2(±0.3, n=4), at P12, was 0(±0, n=4). At P15, this increased to 20.0(±4.0, n=4). At P18, the number of BK positive puncta was 13.0 (±1.0, n=4), and at P20 was 12.0(±1.0, n=4). This clearly shows the sharp increase in the appearance of BK channels after the second postnatal week, which coincides with the onset of hearing for mice.

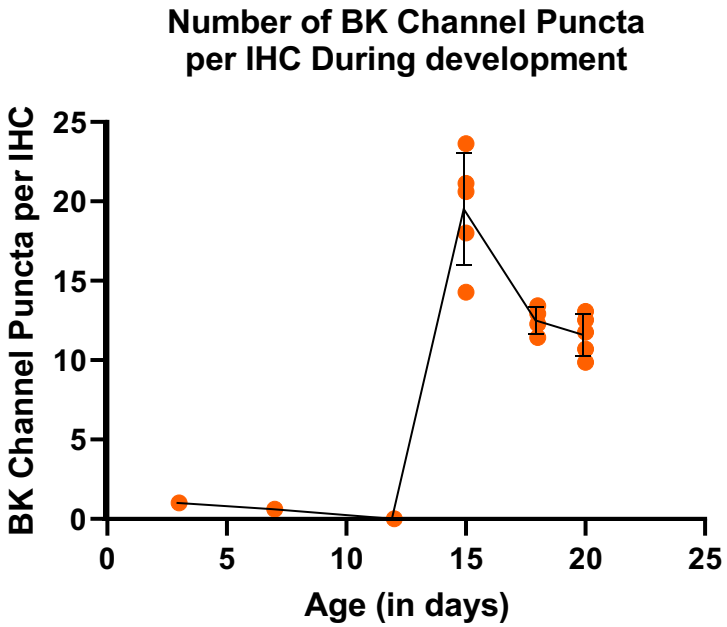

<u>Graphs 4.7</u> Shows number of BK positive puncta in wholemount cochlea for different age intervals between P3 to P20.

Orange dots represent individual values of BK positive puncta from each cochlea; Age intervals used for puncta quantification were: P3, P7, P12, P15, P18 and P20; n=4 for each age interval; n= number of cochleae used for wholemount immunostaining.

4.4.2.2. Determine potassium (BK) channel development in cultures stimulated by optogenetic signalling

BK positive puncta were immunostained and quantified for each for OS (optogenetically stimulated) and control cultures at P10+5DIv (figure 4.5..a-d: apical coil at the 9–12kHz region).

For OS cultures, we found 4.0(±0, n=1) BK positive puncta per IHC. For controls, there were 0 (±0, n=1) BK positive puncta per IHC. As only one mouse was processed for each condition, there was not enough data to make a definitive statement. For this reason, we were unable to conclude whether there was any effect due to optogenetic stimulation.

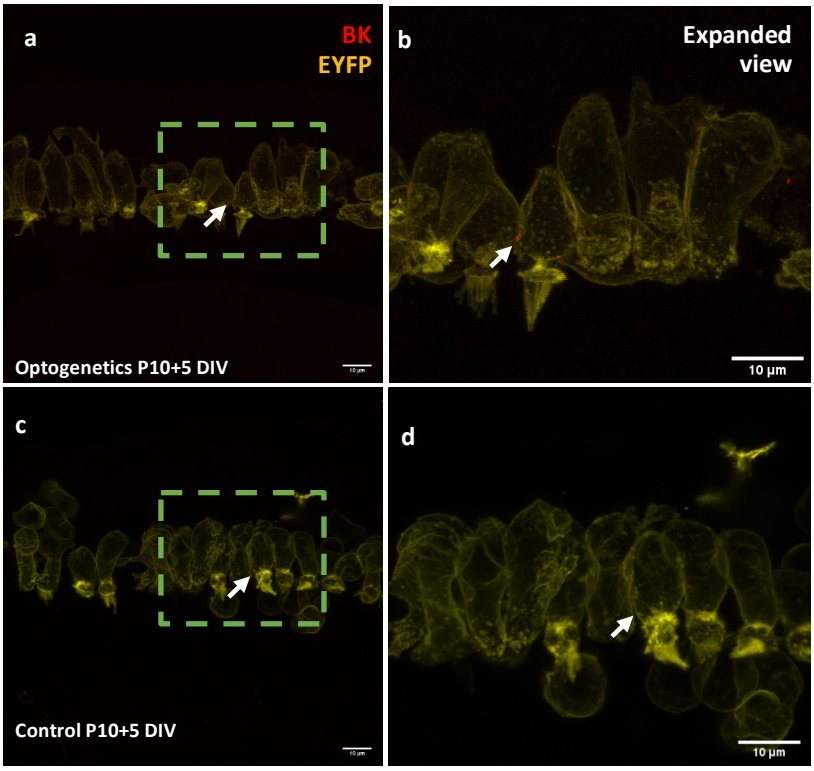

Figure 4.5 Shows the immunostaining of BK positive puncta in cultures at P10+5 DIV with optogenetic stimulation and controls (with no optogenetic stimulation applied).

All images taken at the 9–12kHz region. Graphs show the quantification of BK positive puncta per IHC for each condition. Images for each day in culture show BK positive puncta and EYFP. The cultures were imaged at 5 days *in vitro*, after either being

optogenetically stimulated (OS) or maintained without optogenetic stimulation (control). a, c: BK positive puncta with EYFP; b, d: Expanded view; Images at 63x. Red: BK; Yellow: EYFP. Green box indicates expanded area; Arrows point to BK positive puncta; DIV; Days *in vitro*; All cultures prepared at P10; Scale bar: 10*μm*. n=1 for P10+5; n number signifies the number of cochleae used for culturing.

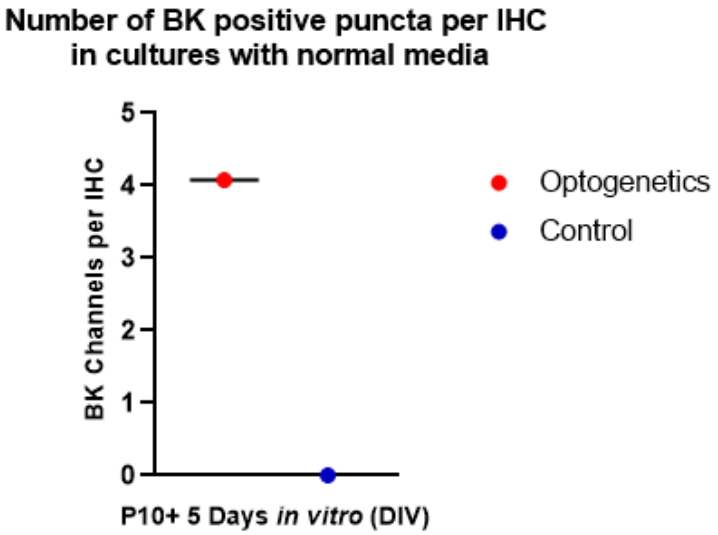

Graphs 4.8 Shows the number of BK positive puncta in cultures stimulated by either optogenetics (OS cultures) or controls (no optogenetic stimulation applied) at P10+5DIV.

There was not enough data for significance testing for the number of BK puncta at 5DIV between OS and control cultures. Red; Cultures stimulated by optogenetics, Blue: Controls. DIV; Days *in vitro*; All cultures prepared at P10. n-number signifies the number of cochleae used for culturing; n=1 cochlea for both OS and control.

4.4.3. Discussion

For this chapter, we wanted to check whether optogenetic stimulation provided to cultures would drive the expression of BK channels. Evidently, we did not see the development of BK channels.

BK channels first appear around hearing onset in mouse IHCs, and are believed to transform mature mammalian IHCs into high-frequency signal transducers (Kros *et al.*, 1998). BK channels also help regulate both the firing of neurons and neurotransmitter release. The expression of BK channels at the end of the second postnatal week is considered to consequently signal the functional maturation of the IHC.

The number of BK channels at P15 are 20.0(±4.0, n=4), as can be observed from graph 4.7. However, neither the OS cultures nor the controls showed these number of puncta (4.0±0, for OS cultures; 0±0, for controls). Additionally, due to fewer n-numbers, we could not make any definitive statistical analysis for these cultures.

Given the results of these experiments, the application of optogenetics in the cultures was inadequate to elicit any identifiable BK channels.

5. General Discussion

The developmental regulation exerted by spontaneous activity in the immature cochlea concerns not only the maturation of hair cells, but also its synaptic fibres, and the subsequent auditory pathway. The main aims of this project were to check whether exogenous activation of IHCs maintained in *ex vivo* preparations would drive their maturation, and to what extent this driving factor would operate. This was checked specifically in the context of ribbon synapses development, as functional ribbon synapses are a hallmark of hair cell maturation in the cochlea. Additionally, spontaneous activity in IHCs is specifically linked to vesicle fusion and glutamate release facilitated by synaptic ribbons, which consequently cause the firing of afferent neurons and help to refine the tonotopic pathway.

If exogenously driven action potentials was enough to drive hair cell maturation in pre-hearing *ex vivo* cochlea preparations, we would expect to observe ribbon counts and volumes similar to those observed in mature IHCs. We would also expect the upregulation basolateral ion channels that would be present in the mature IHCs, which are one of the hallmark characteristics of adult IHCs, such as the Ca^{2+} activated large conductance K+ channels (BK).

Due to the molecular mechanisms controlling the functional development of IHCs as a whole, it becomes tricky to choose a singular readout for IHC maturation whilst in ex vivo culture preparations. Since the cultures are isolated from their *in vivo* environment, they already do not possess some essential neural connections that have been theorised to influence maturation, such as the influence of ACh through the MOC fibres. As such, the ability to provide completely perfect conditions that mimic the *in vivo* environment becomes a challenge.

5.1. The role of optogenetically evoked spontaneous activity in the development of *ex vivo* IHCs with and without the application of growth factors

The data presented here show that stimulation of IHCs using exogenously evoked spontaneous action potentials does not drive the maturation of IHCs or ribbon synapses when placed for up to 10 days in culture.

When placed in culture for up to 10 days, the synaptic ribbons of IHCs did not show ribbon counts similar to mature ribbons (when compared to apical IHCs of normally developing mice). In 10 day cultures, the ribbons did not show any significant differences in volume between the optogenetically stimulated and control (not under optogenetic stimulation) cultures. Incredibly, the volume of CtBP2 positive ribbons at 10 days between optogenetically stimulated cultures ($0.15\mu m^3 \pm 0.02$; n=5) and controls ($0.13\mu m^3 \pm 0.05$; n=4) was comparable to the volumes of ribbons in normal P15 ($0.16\mu m^3 \pm 0.01$; n=2) and P20 ($0.13\mu m^3 \pm 0.035$; n=2) mice. However, since there was no significant difference between the volumes of optogenetically stimulated and control cultures at 10 days, it was postulated that the application of optogenetics at that point did not, at that point, present any observed additional benefit to the cultured IHCs.

Additionally, it was observed that cultures maintained for longer periods i.e., 10 days had begun to appear visually poorer in structure than at 7 days. IHCs had diffused appearance of GluR2 positive puncta, indicating possible synaptic afferent degeneration and uneven tissue topography. Cultures maintained for longer than 10 days presented with further uneven morphology of the sensory epithelium (data not shown). Therefore, for further experiments, we decided that maintaining the cultures for 7 days would be adequate to provide information on ribbon maturation (giving the cultured cochleae a total age of 14 days; P7+7 days) without acquiring the visibly diffused appearance. As such, it was evident that the sole application of optogenetic stimulation was not enough to drive the maturation of ribbon synapses within the IHCs. We therefore supplemented the cultures with growth factors that could help in maintaining the existing sensory epithelium tissue

within the cultures, and also provide the boost towards functional maturation, as is their role in normal auditory functioning.

This was tested over different time periods and with specifically chosen growth factors. The cultures were supplemented with the neurotrophins NT-3 (10ng/ml), BDNF (10ng/ml), and hormone T3(1.8ng/ml) due to their established roles in hair cell development, as well as observed roles in maintenance of neural cultures (He *et al.*, 2003; Sun and Salvi, 2009; Wang and Green, 2011). We observed that the addition of exogenous growth factors was insufficient to drive any significant maturation of ribbons. This was surprising, considering the immense role played by TH and neurotrophins in the general maturation of ribbons *in vivo.*

The role of TH especially is well recognized, the lack of which, is known to affect the maturation of ribbon synapses. It was observed in athyroid $Pax8^{-/-}$ mouse IHCs, that, at P14-P16, ribbon synapse numbers were higher, with a disruption in synaptic pruning, than age-matched controls (Sendin *et al.*, 2007). $Pax8^{-/-}$ mouse IHCs also lacked functional large-conductance BK and KCNQ4 channels, and were seen to still possess immature efferent innervation, even at P15. Additionally, $Pax8^{-/-}$ mice showed action potential firing up until P21 as compared to age-matched control mice (Brandt *et al.*, 2007; Sendin *et al.*, 2007).

The regulation of synaptic pruning of type II SGNs was also attributed to TH (Sundaresan *et al.*, 2016b). Thus, TH is an important regulator of synaptic pruning and IHC development.

We expected that optogenetic stimulation with growth factor supplementation would drive ribbon maturation, afferent pruning and synaptic development in the cultures, such that the number of postsynaptic puncta observed would reduce by half in 7 day culture preparations and would colocalise with synaptic ribbon numbers within each IHC.

Unfortunately, the experiments with supplemented neurotrophins and TH did not show any significant maturation in the IHCs.

There was no difference in the ribbon counts and volumes between the optogenetically stimulated and control cultures. Interestingly, cultures at 3 days showed a significant difference between the number of GluR2 positive puncta between optogenetically stimulated (5.68±0.78; n=2) and control (1.22±0.67; n=2) cultures but did not show any difference at 7 days *in vitro*. Additionally, the percentage of synaptic colocalizations with afferent neurons didn't reflect colocalization percentages with corresponding age-matched controls. As such, it could be concluded that the number of synapses did not necessarily prune, they just were maintained due to the growth factors (as growth factors are proven to function in synaptic maintenance).

5.2. The role of Ca^{2+} in the maturation of IHCs in ex vivo cochlear preparation in concert with optogenetic stimulation

Hair cells subjected to physiological concentrations of Ca^{2+} in the media also showed interesting results. The physiological concentration of endolymphatic Ca^{2+} during the second post-natal week is likely to be in the order of 0.3mM (Johnson *et al.*, 2012).

We expected to see a sharp incline in the developmental progression of IHCs, since the cultures were bathed in media containing the endolymphatic concentration of Ca^{2+}. We expected that this physiologically accurate concentration would help to drive the spontaneous action potentials after exogenous optogenetic stimulation, and we would be able to observe an accurate representation of developmental changes in the ribbons.

However, the results were surprising. At 3 days in culture, the IHC ribbons did not show significant differences between optogenetically stimulated and control cultures. But most surprisingly, the cultured tissue displayed complete disintegration of cells at 7 days *in vitro*. This was an unexpected result, as these low concentrations of Ca^{2+} were previously observed to lead to large mechanotransducer currents that depolarised the IHC membrane potentials and were therefore were able to successfully evoke spontaneous spiking activity in the second postnatal week (Johnson *et al.*, 2012).

We suspect this was due to placing the cochlea in a long culture period of 7 days. Additionally, the dissection process effectively destroyed the separation of endolymph and perilymph fluids in the cultures. There was no way to maintain this fluidic partition in culture, since the entire sensory epithelium was bathed in culture media containing 0.3mM Ca^{2+}, which is not the normal physiological environment for the IHC basilar membrane. Consequently, this might affect the non-sensory SCs, which function to not only provide physical support to the IHCs, but also modulate spontaneous activity in the second postnatal week through waves of extracellular ATP (Tritsch *et al.*, 2007; Johnson *et al.*, 2011a).

Conversely, the application of 5mM Ca^{2+} also did not show any significant difference in the ribbon counts or afferent fibres. Extracellular Ca^{2+} is a blocker of the transducer channel (Marcotti *et al.*, 2005). However, since we used *Otof*:ChR2-EYFP mice, we were able to circumvent the activity of the MET channel. We could depolarise IHCs without MET channel activation, using 470nm wavelength light. In this regard, since the IHCs were still being stimulated, we expected that IHC would still be driven towards maturation. However, IHCs still remained in the immature state.

There was no difference between optogenetically stimulated and control cultures for both synaptic ribbon counts and afferent neuron numbers and volumes. However, one salient difference was that these cells did not show the same kind of degenerative response that was observed in the non-sensory, and sensory cells of the cultures placed in 0.3mM Ca^{2+} media. One can assume that since Ca^{2+} is important for various other processes that involve gene expression, development and other functions of cells, the large-scale removal of Ca^{2+} from the entire sensory epithelium would have a degenerative effect on the cells.

The role of the MET channel has been previously studied by bypassing its functions through the utilisation of optogenetics in hair cells of transgenic zebrafish lateral lines (*myo6b*:ChR2-YFP), and comparing SGN firing activity for both ChR2, and MET activated channels (Monesson-Olson *et al.*, 2014). It was found that optogenetically activated cells showed large variability in first spike latency and a reduction in vector strength during phase-locking of spikes, thereby essentially losing the temporal fidelity (Monesson-Olson *et al.*, 2014). This demonstrates that the MET channel plays a role in high-fidelity stimulus encoding.

In our experiments however, as mentioned above, we did not observe any changes within the synaptic ribbons or afferent fibres stimulated by optogenetics that were significantly different from the controls. Although this would be an additional avenue to explore in the future.

5.3. Checking the expression of BK channels in optogenetically stimulated cultures

The fast-activating K^+ current channel (BK), is expressed in IHCs at around the onset of hearing (P12) and is one of the hallmarks of IHC maturation. We expected that, if optogenetic stimulation was enough to drive hair cell maturation, it would in theory, drive the expression of BK channels (to conduct the K^+ current in mature IHCs). Since sensory epithelia from P7 pups could be too young to drive this expression, we used the cochleae from P10 pups, such that they were still in the prehearing phase, but closer to maturation than the P7 pups. In this regard, we expected the optogenetic stimulation to provide the extra push to the P10 cultured IHCs. We postulated that, even if the IHCs don't fully mature, if the BK channel expression was upregulated with optogenetic stimulation, it would provide us with a jumping point towards driving further maturation.

The immunofluorescence data did not show significant maturation in the cultures made using P10 mice. The cultures did not express BK channels and there were no significant changes between the optogenetically stimulated cultures compared to the control cultures. This, however, could be an area of further investigation, as the appearance of ion channels related to the large K^+ current is an important characteristic that signals the commencement of the mature IHC fate.

5.4. Areas for future investigations

For the purpose of this project, the main aim initially was to drive IHC maturation from ex vivo cultures. Additionally, we also wanted to check the full magnitude to which spontaneous activity plays a role in the development of the ribbon synapse (and holistically, the whole IHC), and to what extent we could drive this maturation.

With respect to this, various additional features linked to hair cell maturation could be used for further investigation. One of these is to evaluate other ion channels classically associated with IHC maturation, such as the $Ca_V1.3$ channels. During prehearing, the $Ca_V1.3$ channels lack organised distribution along the IHC plasma membrane. However, as maturation continues, the $Ca_V1.3$ channels are concentrated close to the synaptic ribbons at the AZ, and any extrasynaptic $Ca_V1.3$ channels are eliminated (Frank *et al.*, 2010; Pangšrič *et al.*, 2010; Wong *et al.*, 2014). Thus, the numbers and distribution of the $Ca_V1.3$ channels with respect to the basolateral membrane could be an indication of maturational progress of the cell.

Additionally, the Ca^{2+} activated small-conductance K^+ (SK2) channels could also provide an indication of IHC maturation. SK2 channels are only present during the prehearing period, wherein they are required for the maintenance of continuous recurring spontaneous activity in IHCs (Johnson *et al.*, 2007). Thus, we would expect that, the downregulation of SK2 channels and simultaneous upregulation of BK channel expression would provide evidence for the maturation of IHCs. This could be achieved through a combination of immunofluorescence microscopy, as well as electrophysiology. Optogenetically stimulated cultures could be observed for the appearance of graded receptor potentials, which could give a more definitive answer to the question of IHC maturation.

Although there was no observation of the appearance of BK channels associated with mature IHCs, even the upregulation of BK-, or subsequent downregulation of SK2- channel associated genes could perhaps provide indication towards maturation of IHCs, even if the final assembly of the BK channels may not be fully observed. This could be achieved in case through qPCR analysis.

An important area of further study could be the Kölliker's organ, which was suggested to produce ATP, leading to Ca^{2+} transients, thus causing hair cell spiking (Tritsch *et al.*, 2007, 2010). Ca^{2+} imaging of the Kölliker's organ could elucidate further, the large influence of Ca^{2+} on spontaneous firing, especially in an *in vitro* context.

Additional super resolution microscopy of the AZ itself, or even individual ribbons, through STochastic Optical Reconstruction Microscopy (STORM) could provide fluorescent axial resolution of up to 50nm, allowing for extremely detailed ribbon shape, size, and synapse evaluation. A more detailed view of the ribbon could also be obtained using electron cryotomography (CryoET), which could provide three-dimensional resolutions up to ~1–4 nm of even smaller precursor ribbons and their tethered vesicles.

Bibliography

1. Adamson, C.L., Reid, M.A. and Davis, R.L. (2002) *Opposite actions of brain-derived neurotrophic factor and neurotrophin-3 on firing features and ion channel composition of murine spiral ganglion neurons*, *Journal of Neuroscience*. Society for Neuroscience. Available at: https://doi.org/10.1523/jneurosci.22-04-01385.2002.
2. Ahmed, Z.M. *et al.* (2006) 'The tip-link antigen, a protein associated with the transduction complex of sensory hair cells, is protocadherin-15', *Journal of Neuroscience*, 26(26), pp. 7022–7034. Available at: https://doi.org/10.1523/JNEUROSCI.1163-06.2006.
3. Alagramam, K.N. *et al.* (2011) 'Mutations in protocadherin 15 and cadherin 23 affect tip links and mechanotransduction in mammalian sensory hair cells', *PLoS ONE*. Edited by M. Coleman, 6(4), p. e19183. Available at: https://doi.org/10.1371/journal.pone.0019183.
4. Atkinson, P.J. *et al.* (2014) 'Hair cell regeneration after ATOH1 gene therapy in the cochlea of profoundly deaf adult guinea pigs', *PLoS ONE*. Edited by B. Riley, 9(7), p. e102077. Available at: https://doi.org/10.1371/journal.pone.0102077.
5. Babola, T.A. *et al.* (2018) 'Homeostatic Control of Spontaneous Activity in the Developing Auditory System', *Neuron*, 99(3), pp. 511-524.e5. Available at: https://doi.org/10.1016/j.neuron.2018.07.004.
6. Bacaj, T. *et al.* (2013) 'Synaptotagmin-1 and Synaptotagmin-7 Trigger Synchronous and Asynchronous Phases of Neurotransmitter Release', *Neuron*, 80(4), pp. 947–959. Available at: https://doi.org/10.1016/j.neuron.2013.10.026.
7. Bailey, G.P. and Sewell, W.F. (2000) 'Contribution of glutamate receptors to spontaneous and stimulus-evoked discharge in afferent fibers innervating hair cells of the Xenopus lateral line organ', *Hearing Research*, 144(1–2), pp. 8–20. Available at: https://doi.org/10.1016/S0378-5955(00)00023-X.
8. Becker, L. *et al.* (2018) 'The presynaptic ribbon maintains vesicle populations at the hair cell afferent fiber synapse', *eLife*, 7. Available at: https://doi.org/10.7554/eLife.30241.
9. Ben-Yosef, T. *et al.* (2003) 'Claudin 14 knockout mice, a model for autosomal recessive deafness DFNB29, are deaf due to cochlear hair cell degeneration', *Human Molecular Genetics*, 12(16), pp. 2049–2061. Available at: https://doi.org/10.1093/hmg/ddg210.
10. Beurg, M. *et al.* (2009) 'Localization of inner hair cell mechanotransducer channels using high-speed calcium imaging', *Nature Neuroscience*, 12(5), pp. 553–558. Available at: https://doi.org/10.1038/nn.2295.
11. Beurg, M. *et al.* (2010) 'Control of exocytosis by synaptotagmins and otoferlin in auditory hair cells', *Journal of Neuroscience*, 30(40), pp. 13281–13290. Available at: https://doi.org/10.1523/JNEUROSCI.2528-10.2010.
12. Blankenship, A.G. and Feller, M.B. (2010) 'Mechanisms underlying spontaneous patterned

activity in developing neural circuits', *Nature Reviews Neuroscience*, 11(1), pp. 18–29. Available at: https://doi.org/10.1038/nrn2759.

13. Bogart, B. (2008) ' Atlas of Anatomy by Anne M. Gilroy, Brian R. MacPherson, and Lawrence M. Ross, illustrated by Markus Voll and Karl Wesker ', *Clinical Anatomy*, 21(7), pp. 738–738. Available at: https://doi.org/10.1002/ca.20701.
14. Bosher, S.K. and Warren, R.L. (1978) 'Very low calcium content of cochlear endolymph, an extracellular fluid', *Nature*, 273(5661), pp. 377–378. Available at: https://doi.org/10.1038/273377a0.
15. Boucher, J., Tseng, Y.H. and Kahn, C.R. (2010) 'Insulin and insulin-like growth factor-1 receptors act as ligand-specific amplitude modulators of a common pathway regulating gene transcription', *Journal of Biological Chemistry*, 285(22), pp. 17235–17245. Available at: https://doi.org/10.1074/jbc.M110.118620.
16. Brandt, N. *et al.* (2007) 'Thyroid hormone deficiency affects postnatal spiking activity and expression of Ca2+ and K+ channels in rodent inner hair cells', *Journal of Neuroscience*, 27(12), pp. 3174–3186. Available at: https://doi.org/10.1523/JNEUROSCI.3965-06.2007.
17. Bucurenciu, I. *et al.* (2008) 'Nanodomain Coupling between Ca2+ Channels and Ca2+ Sensors Promotes Fast and Efficient Transmitter Release at a Cortical GABAergic Synapse', *Neuron*, 57(4), pp. 536–545. Available at: https://doi.org/10.1016/j.neuron.2007.12.026.
18. Buran, B.N. *et al.* (2010) 'Onset coding is degraded in auditory nerve fibers from mutant mice lacking synaptic ribbons', *Journal of Neuroscience*, 30(22), pp. 7587–7597. Available at: https://doi.org/10.1523/JNEUROSCI.0389-10.2010.
19. Burda, H. and Branis, M. (1988) 'Postnatal development of the organ of Corti in the wild house mouse, laboratory mouse, and their hybrid', *Hearing Research*, 36(1), pp. 97–105. Available at: https://doi.org/10.1016/0378-5955(88)90140-2.
20. Burns, M.E. and Augustine, G.J. (1995) 'Synaptic structure and function: Dynamic organization yields architectural precision', *Cell*, 83(2), pp. 187–194. Available at: https://doi.org/10.1016/0092-8674(95)90160-4.
21. Caruso, S. *et al.* (2003) 'Auditory brainstem response in premenopausal women taking oral contraceptives', *Human Reproduction*, 18(1), pp. 85–89. Available at: https://doi.org/10.1093/humrep/deg003.
22. Ceriani, F. *et al.* (2019) 'Coordinated calcium signalling in cochlear sensory and non-sensory cells refines afferent innervation of outer hair cells', *The EMBO Journal*, 38(9), p. e99839. Available at: https://doi.org/10.15252/embj.201899839.
23. Chakrabarti, R., Michanski, S. and Wichmann, C. (2018) 'Vesicle sub-pool organization at inner hair cell ribbon synapses', *EMBO reports*, 19(11). Available at: https://doi.org/10.15252/embr.201744937.
24. Chen, P. *et al.* (2002) 'The role of Math1 in inner ear development: Uncoupling the establishment of the sensory primordium from hair cell fate determination', *Development*,

129(10), pp. 2495–2505. Available at: https://doi.org/10.1242/dev.129.10.2495.

25. Clause, A. *et al.* (2014) 'The Precise Temporal Pattern of Prehearing Spontaneous Activity Is Necessary for Tonotopic Map Refinement', *Neuron*, 82(4), pp. 822–835. Available at: https://doi.org/10.1016/j.neuron.2014.04.001.
26. Coleman, J.R. *et al.* (1994) 'Auditory brainstem responses after ovariectomy and estrogen replacement in rat', *Hearing Research*, 80(2), pp. 209–215. Available at: https://doi.org/10.1016/0378-5955(94)90112-0.
27. Contreras-Jurado, C. *et al.* (2011) 'The thyroid hormone receptors as modulators of skin proliferation and inflammation', *Journal of Biological Chemistry*, 286(27), pp. 24079–24088. Available at: https://doi.org/10.1074/jbc.M111.218487.
28. Contreras-Jurado, C. *et al.* (2015) 'Thyroid hormone signaling controls hair follicle stem cell function', *Molecular Biology of the Cell*, 26(7), pp. 1263–1272. Available at: https://doi.org/10.1091/mbc.E14-07-1251.
29. Corns, L.F. *et al.* (2014) 'Calcium entry into stereocilia drives adaptation of the mechanoelectrical transducer current of mammalian cochlear hair cells', *Proceedings of the National Academy of Sciences of the United States of America*, 111(41), pp. 14918–14923. Available at: https://doi.org/10.1073/pnas.1409920111.
30. Crawford, A.C. and Fettiplace, R. (1986) *Mechanical tuning in turtle cochlear hair cells*, *Hearing Research*. Available at: https://doi.org/10.1016/0378-5955(86)90083-3.
31. Darrow, K.N., Maison, S.F. and Liberman, M.C. (2006) 'Cochlear efferent feedback balances interaural sensitivity', *Nature Neuroscience*, 9(12), pp. 1474–1476. Available at: https://doi.org/10.1038/nn1807.
32. Darrow, K.N., Maison, S.F. and Liberman, M.C. (2007) 'Selective removal of lateral olivocochlear efferents increases vulnerability to acute acoustic injury', *Journal of Neurophysiology*, 97(2), pp. 1775–1785. Available at: https://doi.org/10.1152/jn.00955.2006.
33. Dick, O. *et al.* (2003) 'The presynaptic active zone protein bassoon is essential for photoreceptor ribbon synapse formation in the retina', *Neuron*, 37(5), pp. 775–786. Available at: https://doi.org/10.1016/S0896-6273(03)00086-2.
34. Doser, R.L., Amberg, G.C. and Hoerndli, F.J. (2020) 'Reactive oxygen species modulate activity-dependent AMPA receptor transport in C. Elegans', *Journal of Neuroscience*, 40(39), pp. 7405–7420. Available at: https://doi.org/10.1523/JNEUROSCI.0605-20.2020.
35. Durham, A.C.H. (1983) 'A survey of readily available chelators for buffering calcium ion concentrations in physiological solutions', *Cell Calcium*, 4(1), pp. 33–46. Available at: https://doi.org/10.1016/0143-4160(83)90047-7.
36. Echteler, S.M., Fay, R.R. and Popper, A.N. (1994) 'Structure of the Mammalian Cochlea', in. Springer, New York, NY, pp. 134–171. Available at: https://doi.org/10.1007/978-1-4612-2700-7_5.
37. Eckrich, T. *et al.* (2012) 'Development and Function of the Voltage-Gated Sodium Current in

Immature Mammalian Cochlear Inner Hair Cells', *PLoS ONE*. Edited by S. Barnes, 7(9), p. e45732. Available at: https://doi.org/10.1371/journal.pone.0045732.

38. Ehret, G. (1976) 'Development of absolute auditory thresholds in the house mouse (Mus musculus).', *Journal of the American Audiology Society*, 1(5), pp. 179–184. Available at: https://europepmc.org/article/med/956003 (Accessed: 10 August 2022).
39. Ehret, G. and Frankenreiter, M. (1977) *Quantitative analysis of cochlear structures in the house mouse in relation to mechanisms of acoustical information processing*, *Journal of Comparative Physiology ■ A*. Available at: https://doi.org/10.1007/BF00611249.
40. Elgoyhen, A.B. *et al.* (1994) 'α9: An acetylcholine receptor with novel pharmacological properties expressed in rat cochlear hair cells', *Cell*, 79(4), pp. 705–715. Available at: https://doi.org/10.1016/0092-8674(94)90555-X.
41. Elgoyhen, A.B. *et al.* (2001) 'α10: A determinant of nicotinic cholinergic receptor function in mammalian vestibular and cochlear mechanosensory hair cells', *Proceedings of the National Academy of Sciences of the United States of America*, 98(6), pp. 3501–3506. Available at: https://doi.org/10.1073/pnas.051622798.
42. Elkouby-Naor, L. and Ben-Yosef, T. (2010) 'Functions of claudin tight junction proteins and their complex interactions in various physiological systems', *International Review of Cell and Molecular Biology*, 279(C), pp. 1–32. Available at: https://doi.org/10.1016/S1937-6448(10)79001-8.
43. Emadi, G., Richter, C.P. and Dallos, P. (2004) 'Stiffness of the Gerbil Basilar Membrane: Radial and Longitudinal Variations', *Journal of Neurophysiology*, 91(1), pp. 474–488. Available at: https://doi.org/10.1152/jn.00446.2003.
44. Erixon, E. *et al.* (2009) 'Variational anatomy of the human cochlea: Implications for cochlear implantation', *Otology and Neurotology*, 30(1), pp. 14–22. Available at: https://doi.org/10.1097/MAO.0b013e31818a08e8.
45. Fettiplace, R. (2017) *Hair cell transduction, tuning, and synaptic transmission in the mammalian cochlea*, *Comprehensive Physiology*. Hoboken, NJ, USA: NIH Public Access. Available at: https://doi.org/10.1002/cphy.c160049.
46. Fisher, L.J. (1979) 'Development of retinal synaptic arrays in the inner plexiform layer of dark-reared mice', *Journal of Embryology and Experimental Morphology*, Vol. 54(1), pp. 219–227. Available at: https://doi.org/10.1242/dev.54.1.219.
47. Frank, T. *et al.* (2010) 'Bassoon and the synaptic ribbon organize Ca2+ channels and vesicles to add release sites and promote refilling', *Neuron*, 68(4), pp. 724–738. Available at: https://doi.org/10.1016/j.neuron.2010.10.027.
48. Fridberger, A., De Monvel, J.B. and Ulfendahl, M. (2002) 'Internal shearing within the hearing organ evoked by basilar membrane motion', *Journal of Neuroscience*, 22(22), pp. 9850–9857. Available at: https://doi.org/10.1523/jneurosci.22-22-09850.2002.
49. Fröhlich, A. (1985) 'Freeze-fracture study of an invertebrate multiple-contact synapse: The

fly photoreceptor tetrad', *Journal of Comparative Neurology*, 241(3), pp. 311–326. Available at: https://doi.org/10.1002/cne.902410306.

50. Gao, L. *et al.* (2020) 'Insulin-Like Growth Factor 1 on the Maintenance of Ribbon Synapses in Mouse Cochlear Explant Cultures', *Frontiers in Cellular Neuroscience*, 14, p. 302. Available at: https://doi.org/10.3389/fncel.2020.571155.
51. García-Serrano, L. *et al.* (2011) 'The thyroid hormone receptors modulate the skin response to retinoids', *PLoS ONE*, 6(8). Available at: https://doi.org/10.1371/journal.pone.0023825.
52. Geng, R. *et al.* (2013) 'Noddy, a mouse harboring a missense mutation in protocadherin-15, reveals the impact of disrupting a critical interaction site between tip-link cadherins in inner ear hair cells', *Journal of Neuroscience*, 33(10), pp. 4395–4404. Available at: https://doi.org/10.1523/JNEUROSCI.4514-12.2013.
53. Giraudo, C.G. *et al.* (2006) 'A clamping mechanism involved in SNARE-dependent exocytosis', *Science*, 313(5787), pp. 676–680. Available at: https://doi.org/10.1126/science.1129450.
54. Glowatzki, E. and Fuchs, P.A. (2000) 'Cholinergic synaptic inhibition of inner hair cells in the neonatal mammalian cochlea', *Science*, 288(5475), pp. 2366–2368. Available at: https://doi.org/10.1126/science.288.5475.2366.
55. Glowatzki, E. and Fuchs, P.A. (2002) 'Transmitter release at the hair cell ribbon synapse', *Nature Neuroscience*, 5(2), pp. 147–154. Available at: https://doi.org/10.1038/nn796.
56. Glueckert, R. *et al.* (2003) 'Role of class D L-type Ca2+ channels for cochlear morphology', *Hearing Research*, 178(1–2), pp. 95–105. Available at: https://doi.org/10.1016/S0378-5955(03)00054-6.
57. Goutman, J.D., Elgoyhen, A.B. and Gómez-Casati, M.E. (2015) *Cochlear hair cells: The sound-sensing machines*, *FEBS Letters*. NIH Public Access. Available at: https://doi.org/10.1016/j.febslet.2015.08.030.
58. Grant, L., Yi, E. and Glowatzki, E. (2010) 'Two modes of release shape the postsynaptic response at the inner hair cell ribbon synapse', *Journal of Neuroscience*, 30(12), pp. 4210–4220. Available at: https://doi.org/10.1523/JNEUROSCI.4439-09.2010.
59. Graydon, C.W. *et al.* (2011) 'Sharp Ca 2+ Nanodomains beneath the ribbon promote highly synchronous multivesicular release at hair cell synapses', *Journal of Neuroscience*, 31(46), pp. 16637–16650. Available at: https://doi.org/10.1523/JNEUROSCI.1866-11.2011.
60. Graydon, C.W. *et al.* (2014) 'Passive diffusion as a mechanism underlying ribbon synapse vesicle release and resupply', *Journal of Neuroscience*, 34(27), pp. 8948–8962. Available at: https://doi.org/10.1523/JNEUROSCI.1022-14.2014.
61. Green, S.H. *et al.* (2012) 'The Trk A, B, C's of Neurotrophins in the Cochlea', *Anatomical Record*, 295(11), pp. 1877–1895. Available at: https://doi.org/10.1002/ar.22587.
62. Guinan, J.J. (2006) 'Olivocochlear efferents: Anatomy, physiology, function, and the measurement of efferent effects in humans', *Ear and Hearing*, 27(6), pp. 589–607. Available

at: https://doi.org/10.1097/01.aud.0000240507.83072.e7.

63. Hakizimana, P. and Fridberger, A. (2021) 'Inner hair cell stereocilia are embedded in the tectorial membrane', *Nature Communications*, 12(1), pp. 1–13. Available at: https://doi.org/10.1038/s41467-021-22870-1.
64. He, D.Z.Z., Jia, S. and Feng, F. (2003) 'Thyroid hormone is not necessary for the development of outer hair cell electromotility', *Hearing Research*, 175(SUPPL.), pp. 183–189. Available at: https://doi.org/10.1016/S0378-5955(02)00737-2.
65. Hertzano, R. *et al.* (2008) 'A Myo6 mutation destroys coordination between the myosin heads, revealing new functions of myosin VI in the stereocilia of mammalian inner ear hair cells', *PLoS Genetics*, 4(10). Available at: https://doi.org/10.1371/journal.pgen.1000207.
66. Hinojosa, R. (1977) 'A note on development of corti's organ', *Acta Oto-Laryngologica*, 84(1–6), pp. 238–251. Available at: https://doi.org/10.3109/00016487709123963.
67. Huang, L.C. *et al.* (2007) 'Spatiotemporal definition of neurite outgrowth, refinement and retraction in the developing mouse cochlea', *Development*, 134(16), pp. 2925–2933. Available at: https://doi.org/10.1242/dev.001925.
68. Huang, L.C. *et al.* (2012) 'Synaptic profiles during neurite extension, refinement and retraction in the developing cochlea', *Neural Development*, 7(1), p. 38. Available at: https://doi.org/10.1186/1749-8104-7-38.
69. Jagger, D.J. (2003) 'Membrane Properties of Type II Spiral Ganglion Neurones Identified in a Neonatal Rat Cochlear Slice', *The Journal of Physiology*, 552(Pt 2), p. 525. Available at: https://doi.org/10.1113/jphysiol.2003.052589.
70. Jean, P. *et al.* (2018) 'The synaptic ribbon is critical for sound encoding at high rates and with temporal precision', *eLife*, 7, pp. 1–39. Available at: https://doi.org/10.7554/eLife.29275.
71. Jeong, M. *et al.* (2018) 'Generating inner ear organoids containing putative cochlear hair cells from human pluripotent stem cells', *Cell Death and Disease*, 9(9), pp. 1–13. Available at: https://doi.org/10.1038/s41419-018-0967-1.
72. Johnson, S.L. *et al.* (2008) 'Tonotopic variation in the calcium dependence of neurotransmitter release and vesicle pool replenishment at mammalian auditory ribbon synapses', *Journal of Neuroscience*, 28(30), pp. 7670–7678. Available at: https://doi.org/10.1523/JNEUROSCI.0785-08.2008.
73. Johnson, S.L. *et al.* (2009) 'Functional maturation of the exocytotic machinery at gerbil hair cell ribbon synapses', *Journal of Physiology*, 587(8), pp. 1715–1726. Available at: https://doi.org/10.1113/jphysiol.2009.168542.
74. Johnson, S.L. *et al.* (2010) 'Synaptotagmin IV determines the linear Ca 2+ dependence of vesicle fusion at auditory ribbon synapses', *Nature Neuroscience*, 13(1), pp. 45–52. Available at: https://doi.org/10.1038/nn.2456.
75. Johnson, S.L., Eckrich, T., *et al.* (2011) 'Position-dependent patterning of spontaneous action potentials in immature cochlear inner hair cells', *Nature Neuroscience*, 14(6), pp. 711–717.

Available at: https://doi.org/10.1038/nn.2803.

76. Johnson, S.L., Beurg, M., *et al.* (2011) 'Prestin-Driven Cochlear Amplification Is Not Limited by the Outer Hair Cell Membrane Time Constant', *Neuron*, 70(6), pp. 1143–1154. Available at: https://doi.org/10.1016/j.neuron.2011.04.024.
77. Johnson, S.L. *et al.* (2012) 'The resting transducer current drives spontaneous activity in prehearing mammalian cochlear inner hair cells', *Journal of Neuroscience*, 32(31), pp. 10479–10483. Available at: https://doi.org/10.1523/JNEUROSCI.0803-12.2012.
78. Johnson, S.L. *et al.* (2013) 'Presynaptic maturation in auditory hair cells requires a critical period of sensory-independent spiking activity', *Proceedings of the National Academy of Sciences of the United States of America*, 110(21), pp. 8720–8725. Available at: https://doi.org/10.1073/pnas.1219578110.
79. Johnson, S.L., Ceriani, F., *et al.* (2017) 'Connexin-mediated signaling in nonsensory cells is crucial for the development of sensory inner hair cells in the mouse cochlea', *Journal of Neuroscience*, 37(2), pp. 258–268. Available at: https://doi.org/10.1523/JNEUROSCI.2251-16.2016.
80. Johnson, S.L., Olt, J., *et al.* (2017) 'The coupling between Ca2+ channels and the exocytotic Ca2+ sensor at hair cell ribbon synapses varies tonotopically along the mature cochlea', *Journal of Neuroscience*, 37(9), pp. 2471–2484. Available at: https://doi.org/10.1523/JNEUROSCI.2867-16.2017.
81. Johnson, S.L., Adelman, J.P. and Marcotti, W. (2007) 'Genetic deletion of SK2 channels in mouse inner hair cells prevents the developmental linearization in the Ca2+ dependence of exocytosis', *Journal of Physiology*, 583(2), pp. 631–646. Available at: https://doi.org/10.1113/jphysiol.2007.136630.
82. Johnson, S.L., Marcotti, W. and Kros, C.J. (2005) 'Increase in efficiency and reduction in Ca2+ dependence of exocytosis during development of mouse inner hair cells', *Journal of Physiology*, 563(1), pp. 177–191. Available at: https://doi.org/10.1113/jphysiol.2004.074740.
83. Johnstone, B.M. *et al.* (1989) 'Stimulus-related potassium changes in the organ of Corti of guinea-pig.', *The Journal of Physiology*, 408(1), pp. 77–92. Available at: https://doi.org/10.1113/jphysiol.1989.sp017448.
84. Kalluri, R. and Monges-Hernandez, M. (2017) 'Spatial Gradients in the Size of Inner Hair Cell Ribbons Emerge Before the Onset of Hearing in Rats', *JARO - Journal of the Association for Research in Otolaryngology*, 18(3), pp. 399–413. Available at: https://doi.org/10.1007/s10162-017-0620-1.
85. Kaltenbach, J.A., Falzarano, P.R. and Simpson, T.H. (1994) 'Postnatal development of the hamster cochlea. II. Growth and differentiation of stereocilia bundles', *Journal of Comparative Neurology*, 350(2), pp. 187–198. Available at: https://doi.org/10.1002/cne.903500204.
86. Kandler, K., Clause, A. and Noh, J. (2009) 'Tonotopic reorganization of developing auditory brainstem circuits', *Nature Neuroscience*, 12(6), pp. 711–717. Available at:

https://doi.org/10.1038/nn.2332.

87. Kawasaki, F. *et al.* (2004) 'Active Zone Localization of Presynaptic Calcium Channels Encoded by the cacophony Locus of Drosophila', *Journal of Neuroscience*, 24(1), pp. 282–285. Available at: https://doi.org/10.1523/JNEUROSCI.3553-03.2004.
88. Kersigo, J. and Fritzsch, B. (2015) 'Inner Ear hair cells deteriorate in mice engineered to have no or diminished innervation', *Frontiers in Aging Neuroscience*, 7(FEB), p. 33. Available at: https://doi.org/10.3389/fnagi.2015.00033.
89. Khimich, D. *et al.* (2005) 'Hair cell synaptic ribbons are essential for synchronous auditory signalling', *Nature*, 434(7035), pp. 889–894. Available at: https://doi.org/10.1038/nature03418.
90. Kim, J. and Koo, M. (2015) 'Mass and stiffness impact on the middle ear and the cochlear partition', *Korean Journal of Audiology*, 19(1), pp. 1–6. Available at: https://doi.org/10.7874/jao.2015.19.1.1.
91. Kim, J.H. *et al.* (2011) 'Early Fetal Development of the Human Cochlea', *Anatomical Record*, 294(6), pp. 996–1002. Available at: https://doi.org/10.1002/ar.21387.
92. Kim, M.H., Li, G.L. and von Gersdorff, H. (2013) 'Single Ca2+ channels and exocytosis at sensory synapses', *Journal of Physiology*, 591(13), pp. 3167–3178. Available at: https://doi.org/10.1113/jphysiol.2012.249482.
93. Kim, W.Y. *et al.* (2001) 'NeuroD-null mice are deaf due to a severe loss of the inner ear sensory neurons during development', *Development*, 128(3), pp. 417–426. Available at: https://doi.org/10.1242/dev.128.3.417.
94. Kirkby, L.A. *et al.* (2013) 'A role for correlated spontaneous activity in the assembly of neural circuits', *Neuron*, 80(5), pp. 1129–1144. Available at: https://doi.org/10.1016/j.neuron.2013.10.030.
95. Koundakjian, E.J., Appler, J.L. and Goodrich, L. V. (2007) 'Auditory neurons make stereotyped wiring decisions before maturation of their targets', *Journal of Neuroscience*, 27(51), pp. 14078–14088. Available at: https://doi.org/10.1523/JNEUROSCI.3765-07.2007.
96. Kros, C.J. (1996) 'Physiology of Mammalian Cochlear Hair Cells', pp. 318–385. Available at: https://doi.org/10.1007/978-1-4612-0757-3_6.
97. Kros, C.J., Ruppersberg, J.P. and Rüsch, A. (1998) 'Expression of a potassium current inner hair cells during development of hearing in mice', *Nature*, 394(6690), pp. 281–284. Available at: https://doi.org/10.1038/28401.
98. Lee, Y.S., Liu, F. and Segil, N. (2006) 'A morphogenetic wave of p27Kip1 transcription directs cell cycle exit during organ of Corti development', *Development*, 133(15), pp. 2817–2826. Available at: https://doi.org/10.1242/dev.02453.
99. Liberman, L.D., Wang, H. and Liberman, M.C. (2011) 'Opposing gradients of ribbon size and AMPA receptor expression underlie sensitivity differences among cochlear-nerve/hair-cell synapses', *Journal of Neuroscience*, 31(3), pp. 801–808. Available at:

https://doi.org/10.1523/JNEUROSCI.3389-10.2011.

100. Liberman, M.C. (1980) ‘Morphological differences among radial afferent fibers in the cat cochlea: An electron-microscopic study of serial sections’, *Hearing Research*, 3(1), pp. 45–63. Available at: https://doi.org/10.1016/0378-5955(80)90007-6.

101. Liberman, M.C. (2017) ‘Noise-induced and age-related hearing loss: New perspectives and potential therapies’, *F1000Research*, 6. Available at: https://doi.org/10.12688/f1000research.11310.1.

102. Liberman, M.C., Dodds, L.W. and Pierce, S. (1990) ‘Afferent and efferent innervation of the cat cochlea: Quantitative analysis with light and electron microscopy’, *Journal of Comparative Neurology*, 301(3), pp. 443–460. Available at: https://doi.org/10.1002/cne.903010309.

103. Lim, D.J. and Anniko, M. (1985) ‘Developmental morphology of the mouse inner ear: A scanning electron microscopic observation’, *Acta Oto-Laryngologica*, 99(S422), pp. 5–69. Available at: https://doi.org/10.3109/00016488509121766.

104. Magupalli, V.G. *et al.* (2008) ‘Multiple RIBEYE-RIBEYE interactions create a dynamic scaffold for the formation of synaptic ribbons’, *Journal of Neuroscience*, 28(32), pp. 7954–7967. Available at: https://doi.org/10.1523/JNEUROSCI.1964-08.2008.

105. Marcotti, W. *et al.* (1999) ‘Transient expression of an inwardly rectifying potassium conductance in developing inner and outer hair cells along the mouse cochlea’, *Pflügers Archiv - European Journal of Physiology*, 439(1), pp. 113–122. Available at: https://doi.org/10.1007/s004249900157.

106. Marcotti, W. *et al.* (2003) ‘Development of changes in the expression of potassium currents of embryonic, neonatal and mature mouse inner hair cells’, *Journal of Physiology*, 548(2), pp. 383–400. Available at: https://doi.org/10.1113/jphysiol.2002.034801.

107. Marcotti, W. *et al.* (2016) ‘The acquisition of mechano-electrical transducer current adaptation in auditory hair cells requires myosin VI’, *Journal of Physiology*, 594(13), pp. 3667–3681. Available at: https://doi.org/10.1113/JP272220.

108. Marcotti, W., Johnson, S.L. and Kros, C.J. (2004) ‘A transiently expressed SK current sustains and modulates action potential activity in immature mouse inner hair cells’, *Journal of Physiology*, 560(3), pp. 691–708. Available at: https://doi.org/10.1113/jphysiol.2004.072868.

109. Marcotti, W. and Kros, C.J. (1999) ‘Developmental expression of the potassium current I(K,n) contributes to maturation of mouse outer hair cells’, *Journal of Physiology*, 520(3), pp. 653–660. Available at: https://doi.org/10.1111/j.1469-7793.1999.00653.x.

110. Marcotti, W., van Netten, S.M. and Kros, C.J. (2005) ‘The aminoglycoside antibiotic dihydrostreptomycin rapidly enters mouse outer hair cells through the mechano-electrical transducer channels’, *Journal of Physiology*, 567(2), pp. 505–521. Available at: https://doi.org/10.1113/jphysiol.2005.085951.

111. Matsubara, A. *et al.* (1996) *Organization of AMPA receptor subunits at a glutamate synapse: A quantitative immunogold analysis of hair cell synapses in the rat organ of corti*, *Journal of Neuroscience*. Society for Neuroscience. Available at: https://doi.org/10.1523/jneurosci.16-14-04457.1996.

112. Matthews, G. and Fuchs, P. (2010) 'The diverse roles of ribbon synapses in sensory neurotransmission', *Nature Reviews Neuroscience*, 11(12), pp. 812–822. Available at: https://doi.org/10.1038/nrn2924.

113. Mburu, P. *et al.* (2010) 'Gelsolin plays a role in the actin polymerization complex of hair cell stereocilia', *PLoS ONE*. Edited by R.C. May, 5(7), p. e11627. Available at: https://doi.org/10.1371/journal.pone.0011627.

114. McGrath, J., Roy, P. and Perrin, B.J. (2017) 'Stereocilia morphogenesis and maintenance through regulation of actin stability', *Seminars in Cell and Developmental Biology*, 65, pp. 88–95. Available at: https://doi.org/10.1016/j.semcdb.2016.08.017.

115. McKay, S.M. and Oleskevich, S. (2007) 'The role of spontaneous activity in development of the endbulb of Held synapse', *Hearing Research*, 230(1–2), pp. 53–63. Available at: https://doi.org/10.1016/j.heares.2007.05.006.

116. McPherson, D.R. (2018) *Sensory hair cells: An introduction to structure and physiology*, *Integrative and Comparative Biology*. Oxford University Press. Available at: https://doi.org/10.1093/icb/icy064.

117. Menting, J.G. *et al.* (2013) 'How insulin engages its primary binding site on the insulin receptor', *Nature*, 493(7431), pp. 241–245. Available at: https://doi.org/10.1038/nature11781.

118. Merchan-Perez, A. and Liberman, M.C. (1996) 'Ultrastructural differences among afferent synapses on cochlear hair cells: Correlations with spontaneous discharge rate', *Journal of Comparative Neurology*, 371(2), pp. 208–221. Available at: https://doi.org/10.1002/(SICI)1096-9861(19960722)371:2<208::AID-CNE2>3.3.CO;2-P.

119. Meyer, A.C. *et al.* (2009) 'Tuning of synapse number, structure and function in the cochlea', *Nature Neuroscience*, 12(4), pp. 444–453. Available at: https://doi.org/10.1038/nn.2293.

120. Michael, G.J. *et al.* (1997) *Nerve growth factor treatment increases brain-derived neurotrophic factor selectively in TrkA-expressing dorsal root ganglion cells and in their central terminations within the spinal cord*, *Journal of Neuroscience*. Available at: https://doi.org/10.1523/jneurosci.17-21-08476.1997.

121. Michalski, N. *et al.* (2017) 'Otoferlin acts as a Ca2+ sensor for vesicle fusion and vesicle pool replenishment at auditory hair cell ribbon synapses', *eLife*, 6. Available at: https://doi.org/10.7554/eLife.31013.

122. Michanski, S. *et al.* (2019) 'Mapping developmental maturation of inner hair cell ribbon synapses in the apical mouse cochlea', *Proceedings of the National Academy of Sciences of the United States of America*, 116(13), pp. 6415–6424. Available at:

https://doi.org/10.1073/pnas.1812029116.

123. Moglie, M.J. *et al.* (2018) 'Compartmentalization of antagonistic Ca2+ signals in developing cochlear hair cells', *Proceedings of the National Academy of Sciences of the United States of America*, 115(9), pp. E2095–E2104. Available at: https://doi.org/10.1073/pnas.1719077115.

124. Monesson-Olson, B.D. *et al.* (2014) 'Optical stimulation of zebrafish hair cells expressing channelrhodopsin-2', *PLoS ONE*, 9(5), p. 96641. Available at: https://doi.org/10.1371/journal.pone.0096641.

125. Moody, W.J. and Bosma, M.M. (2005) 'Ion channel development, spontaneous activity, and activity-dependent development in nerve and muscle cells', *Physiological Reviews*, 85(3), pp. 883–941. Available at: https://doi.org/10.1152/physrev.00017.2004.

126. Moser, T. and Beutner, D. (2000) 'Kinetics of exocytosis and endocytosis at the cochlear inner hair cell afferent synapse of the mouse', *Proceedings of the National Academy of Sciences of the United States of America*, 97(2), pp. 883–888. Available at: https://doi.org/10.1073/pnas.97.2.883.

127. Moser, T., Grabner, C.P. and Schmitz, F. (2020) 'Sensory processing at ribbon synapses in the retina and the cochlea', *Physiological Reviews*, 100(1), pp. 103–144. Available at: https://doi.org/10.1152/physrev.00026.2018.

128. Müller, U. (2008) 'Cadherins and mechanotransduction by hair cells', *Current Opinion in Cell Biology*, 20(5), pp. 557–566. Available at: https://doi.org/10.1016/j.ceb.2008.06.004.

129. Neher, E. (1998) 'Vesicle pools and Ca2+ microdomains: New tools for understanding their roles in neurotransmitter release', *Neuron*, 20(3), pp. 389–399. Available at: https://doi.org/10.1016/S0896-6273(00)80983-6.

130. Ng, L., Kelley, M.W. and Forrest, D. (2013) 'Making sense with thyroid hormone-the role of T 3 in auditory development', *Nature Reviews Endocrinology*, 9(5), pp. 296–307. Available at: https://doi.org/10.1038/nrendo.2013.58.

131. Nouvian, R. *et al.* (2006) 'Structure and function of the hair cell ribbon synapse', *Journal of Membrane Biology*, 209(2–3), pp. 153–165. Available at: https://doi.org/10.1007/s00232-005-0854-4.

132. Nouvian, R. *et al.* (2011) 'Exocytosis at the hair cell ribbon synapse apparently operates without neuronal SNARE proteins', *Nature Neuroscience*, 14(4), pp. 411–413. Available at: https://doi.org/10.1038/nn.2774.

133. O'Malley, B.W., Li, D. and Turner, D.S. (1995) 'Hearing loss and cochlear abnormalities in the congenital hypothyroid (hyt/hyt) mouse', *Hearing Research*, 88(1–2), pp. 181–189. Available at: https://doi.org/10.1016/0378-5955(95)00111-G.

134. Ogier, J.M. *et al.* (2019) 'Organotypic culture of neonatal murine inner ear explants', *Frontiers in Cellular Neuroscience*, 13, p. 170. Available at: https://doi.org/10.3389/fncel.2019.00170.

135. Oliver, D. *et al.* (2003) *Resting potential and submembrane calcium concentration of inner hair cells in the isolated mouse cochlea are set by KCNQ-type potassium channels*, *Journal of Neuroscience*. Society for Neuroscience. Available at: https://doi.org/10.1523/jneurosci.23-06-02141.2003.

136. Palmer, A.R. and Russell, I.J. (1986) 'Phase-locking in the cochlear nerve of the guinea-pig and its relation to the receptor potential of inner hair-cells', *Hearing Research*, 24(1), pp. 1–15. Available at: https://doi.org/10.1016/0378-5955(86)90002-X.

137. Pangšrič, T. *et al.* (2010) 'Hearing requires otoferlin-dependent efficient replenishment of synaptic vesicles in hair cells', *Nature Neuroscience*, 13(7), pp. 869–876. Available at: https://doi.org/10.1038/nn.2578.

138. Peng, A.W. *et al.* (2009) 'Twinfilin 2 regulates actin filament lengths in cochlear stereocilia', *Journal of Neuroscience*, 29(48), pp. 15083–15088. Available at: https://doi.org/10.1523/JNEUROSCI.2782-09.2009.

139. Peng, A.W. *et al.* (2011) 'Integrating the biophysical and molecular mechanisms of auditory hair cell mechanotransduction', *Nature Communications*, 2(1), p. 523. Available at: https://doi.org/10.1038/ncomms1533.

140. Petit, C. and Richardson, G.P. (2009) 'Linking genes underlying deafness to hair-bundle development and function', *Nature Neuroscience*. Europe PMC Funders, pp. 703–710. Available at: https://doi.org/10.1038/nn.2330.

141. Platzer, J. *et al.* (2000) 'Congenital deafness and sinoatrial node dysfunction in mice lacking class D L-type Ca2+ channels', *Cell*, 102(1), pp. 89–97. Available at: https://doi.org/10.1016/S0092-8674(00)00013-1.

142. Prokop, A. (1999) 'Integrating bits and pieces: Synapse structure and formation in Drosophila embryos', *Cell and Tissue Research*, 297(2), pp. 169–186. Available at: https://doi.org/10.1007/s004410051345.

143. Pujol, R., Lavigne-Rebillard, M. and Lenoir, M. (1998) 'Development of Sensory and Neural Structures in the Mammalian Cochlea', *Development of the Auditory System*, pp. 146–192. Available at: https://doi.org/10.1007/978-1-4612-2186-9_4.

144. Pumplin, D.W., Reese, T.S. and Llinás, R. (1981) 'Are the presynaptic membrane particles the calcium channels?', *Proceedings of the National Academy of Sciences of the United States of America*, 78(11), pp. 7210–7213. Available at: https://doi.org/10.1073/pnas.78.11.7210.

145. Pylypenko, O. *et al.* (2015) 'Myosin VI deafness mutation prevents the initiation of processive runs on actin', *Proceedings of the National Academy of Sciences of the United States of America*, 112(11), pp. E1201–E1209. Available at: https://doi.org/10.1073/pnas.1420989112.

146. Pyott, S.J. *et al.* (2004) 'Extrasynaptic localization of inactivating calcium-activated potassium channels in mouse inner hair cells', *Journal of Neuroscience*, 24(43), pp. 9469–

9474. Available at: https://doi.org/10.1523/JNEUROSCI.3162-04.2004.

147. Qiu, X. and Müller, U. (2018) *Mechanically gated ion channels in mammalian hair cells*, *Frontiers in Cellular Neuroscience*. Frontiers Media SA. Available at: https://doi.org/10.3389/fncel.2018.00100.

148. Raphael, Y. (2002) 'Cochlear pathology, sensory cell death and regeneration', *British Medical Bulletin*, pp. 25–38. Available at: https://doi.org/10.1093/bmb/63.1.25.

149. Regus-Leidig, H. *et al.* (2013) 'Identification and Immunocytochemical Characterization of Piccolino, a Novel Piccolo Splice Variant Selectively Expressed at Sensory Ribbon Synapses of the Eye and Ear', *PLoS ONE*. Edited by K.-W. Koch, 8(8), p. e70373. Available at: https://doi.org/10.1371/journal.pone.0070373.

150. Regus-Leidig, H. *et al.* (2014) 'In vivo knockdown of Piccolino disrupts presynaptic ribbon morphology in mouse photoreceptor synapses', *Frontiers in Cellular Neuroscience*, 8(SEP), p. 259. Available at: https://doi.org/10.3389/fncel.2014.00259.

151. Robles, L. and Ruggero, M.A. (2001) 'Mechanics of the mammalian cochlea', *Physiological Reviews*, 81(3), pp. 1305–1352. Available at: https://doi.org/10.1152/physrev.2001.81.3.1305.

152. Roux, I. *et al.* (2006) 'Otoferlin, Defective in a Human Deafness Form, Is Essential for Exocytosis at the Auditory Ribbon Synapse', *Cell*, 127(2), pp. 277–289. Available at: https://doi.org/10.1016/j.cell.2006.08.040.

153. Rüsch, A. *et al.* (2001) *Retardation of cochlear maturation and impaired hair cell function caused by deletion of all known thyroid hormone receptors*, *Journal of Neuroscience*. Available at: https://doi.org/10.1523/jneurosci.21-24-09792.2001.

154. Rutherford, M.A. and Moser, T. (2016) *The Ribbon Synapse Between Type I Spiral Ganglion Neurons and Inner Hair Cells*. Available at: https://doi.org/10.1007/978-1-4939-3031-9_5.

155. Safieddine, S. and Wenthold, R.J. (1999) 'SNARE complex at the ribbon synapses of cochlear hair cells: Analysis of synaptic vesicle- and synaptic membrane-associated proteins', *European Journal of Neuroscience*, 11(3), pp. 803–812. Available at: https://doi.org/10.1046/j.1460-9568.1999.00487.x.

156. Santarelli, R. *et al.* (2015) 'Audibility, speech perception and processing of temporal cues in ribbon synaptic disorders due to OTOF mutations', *Hearing Research*, 330, pp. 200–212. Available at: https://doi.org/10.1016/j.heares.2015.07.007.

157. Scheibe, F., Haupt, H. and Ising, H. (1999) 'Total magnesium concentrations of perilymph, cerebrospinal fluid and blood in guinea pigs fed different magnesium-containing diets', *European Archives of Oto-Rhino-Laryngology*, 256(5), pp. 215–219. Available at: https://doi.org/10.1007/s004050050144.

158. Schindelin, J. *et al.* (2012) 'Fiji: An open-source platform for biological-image analysis', *Nature Methods*, 9(7), pp. 676–682. Available at: https://doi.org/10.1038/nmeth.2019.

159. Schmitz, F., Königstorfer, A. and Südhof, T.C. (2000) 'RIBEYE, a component of synaptic ribbons: A protein's journey through evolution provides insight into synaptic ribbon function', *Neuron*, 28(3), pp. 857–872. Available at: https://doi.org/10.1016/S0896-6273(00)00159-8.

160. Schnee, M.E. *et al.* (2005) 'Auditory hair cell-afferent fiber synapses are specialized to operate at their best frequencies', *Neuron*, 47(2), pp. 243–254. Available at: https://doi.org/10.1016/j.neuron.2005.06.004.

161. Schoenmakers, T.J.M. *et al.* (1992) 'CHELATOR: An improved method for computing metal ion concentrations in physiological solutions', *BioTechniques*, 12(6), pp. 870-872+874+876+878. Available at: https://pubmed.ncbi.nlm.nih.gov/1642895/ (Accessed: 28 August 2022).

162. Schwander, M., Kachar, B. and Müller, U. (2010) 'The cell biology of hearing', *Journal of Cell Biology*, 190(1), pp. 9–20. Available at: https://doi.org/10.1083/jcb.201001138.

163. Schwieger, J. *et al.* (2015) 'Neuronal survival, morphology and outgrowth of spiral ganglion neurons using a defined growth factor combination', *PLoS ONE*, 10(8). Available at: https://doi.org/10.1371/journal.pone.0133680.

164. Seal, R.P. *et al.* (2008) 'Sensorineural Deafness and Seizures in Mice Lacking Vesicular Glutamate Transporter 3', *Neuron*, 57(2), pp. 263–275. Available at: https://doi.org/10.1016/j.neuron.2007.11.032.

165. Sendin, G. *et al.* (2007) 'Maturation of ribbon synapses in hair cells is driven by thyroid hormone', *Journal of Neuroscience*, 27(12), pp. 3163–3173. Available at: https://doi.org/10.1523/JNEUROSCI.3974-06.2007.

166. Shapira, M. *et al.* (2003) 'Unitary assembly of presynaptic active zones from Piccolo-Bassoon transport vesicles', *Neuron*, 38(2), pp. 237–252. Available at: https://doi.org/10.1016/S0896-6273(03)00207-1.

167. Sharlin, D.S. *et al.* (2018) 'Deafness and loss of cochlear hair cells in the absence of thyroid hormone transporters Slc16a2 (Mct8) and Slc16a10 (Mct10)', *Scientific Reports*, 8(1). Available at: https://doi.org/10.1038/s41598-018-22553-w.

168. Simmons, D.D., Mansdorf, N.B. and Kim, J.H. (1996) 'Olivocochlear innervation of inner and outer hair cells during postnatal maturation: Evidence for a waiting period', *Journal of Comparative Neurology*, 370(4), pp. 551–562. Available at: https://doi.org/10.1002/(SICI)1096-9861(19960708)370:4<551::AID-CNE10>3.0.CO;2-M.

169. Slepecky, N., Hamernik, R.P. and Henderson, D. (1980) 'Re-examination of a hair cell organelle in the cuticular late region and its possible relation to active processes in he cochlea', *Hearing Research*, 2(3–4), pp. 413–421. Available at: https://doi.org/10.1016/0378-5955(80)90077-5.

170. Slepecky, N.B. (1996) 'Structure of the Mammalian Cochlea', pp. 44–129. Available at: https://doi.org/10.1007/978-1-4612-0757-3_2.

171. Smith, C.A. and Sjöstrand, F.S. (1961) ‘A synaptic structure in the hair cells of the guinea pig cochlea’, *Journal of Ultrasructure Research*, 5(2), pp. 184–192. Available at: https://doi.org/10.1016/S0022-5320(61)90013-2.

172. Sobkowicz, H.M. *et al.* (1982) *Ribbon synapses in the developing intact and cultured organ of corti in the mouse*, *Journal of Neuroscience*. Society for Neuroscience. Available at: https://doi.org/10.1523/jneurosci.02-07-00942.1982.

173. Sobkowicz, H.M. *et al.* (1986) ‘Distribution of synaptic ribbons in the developing organ of Corti’, *Journal of Neurocytology*, 15(6), pp. 693–714. Available at: https://doi.org/10.1007/BF01625188.

174. Sobkowicz, H.M., August, B.K. and Slapnick, S.M. (2002) ‘Influence of neurotrophins on the synaptogenesis of inner hair cells in the deaf Bronx waltzer (bv) mouse organ of Corti in culture’, *International Journal of Developmental Neuroscience*, 20(7), pp. 537–554. Available at: https://doi.org/10.1016/S0736-5748(02)00084-9.

175. Soto, F. *et al.* (2012) ‘Spontaneous activity promotes synapse formation in a cell-type-dependent manner in the developing retina’, *Journal of Neuroscience*, 32(16), pp. 5426–5439. Available at: https://doi.org/10.1523/JNEUROSCI.0194-12.2012.

176. Sotomayor, M. *et al.* (2012) ‘Structure of a force-conveying cadherin bond essential for inner-ear mechanotransduction’, *Nature*, 492(7427), pp. 128–132. Available at: https://doi.org/10.1038/nature11590.

177. Staecker, H. *et al.* (1996) ‘NGF, BDNF and NT-3 play unique roles in the in vitro development and patterning of innervation of the mammalian inner ear’, *Developmental Brain Research*, 92(1), pp. 49–60. Available at: https://doi.org/10.1016/0165-3806(95)00198-0.

178. Sterkers, O., Ferrary, E. and Amiel, C. (1988) ‘Production of inner ear fluids’, *Physiological Reviews*, 68(4), pp. 1083–1128. Available at: https://doi.org/10.1152/physrev.1988.68.4.1083.

179. Sun, W. and Salvi, R.J. (2009) ‘Brain derived neurotrophic factor and neurotrophic factor 3 modulate neurotransmitter receptor expressions on developing spiral ganglion neurons’, *Neuroscience*, 164(4), pp. 1854–1866. Available at: https://doi.org/10.1016/j.neuroscience.2009.09.037.

180. Sundaresan, Srividya *et al.* (2016) ‘Thyroid hormone is required for pruning, functioning and long-term maintenance of afferent inner hair cell synapses’, *European Journal of Neuroscience*, 43(2), pp. 148–161. Available at: https://doi.org/10.1111/ejn.13081.

181. Sundaresan, S., Balasubbu, S. and Mustapha, M. (2016) ‘Thyroid hormone is required for the pruning of afferent type II spiral ganglion neurons in the mouse cochlea’, *Neuroscience*, 312(November), pp. 165–178. Available at: https://doi.org/10.1016/j.neuroscience.2015.11.020.

182. Sutton, R.B. *et al.* (1995) ‘Structure of the first C2 domain of synaptotagmin I: A novel Ca2+/phospholipid-binding fold’, *Cell*, 80(6), pp. 929–938. Available at:

https://doi.org/10.1016/0092-8674(95)90296-1.

183. Szarama, K.B. *et al.* (2013) 'Thyroid hormone increases fibroblast growth factor receptor expression and disrupts cell mechanics in the developing organ of corti', *BMC Developmental Biology*, 13(1), p. 6. Available at: https://doi.org/10.1186/1471-213X-13-6.

184. Szobota, S. *et al.* (2019) 'BDNF, NT-3 and Trk receptor agonist monoclonal antibodies promote neuron survival, neurite extension, and synapse restoration in rat cochlea ex vivo models relevant for hidden hearing loss', *PLoS ONE*, 14(10). Available at: https://doi.org/10.1371/journal.pone.0224022.

185. Teudt, I.U. and Richter, C.P. (2014) 'Basilar membrane and tectorial membrane stiffness in the CBA/CaJ mouse', *JARO - Journal of the Association for Research in Otolaryngology*, 15(5), pp. 675–694. Available at: https://doi.org/10.1007/s10162-014-0463-y.

186. Tilney, L.G., Tilney, M.S. and DeRosier, D.J. (1992) 'Actin filaments, stereocilia, and hair cells: How cells count and measure', *Annual Review of Cell Biology*, 8(1), pp. 257–274. Available at: https://doi.org/10.1146/annurev.cb.08.110192.001353.

187. Tom Dieck, S. *et al.* (2005) 'Molecular dissection of the photoreceptor ribbon synapse: Physical interaction of Bassoon and RIBEYE is essential for the assembly of the ribbon complex', *Journal of Cell Biology*, 168(5), pp. 825–836. Available at: https://doi.org/10.1083/jcb.200408157.

188. Tritsch, N.X. *et al.* (2007) 'The origin of spontaneous activity in the developing auditory system', *Nature*, 450(7166), pp. 50–55. Available at: https://doi.org/10.1038/nature06233.

189. Tritsch, N.X. *et al.* (2010) 'Calcium action potentials in hair cells pattern auditory neuron activity before hearing onset', *Nature Neuroscience*, 13(9), pp. 1050–1052. Available at: https://doi.org/10.1038/nn.2604.

190. Tritsch, N.X. and Bergles, D.E. (2010) 'Developmental regulation of spontaneous activity in the mammalian cochlea', *Journal of Neuroscience*, 30(4), pp. 1539–1550. Available at: https://doi.org/10.1523/JNEUROSCI.3875-09.2010.

191. Ubaidah, M.A. *et al.* (2015) 'Effect of growth factor supplementation on the hair cell specific markers of cells harvested from basilar membrane', *Journal of International Advanced Otology*, 11(1), pp. 23–29. Available at: https://doi.org/10.5152/iao.2015.539.

192. Uetsuka, S. *et al.* (2015) 'Molecular architecture of the stria vascularis membrane transport system, which is essential for physiological functions of the mammalian cochlea', *European Journal of Neuroscience*, 42(3), pp. 1984–2002. Available at: https://doi.org/10.1111/ejn.12973.

193. Uthaiah, R.C. and Hudspeth, A.J. (2010) 'Molecular anatomy of the hair cell's ribbon synapse', *Journal of Neuroscience*, 30(37), pp. 12387–12399. Available at: https://doi.org/10.1523/JNEUROSCI.1014-10.2010.

194. Vélez-Ortega, A.C. *et al.* (2017) 'Mechanotransduction current is essential for stability of the transducing stereocilia in mammalian auditory hair cells', *eLife*, 6. Available at: https://doi.org/10.7554/eLife.24661.

195. Verpy, E. *et al.* (2011) 'Stereocilin connects outer hair cell stereocilia to one another and to the tectorial membrane', *Journal of Comparative Neurology*, 519(2), pp. 194–210. Available at: https://doi.org/10.1002/cne.22509.

196. Vetter, D.E. *et al.* (1999) 'Role of α9 nicotinic ACh receptor subunits in the development and function of cochlear efferent innervation', *Neuron*, 23(1), pp. 93–103. Available at: https://doi.org/10.1016/S0896-6273(00)80756-4.

197. Voorn, R.A. and Vogl, C. (2020) 'Molecular Sciences Molecular Assembly and Structural Plasticity of Sensory Ribbon Synapses-A Presynaptic Perspective', *International Journal of Molecular Sciences* [Preprint]. Available at: https://doi.org/10.3390/ijms21228758.

198. Wan, G. *et al.* (2014) 'Neurotrophin-3 regulates ribbon synapse density in the cochlea and induces synapse regeneration after acoustic trauma', *eLife*, 2014-Octob, pp. 1–35. Available at: https://doi.org/10.7554/eLife.03564.

199. Wang, H.C. *et al.* (2015) 'Spontaneous Activity of Cochlear Hair Cells Triggered by Fluid Secretion Mechanism in Adjacent Support Cells', *Cell*, 163(6), pp. 1348–1359. Available at: https://doi.org/10.1016/j.cell.2015.10.070.

200. Wang, J. *et al.* (2014) 'Calcium sensitive ring-like oligomers formed by synaptotagmin', *Proceedings of the National Academy of Sciences of the United States of America*, 111(38), pp. 13966–13971. Available at: https://doi.org/10.1073/pnas.1415849111.

201. Wang, Q. and Green, S.H. (2011) 'Functional role of neurotrophin-3 in synapse regeneration by spiral ganglion neurons on inner hair cells after excitotoxic trauma in vitro', *Journal of Neuroscience*, 31(21), pp. 7938–7949. Available at: https://doi.org/10.1523/JNEUROSCI.1434-10.2011.

202. Wangemann, P. (2006) 'Supporting sensory transduction: Cochlear fluid homeostasis and the endocochlear potential', *Journal of Physiology*, 576(1), pp. 11–21. Available at: https://doi.org/10.1113/jphysiol.2006.112888.

203. Warr, W.B. and Guinan, J.J. (1979) 'Efferent innervation of the organ of corti: two separate systems', *Brain Research*, 173(1), pp. 152–155. Available at: https://doi.org/10.1016/0006-8993(79)91104-1.

204. Williamson, T.T. *et al.* (2020) 'Understanding hormone and hormone therapies' impact on the auditory system', *Journal of Neuroscience Research*. John Wiley and Sons Inc., pp. 1721–1730. Available at: https://doi.org/10.1002/jnr.24588.

205. Wong, A.B. *et al.* (2014) 'Developmental refinement of hair cell synapses tightens the coupling of Ca2+ influx to exocytosis', *EMBO Journal*, 33(3), pp. 247–264. Available at: https://doi.org/10.1002/embj.201387110.

206. Wu, Y.J. *et al.* (2004) 'Nerve Growth Factor, Brain-Derived Neurotrophic Factor, and

Neurotrophin-3 Are Sorted to Dense-Core Vesicles and Released Via the Regulated Pathway in Primary Rat Cortical Neurons', *Journal of Neuroscience Research*, 75(6), pp. 825–834. Available at: https://doi.org/10.1002/jnr.20048.

207. Yamahara, K. *et al.* (2019) 'Insulin-like growth factor 1 promotes cochlear synapse regeneration after excitotoxic trauma in vitro', *Hearing Research*, 374, pp. 5–12. Available at: https://doi.org/10.1016/j.heares.2019.01.008.

208. Yang, H. *et al.* (2010) 'Generation and characterization of Atoh1-Cre knock-in mouse line', *Genesis*, 48(6), pp. 407–413. Available at: https://doi.org/10.1002/dvg.20633.

209. Yasunaga, ichiro *et al.* (1999) 'A mutation in OTOF, encoding otoferlin, a FER-1-like protein, causes DFNB9, a nonsyndromic form of deafness', 21, p. 363. Available at: http://genetics.nature.com (Accessed: 29 November 2022).

210. Yasunaga, S. *et al.* (2000) 'OTOF encodes multiple long and short isoforms: Genetic evidence that the long ones underlie recessive deafness DFNB9', *American Journal of Human Genetics*, 67(3), pp. 591–600. Available at: https://doi.org/10.1086/303049.

211. Zampini, V. *et al.* (2011) 'Eps8 regulates hair bundle length and functional maturation of mammalian auditory hair cells', *PLoS Biology*. Edited by A. Groves, 9(4), p. e1001048. Available at: https://doi.org/10.1371/journal.pbio.1001048.

212. Zdebik, A.A., Wangemann, P. and Jentsch, T.J. (2009) 'Potassium ion movement in the inner ear: Insights from genetic disease and mouse models', *Physiology*, 24(5), pp. 307–316. Available at: https://doi.org/10.1152/physiol.00018.2009.

213. Zhai, R.G. *et al.* (2001) 'Assembling the presynaptic active zone: A characterization of an active zone precursor vesicle', *Neuron*, 29(1), pp. 131–143. Available at: https://doi.org/10.1016/S0896-6273(01)00185-4.

214. Zhang-Hooks, Y.X. *et al.* (2016) 'NMDA Receptors Enhance Spontaneous Activity and Promote Neuronal Survival in the Developing Cochlea', *Neuron*, 89(2), pp. 337–350. Available at: https://doi.org/10.1016/j.neuron.2015.12.016.

215. Zhang, L. wen *et al.* (2019) 'In vitro culture of mammalian inner ear hair cells', *Journal of Zhejiang University: Science B*, 20(2), pp. 170–179. Available at: https://doi.org/10.1631/jzus.B1700613.

216. Zhou, Y. *et al.* (2020) 'Distribution and Functional Characteristics of Voltage-Gated Sodium Channels in Immature Cochlear Hair Cells', *Neuroscience Bulletin*, 36(1), pp. 49–65. Available at: https://doi.org/10.1007/s12264-019-00415-3.

217. Zhou, Z., Liu, Q. and Davis, R.L. (2005) 'Complex regulation of spiral ganglion neuron firing patterns by neurotrophin-3', *Journal of Neuroscience*, 25(33), pp. 7558–7566. Available at: https://doi.org/10.1523/JNEUROSCI.1735-05.2005.